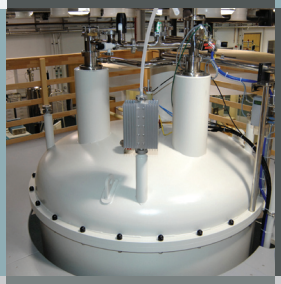

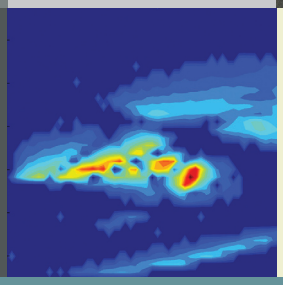

The UK 850 MHz Solid-State NMR Facility

Annual Report 2011

The UK 850 MHz Solid-State NMR Facility

In the first **2** years of operation:

626 days have been allocated to

28 PIs from **16** different UK institutions

with **991** days being requested

The National Management Committee with David Delpy at the formal opening in 2010. From left to right: Front: Steven Brown (Warwick, NMC Chair), David Delpy (EPSRC), Sharon Ashbrook (St Andrews), Robin Harris (Durham), Mark Smith (Warwick). Back: Stephen Wimperis (Glasgow), Ray Dupree (Warwick), Jeremy Titman (Nottingham), Melinda Duer (Cambridge), Dinu Iuga (Facility Manager)

Contents

Introduction

This annual report celebrates two years of operation of the UK 850 MHz solid-state NMR facility, which was enabled by a £3.7 M grant from EPSRC (with a 10% contribution from BBSRC) to a consortium of UK solid-state NMR spectroscopists who form the National Management Committee of the Facility, with additional financial contributions from the University of Warwick (in part through the Birmingham Science City Advanced Materials Projects 1 and 2, supported by Advantage West Midlands) and the European Regional Development Fund. Since welcoming the first visitors in February 2010, the facility has been used by spectroscopists from 16 different UK universities, whose research projects have spanned chemistry, materials, pharmaceuticals, earth sciences, biology and physics.

In NMR, higher magnetic fields bring the advantage of increased resolution and sensitivity. The 850 MHz magnet at the heart of the Facility thus allows experiments to be performed that simply cannot be done successfully at lower fields, as is attested to by the detailed descriptions of the research enabled by the Facility in its second year of operation presented here. For quadrupolar nuclei that constitute two-thirds of all NMR-active nuclear isotopes, the linebroadening decreases markedly with increasing magnetic field strength, which combined with the increase in sensitivity, presents a win-win situation for the spectroscopist. This is illustrated in the publications of research from the Facility that have appeared in 2011 as well as the detailed research descriptions presented in this annual report for, e.g., ^{14}N NMR of pharmaceuticals, ^{17}O NMR of electrochemical products in lithium oxide batteries, geological minerals and zeolites, ^{25}Mg NMR of hydrogen-storage materials, ^{27}Al and ^{71}Ga NMR of solid-oxide fuel cell electrolyte materials, ^{43}Ca NMR of fluroapatites and bioactive glasses, ^{45}Sc NMR of framework materials and ^{87}Sr NMR of inorganic-organic compounds.

In solid-state NMR, most experiments are performed using the technique of magic-angle spinning (MAS). Through the supportive interaction with Bruker who supplied the Facility's existing 10 MAS probes, the Facility allows the spectroscopist to choose from a range of setups from small diameter rotors (down to 1.3 mm) that enable higher rotation frequencies and higher rf nutation frequencies to large diameter rotors (up to 7 mm) that benefit from improved sensitivity associated with higher sample volumes. To stay equipped with the latest technology, the Facility has recently placed an order with Jeol for Europe's first 1 mm double-resonance MAS probe that will enable rotation frequencies up to 80 kHz, with delivery expected in the second half of 2012. In addition, through a partnership with Ago Samoson's laboratory in Estonia, the Facility also possesses a unique double-rotation (DOR) probe that provides high-resolution spectra free of second-order quadrupolar broadening for nuclei with spin equal to 3/2, 5/2, 7/2 or 9/2 – the report gives examples of the impressive resolution achievable using this technique.

The Facility is providing a focus for solid-state NMR spectroscopy in the UK, for example, the first annual symposium in April 2011 attracted over 60 attendees, with talks by scientists from 10 different UK universities. The Facility is keen to welcome new users – the Facility Manager is available to advise those less familiar with the technique, before, during and after a visit.

In conclusion, we are excited by the science being enabled by the UK 850 MHz solid-state NMR facility, which we hope you will enjoy reading about in this annual report.

Further details of the Facility can be found at the Facility website:
http://go.warwick.ac.uk/850mhz/

The National Management Committee

Sharon E Ashbrook
(St Andrews)

Steven P Brown
(Chair, Warwick)

Melinda J Duer
(Cambridge)

Ray Dupree
(Warwick)

Robin K Harris
(Durham)

Mark E Smith
(Lancaster)

Jeremy J Titman
(Nottingham)

Stephen Wimperis
(Glasgow)

Organization and Management of the Facility

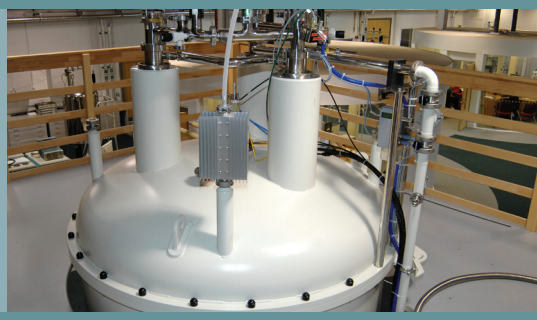

The UK 850 MHz solid-state NMR Facility was established with the aid of several linked research grants from EPSRC. The eight investigators on the grant comprise the National Management Committee (NMC) which determines the strategic objectives for the Facility and the procedures by that these are to be achieved. The NMC meets twice a year, communicating informally more frequently as the need arises. The operation of the Facility is the responsibility of the Local Management Team (LMT) comprising the Facility Manager (FM) who is an ex-officio member of the NMC and the Warwick-based NMC chair. The duties of the Facility Manager include maintaining the instrumentation and assisting visitors to the Facility with their experiments. The management of the Facility is overseen by the International Advisory Board (IAB) which is made up of three eminent solid-state NMR spectroscopists from overseas: Marc Baldus (Utrecht), Arno Kentgens (Nijmegen), Roderick Wasylishen (Alberta). The terms of reference of the NMC and IAB, the remit of the LMT and the duties of the FM are available on the Facility website.

Time Allocation Process

All UK academics who are eligible to apply for Research Council funding, as well as UK researchers of similar standing in industry, may apply for an allocation of spectrometer time at the Facility. Users are expected to run their own experiments with the assistance of the Facility Manager, so personnel with previous solid-state NMR experience should be identified to visit the Facility and carry out the research (inexperienced users should contact the facility manager in advance, to agree a collaborative arrangement with the Facility Manager relating to the Facility Manager's role in carrying out the experiments). A minimum of 80% of the available time is allocated by an independent Time Allocation Panel (TAP) that comprises three UK scientists, including one member of the NMC, as well as the Facility Manager in an ex-officio capacity. The balance is allocated by the NMC and is reserved for fast-track applications, measurements referred from the EPSRC solid-state NMR service, the Facility Manager's designated research time, to compensate users who were unable to take up their allocated time because of instrument down-time, and a small number of maintenance days. Members of the TAP normally serve for a two-year term.

There are two allocation rounds each year for time, each covering a six-month period, starting in either February or August, corresponding to deadlines of November 30th and May 31st. Previous users of the Facility are notified of upcoming deadlines by email. Previous time allocations and instructions for applicants are given on the Facility website. The main criterion for allocating time is overall scientific merit, as well as the quality of the case made for high-field solid-state NMR. Where appropriate, the TAP will consider additional factors, such as the quality of publications arising from previous allocations of time and whether the research is supported by peer-reviewed grants or involves students funded by EPSRC or BBSRC. The TAP is charged with ensuring that the balance of the allocated time broadly reflects the research objectives of the original grant and with providing feedback for unsuccessful applicants. During the TAP meeting, the Facility Manager gives advice on the feasibility of the proposed experiments and the spectrometer time required.

The maximum time that can be requested by an individual applicant during any allocation round is 28 days, but this can be split between several applications. It is a condition that the Facility is mentioned in any publication arising wholly or partly from an allocation of time. Furthermore, a user report must be produced by the original applicant no later than the 7th of the month following the end of the specific six-month time-allocation period, i.e., 7th February or 7th August. Applications are not accepted from users who have outstanding reports from previous allocations of time. The code for all NMR pulse sequences implemented by users on the Facility's spectrometer must be deposited in a shared database. If the experiment is a new one, the code will only be made available to other users after the pulse sequence has been published. Reasonable travel costs associated with the use of the facility will be paid to academic users. The Facility rents accommodation on the University of Warwick campus for use by Facility visitors.

TAP membership (2011): Chair: Jeremy Titman, Nottingham; non-NMC members: David Middleton, Liverpool & Mike Anderson, Manchester (for the February 2011 round) & Kenneth Harris, Cardiff (for the August 2011 round onwards).

What is the Facility?

UK 850 MHz solid-state NMR facility probes

No	Probe
1	1.3 mm probe HXY (+19F) conventional insert design H13863
2	2.5 mm HXY DBB (double-broadband) H13856
3	2.5 mm HX (+19F) H13889
4	2.5 mm HFX H13894
5	3.2 mm HXY DBB (double-broadband) H13857
6	3.2 mm HXY low E field for biosolids LLC H13900
7	3.2 mm HXY conventional insert design H13888
8	4 mm HXY conventional insert design (+19F) H13694
9	4 mm HX (low gamma) H13892
10	7 mm X (low gamma) H13895
11	Static
12	DOR probe (produced by Samoson group, Tallinn, Estonia)

Probes 1 to 11 were supplied by Bruker. Maximum MAS frequencies: 4 mm probes 15 kHz; 3.2 mm probes 24 kHz, 2.5 mm probes 35 kHz; 1.3 mm probe 65 kHz. All 3.2 mm and 4 mm MAS probes are equipped with DVT stators and can operate between -140 ^{O}C + 150 ^{O}C.

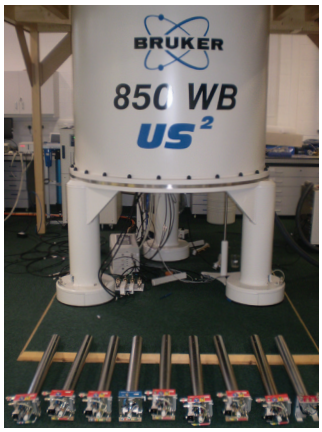

850 MHz spectrometer and probes

Probes usage 2010 and 2011

Year 1 + Year 2 (Round 1 to Round 4)

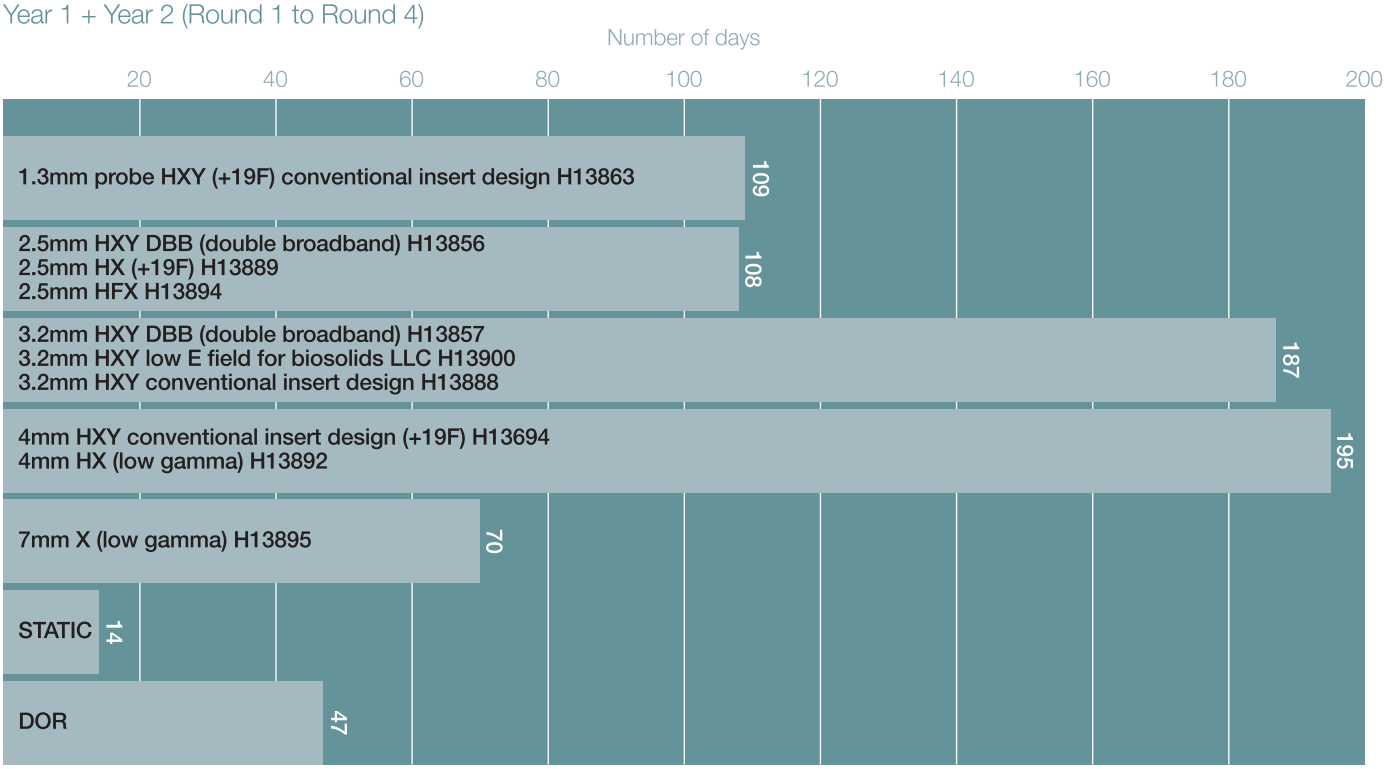

Nuclei tested in Double Resonance Mode

Probe in double Resonance mode	Mode	X-Nucleus																								
		^{31}P	^{87}Rb	^{11}B	^{71}Ga	^{65}Cu	^{23}Na	^{27}Al	^{13}C	^{79}Br	^{93}Nb	^{45}Sc	^{29}Si	^{2}H	^{6}Li	^{17}O	^{135}Ba	^{15}N	^{35}Cl	^{14}N	^{91}Zr	^{43}Ca	^{25}Mg	^{89}Y	^{39}K	^{87}Sr
1.3 mm probe HXY (+19F) conventional insert design	DR ^{1}H-X DR ^{19}F-X●				■	✸	✸	✸	■ ■	■	■	✸	✸	✸	✸	■	✸	■	✸	■						
2.5 mm HX (+19F) 2.5 mm HFX 2.5mm HXY DBB	DR ^{1}H-X DR ^{19}F-X●	■	■	✸	■	✸	✸	■ ■	■ ■	■	✸	■	✸	■	✸	■	✸	■	✸	■	✸	✸	■			
3.2 mm HXY low E field for biosolids LLC	DR ^{1}H-X		✸	✸	✸	✸	✸	✸	■	■	✸	✸	✸	✸	✸	✸	✸	■	✸	✸						
3.2 mm HXY conventional insert design 3.2mm HXY DBB	DR ^{1}H-X		■	■	■	✸	✸	■	■	■	✸	✸	✸	✸	✸	■	✸	■	■	■						
4 mm HXY conventional insert design (+19F)	DR ^{1}H-X DR ^{19}F-X●	■	✸	✸	✸	✸	■	■	■ ■	■	✸	✸	■	✸	✸	✸	✸	■ ■	✸	✸						
4 mm HX (low gamma)	DR ^{1}H-X								■	■	■	✸	✸	■	■	■	✸	■	✸	■	■	■	■	■	■	
7 mm X (low gamma)	X															✸	■	✸	■	■	✸	■	✸	■	■	■
Static	X	■	✸	✸	■	■	✸	✸	■	✸	■	✸	✸	■	✸	✸	✸	✸	■	■	✸	✸	✸	✸	■	✸
DOR	X			■	■	✸	✸	■	✸	✸	✸	✸	✸	✸	✸	■	✸	✸	✸	✸	✸	■	✸			

■ *Experiments performed at the facility to date*
✸ *Bench tests indicate should be possible*
● *Other ^{19}F-X DR combinations have not yet been investigated*
For triple-resonance capabilities, refer to the facility website

Time Allocation

440 days requested by 26 PIs from 15 different institutions (Aberdeen, Aston, Birmingham, Cambridge, Cardiff, Durham, Glasgow, Liverpool, Nottingham, Oxford, Queen Mary College London, Southampton, St. Andrews, University College London and Warwick). 306 days allocated by the Time Allocation Panel.

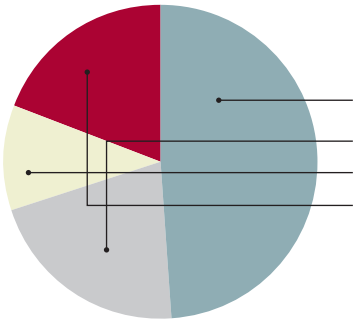

Requested time

Outside Warwick and non-NMC **49%**
NMC outside Warwick **21%**
Warwick NMC **11%**
Warwick non-NMC **19%**

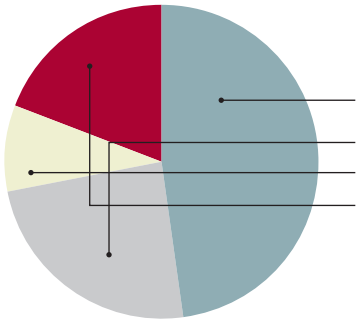

Allocated time

Outside Warwick and non-NMC **48%**
NMC outside Warwick **24%**
Warwick NMC **9%**
Warwick non-NMC **19%**

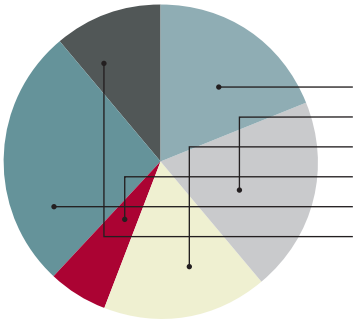

Requested time

Advanced materials **19%**
Bio materials **20%**
Energy materials **17%**
Methods development **6%**
Proteins **27%**
Pharmaceuticals and self assembly **11%**

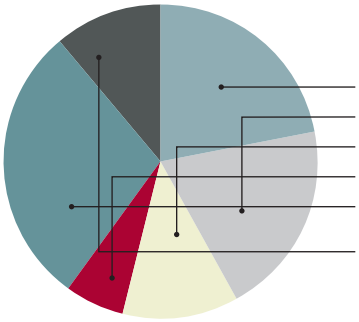

Allocated time

Advanced materials **22%**
Bio materials **20%**
Energy materials **12%**
Methods development **6%**
Proteins **29%**
Pharmaceuticals and self assembly **11%**

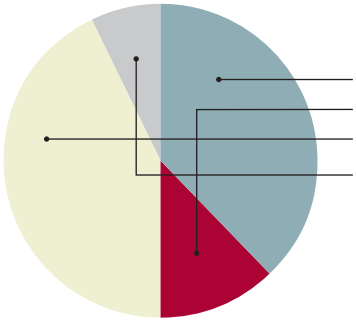

Requested time

EPSRC **38%**
BBSRC **12%**
Other agencies **43%**
No external funding **7%**

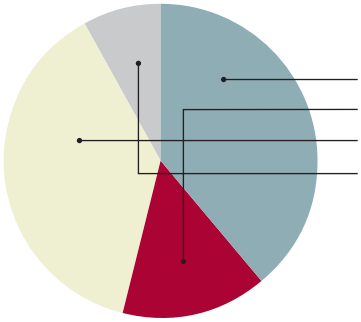

Allocated time

EPSRC **39%**
BBSRC **15%**
Other agencies **38%**
No external funding **8%**

Projects with more than one funding source were counted only once. Other agencies that are funding facility users are: MRC, STFC, Leverhulme Trust, Wellcome Trust, British Heart Foundation, Royal Society, Industry, EU, and Swedish & US funding agencies.

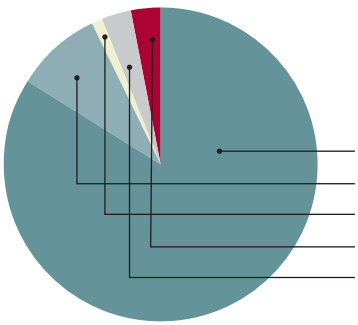

Spectrometer time
Feb 1 2011 – Jan 31 2012
(the facility operates 24 hours a day, 7 days a week)

TAP allocated days **84%**
Facility manager research **9%**
Maintenance **1%**
Fast track **3%**
Compensation **3%**

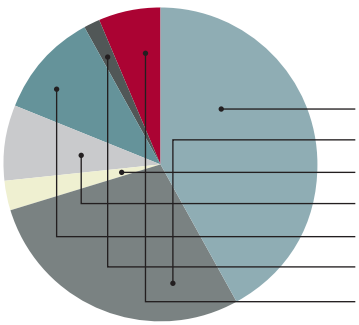

Facility users
Feb 1 2011 – Jan 31 2012

PIs + 1 UK academic **27**
EPSRC PhD students* **18**
BBSRC PhD students **2**
Other PhD students** **5**
PDRA*** **7**
Research staff **1**
Overseas collaborators **4**

* *Some students are partially funded by STFC and industry*
** *2 MRC funded, 1 Cambridge Commonwealth Trust and 2 self funded*
*** *2 EPSRC, 1 MRC, 1 Leverhulme Trust, 1 Wellcome Trust, 1 EU and 1 US funding agency*

Results from User Questionnaire Feb 2011 – Jan 2012

Feedback questionnaires are provided for each visit to the facility and contain a series of questions and the opportunity for visitors to make comments and suggestions. The responses are graded from 1 (least satisfied) to 5 (most satisfied). Figure 1 shows the average scores based on results from 31 responses from visits over the period February 2011 to January 2012.

Section 1 to be completed by the PI

Application for time

1 Ease of the application process
2 Transparency of the application process
3 Feedback on any unsuccessful time requests

Scheduling of time awarded

4 Scheduling of your time by the facility

Section 2 to be completed by the visitor

Accommodation

5 Ease of arranging accommodation
6 Quality of the accommodation
7 Location of the accommodation

At the 850 facility

8 Support from the Facility Manager upon arrival
9 Support from the Facility Manager throughout your visit
10 Quality of the NMR facilities
11 Quality of the office facilities
12 Quality of the sample preparation area and storage facilities
13 Ease of access to the facility out of hours
14 Your overall time at the facility

Post visit experience

15 Arrangements for accessing data
16 Arrangements for returning any samples
17 Reimbursement of any expenses

Average scores from feedback questionnaire over period Feb 2011 – Jan 2012

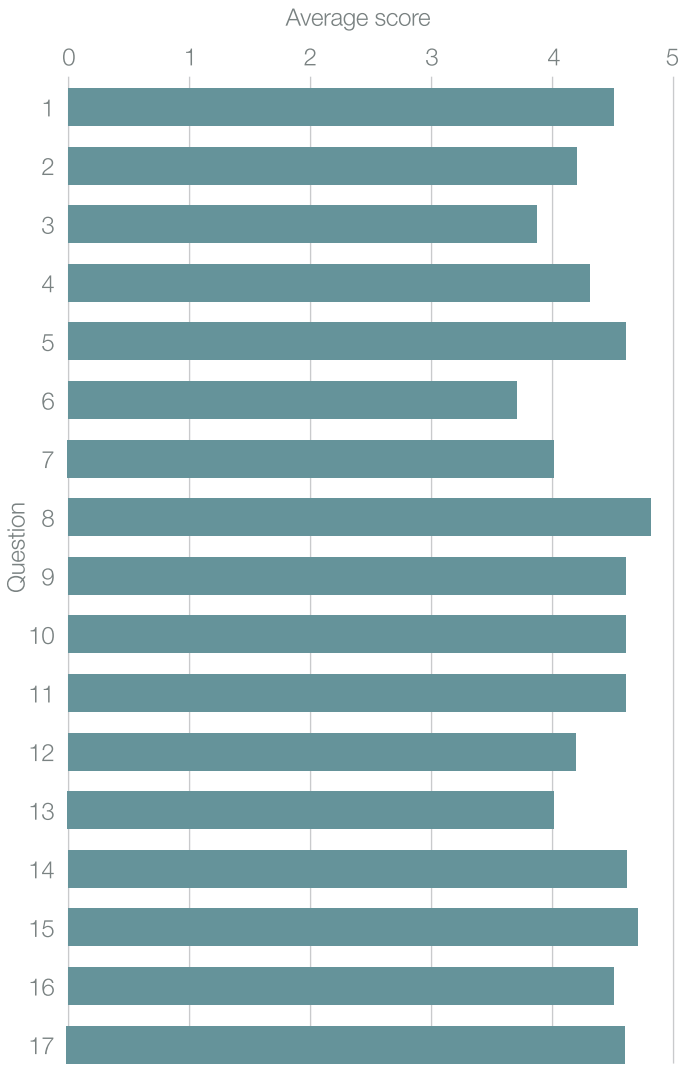

UK 850 MHz Solid-State NMR Facility
1st Annual Symposium

Monday 4 April 2011
Millburn House, University of Warwick
Symposium Organiser: **Stephen Wimperis** (Glasgow)

List of talks

1 ***'High-resolution solid-state NMR of inner-Earth minerals'***
John Griffin *(St Andrews)*

2 ***'Using solution and solid-state NMR to study complexes of F-actin'***
Mark Pfuhl *(Kings College)*

3 ***'Measurements of proton-oxygen-17 distances in solids'***
David Bennett *(Nottingham)*

4 ***'Exploring hydrogen bonding in amyloid fibrils of Alzheimer's Aβ fragment $A\beta_{(16\text{-}22)}$ using $^{15}N(^{17}O)$ REAPDOR NMR'***
Oleg Antzukin *(Warwick)*

5 ***'Structural modulation of amyloid fibrils and intermediates by glycosaminoglycans'***
David Middleton *(Liverpool)*

6 ***'^{14}N-^{1}H correlation spectra at 850 MHz'***
Andrew Tatton *(Warwick)*

7 ***'Double resonance NMR study in ionomer glasses and low-gamma nuclei NMR for the cation substitutions in fluorapatite'***
Natalia Karpukhina *(Queen Mary)*

8 ***'Structural analysis of lantibiotic/lipid II complexes in lipid membranes'***
Filip Ciesielski *(Nottingham)*

9 ***'Solid-state NMR observation of quadrupolar nuclei at high field including ^{43}Ca and ^{87}Sr'***
Mark Smith *(Warwick)*

10 ***'^{17}O NMR of biominerals gives new insight into mineral formation and the process of crystal organisation'***
Melinda Duer *(Cambridge)*

11 ***'Acidic residues of β2m fibrils essential for binding the fibril stabiliser Serum Amyloid P component'***
Garrick Taylor *(Southampton)*

12 ***'Natural abundance high-resolution ^{2}H NMR of organic solids'***
Abil Aliev *(UCL)*

13 ***'In-situ solid-state NMR studies of crystallization processes'***
Kenneth Harris *(Cardiff)*

Publications

'Natural-Abundance Solid-State ^{2}H NMR Spectroscopy at High Magnetic Field'

A. E. Aliev, S. E. Mann, D. Iuga, C. E. Hughes, and K. D. M. Harris

Journal of Physical Chemistry A, 115, 5568 – 5578, (2011)

'High-Resolution Solid-State ^{2}H NMR Spectroscopy of Polymorphs of Glycine'

A. E. Aliev, S. E. Mann, A. S. Rahman, P. F. McMillan, F. Corà, D. Iuga, C. E. Hughes, and K. D. M. Harris

Journal of Physical Chemistry A, 115, 12201 – 12211, (2011)

'Defects in Doped $LaGaO_3$ Anionic Conductors: Linking NMR Spectral Features, Local Environments and Defect Thermodynamics"

F. Blanc, D. S. Middlemiss, Z. Gan, and C. P. Grey

Journal of the American Chemical Society, 133, 17662 – 17672, (2011)

'Probing Intermolecular Crystal Packing in γ-Indomethacin by High-Resolution ^{1}H Solid-State NMR Spectroscopy'

J. P. Bradley, S. P. Velaga, O. N. Antzutkin, and S. P. Brown

Crystal Growth & Design, 11, 3463 – 3471, (2011)

'Observation of 'hidden' magnesium: First-principles calculations and ^{25}Mg solid-state NMR of enstatite'

J. M. Griffin, A. J. Berry, and S. E. Ashbrook

Solid State Nuclear Magnetic Resonance, 40, 91 – 99, (2011)

'Boron environments in Pyrex® glass – a high resolution, Double-Rotation NMR and thermodynamic modelling study'

A. P. Howes, N. M. Vedishcheva, A. Samoson, J. V. Hanna, M. E. Smith, D. Holland, and R. Dupree

Physical Chemistry Chemical Physics, 13, 11919 – 11928, (2011)

'Double-quantum homonuclear correlations of spin I = 5/2 nuclei'

D. Iuga

Journal of Magnetic Resonance, 208, 225 – 234, (2011)

'^{93}Nb NMR and DFT investigation of the polymorphs of $NaNbO_3$'

K. E. Johnston, J. M. Griffin, R. I. Walton, D. M. Dawson, P. Lightfoot, and S. E. Ashbrook

Physical Chemistry Chemical Physics, 13, 7565 – 7576, (2011)

'Insights into new calcium phosphosilicate xerogels using an advanced characterization methodology'

A. Li, D. Wang, J. Xiang, R. J. Newport, M. X. Reinholdt, P. H. Mutin, D. Vantelon, C. Bonhomme, M. E. Smith, D. Laurencin, and D. Qiu

Journal of Non Crystalline Solids, 357, 3548 – 3555, (2011)

'Synthesis and Characterization of Crystalline Structures Based on Phenylboronate Ligands Bound to Alkaline Earth Cations'

M. Reinholdt, J. Croissant, L. Di Carlo, D. Granier, P. Gaveau, S. Bégu, J.M. Devoisselle, P. H. Mutin, M. E. Smith, C. Bonhomme, C. Gervais, A. van der Lee, and D. Laurencin

Inorganic Chemistry, 50, 7802 – 7810, (2011)

'Identifying Guanosine Self Assembly at Natural Isotopic Abundance by High-Resolution ^{1}H and ^{13}C Solid-State NMR Spectroscopy'

A. L. Webber, S. Masiero, S. Pieraccini, J. C. Burley, A. S. Tatton, D. Iuga, T. N. Pham, G. P. Spada, and S. P. Brown

Journal of the American Chemical Society, 133. 19777 – 19795, (2011)

In addition, there were 32 talks and 22 posters at conferences and seminars in 2011, where results obtained at the UK 850 MHz solid-state NMR facility were presented.

PhD Theses

Student	Department	University	Supervisor	Title	Date
Garrick Foster Taylor	Centre for Biological Sciences	Southampton	Philip Williamson	*'The interaction between fibrillar beta-2 micro globulin and serum amyloid-P component'*	Dec 2011
Martin Mee	Physics	Warwick	Diane Holland	*'Cation substitution of beta-tricalcium phosphate'*	Sep 2011
Jonathan Bradley	Physics	Warwick	Steven Brown	*'Development and Application of High-Resolution Solid-State NMR Methods for Probing Polymorphism of Active Pharmaceutical Ingredients'*	Jun 2011
Lucienne Buannic	Chemistry	State University of New York at Stony Brook	Clare Grey	*'Solid state NMR study of protonic conductors for applications as electrolyte materials in Solid Oxide Fuel Cells'*	Jun 2011
Daniel Lee	School of Chemistry	Nottingham	Jeremy Titman	*'Development of Two-dimensional Correlation Spectroscopy in Solid-state NMR: Applications to Nano-composites and Fullerides'*	Jun 2011
Teresa Kurkiewicz	School of Chemistry	Glasgow	Stephen Wimperis	*'New NMR methods for studying dynamics in solids'*	Mar 2011
Karen Johnston	School of Chemistry	St Andrews	Sharon Ashbrook Philip Lightfoot	*'A Complementary Study of Perovskites: Combining Diffraction, Solid-State NMR and First-Principles DFT Calculations'*	Aug 2010

The UK 850 MHz Solid-State NMR Facility PhD Travel Fund

Supported by Bruker

The UK 850 MHz Solid-State NMR Facility PhD travel fund supported by Bruker provides funding for: (a) attendance at an internationally recognised, high-profile conference where a PhD student presents results he/she obtained at the 850 MHz Facility, or (b) a "start-up" visit to another lab to learn new methods to be implemented at the 850 MHz Facility. For further details see: **http://go.warwick.ac.uk/850mhz/travel_fund/**

2011 Awards

- **Andrew P. Williams** (Cardiff University) awarded £400 to attend the Annual Conference of the British Association for Crystal Growth (BACG), London (July 2011) and present a poster entitled *In-Situ NMR Studies of Crystallization using combined Solution- and Solid-State NMR*.
- **Oliver Alderman** (University of Warwick) awarded £700 to attend the 7th International Conference on Borate Glasses, Crystals, and Melts, Canada, (August 2011) and present a talk entitled *B-11 double rotation spin diffusion NMR as a probe of local and intermediate structure in borate crystals and glasses*.
- **David Bennett** (University of Nottingham) awarded £800 to attend the 7th Alpine Conference on Solid-State NMR (September 2011) and present a poster entitled *Measurements of Proton-Oxygen-17 Distances in Solids*.
- **Erika Davies** (University of Cambridge) awarded £850 to attend the 7th Alpine Conference on Solid-State NMR (September 2011) and present a poster entitled *Probing the Surface Structure of Bone Mineral by ^{17}O NMR studies at 850 MHz*.
- **Valerie Seymour** (University of St. Andrews) awarded £900 to attend the 7th Alpine Conference on Solid-State NMR (September 2011) and present a poster entitled *Solid-State NMR Investigation into Local Structure and Order in the Aluminophosphate STA-2*.
- **Andrew Tatton** (University of Warwick) awarded £800 to attend the 7th Alpine Conference on Solid-State NMR (September 2011) and present a poster entitled *^{14}N-^{1}H Correlation Spectra at 850 MHz*.

User Reports

Structure and Dynamics of Molecular Solids from Solid-State ^{2}H NMR Spectroscopy

Abil E. Aliev,[1] Sam E. Mann,[1] Aisha S. Rahman,[1] Paul F. McMillan,[1] Furio Corà,[1] Dinu Iuga,[2] Colan E. Hughes[3] and Kenneth D.M. Harris[3]

[1]*Department of Chemistry, University College London,*
[2]*Department of Physics, University of Warwick,* [3]*School of Chemistry, Cardiff University*

Overview

^{1}H and ^{2}H NMR measurements have the potential to yield significant insights concerning differences in the structural and dynamic properties of polymorphs in the solid state. However, the routine measurement of well-resolved ^{1}H NMR spectra for solids is complicated significantly by strong homonuclear ^{1}H···^{1}H interactions. As ^{1}H and ^{2}H NMR chemical shifts are essentially the same, ^{1}H chemical shifts can be determined straightforwardly *via* high-resolution solid-state ^{2}H NMR measurements.[1-4] An additional advantage of high-resolution solid-state ^{2}H NMR is that ^{2}H quadrupole interaction parameters (i.e., the quadrupole coupling constant χ and asymmetry parameter η) can be estimated from the same spectra used for chemical shift measurements. ^{2}H quadrupole coupling constants for organic materials are typically of the order of ~200 kHz, which is of a similar order of magnitude to the frequencies of various reorientational motions that can occur in organic solids in an appropriate temperature regime. Thus, the ^{2}H quadrupole interaction is sensitive to motional averaging effects due to dynamic processes of this type, and measurements of ^{2}H quadrupole interaction parameters can yield detailed information on solid-state dynamics.

We have explored the opportunities provided by high-resolution solid-state ^{2}H NMR, employing both experimental and computational techniques in studies of the α and γ polymorphs of fully deuterated glycine (glycine-d_5).[5] One of the primary objectives of this study was to prepare grounds for future high-resolution solid-state ^{2}H NMR measurements on materials with natural isotopic abundances. In spite of the low natural abundance of the ^{2}H isotope, the increasing availability of high-field NMR instruments creates the prospect of carrying out natural-abundance solid-state ^{2}H NMR measurements on a routine basis, particularly for full characterization of structural and dynamics aspects of polymorphism in organic solids (including pharmaceutical materials) as well as for fundamental studies of intermolecular and intramolecular interactions in the solid state.

Spinning Sideband Analysis of ^{2}H MAS NMR Spectra

We have shown that numerical analysis of spinning sideband patterns (Figure 1) yields values of ^{2}H quadrupole interaction parameters that are in good agreement with the corresponding parameters determined from single-crystal ^{2}H NMR measurements. In particular, the maximum deviation in ^{2}H quadrupole coupling constants determined from these two approaches is only 1% for the α and γ polymorphs of glycine-d_5. These findings suggest that, in principle, the resolution provided by ^{2}H MAS NMR may be sufficient for accurate determination of ^{2}H quadrupole interaction parameters without the need to grow suitable single crystals for single-crystal ^{2}H NMR studies, and without the requirement to have suitable equipment for carrying out single-crystal NMR measurements.

Sensitivity of ^{2}H MAS NMR Spectra to Reorientational Motions

As demonstrated recently,[4] solid-state ^{2}H MAS NMR spectra are sensitive to dynamic processes, and may therefore be exploited to provide insights on molecular motions in solids. The dynamics of the $-N^+D_3$ group in the α and γ polymorphs of glycine-d_5 allows an assessment of the effect of the rate of molecular motion on the measured spectra. From an analysis of simulated ^{2}H MAS NMR sideband patterns as a function of reorientational jump frequency (κ) for the $-N^+D_3$ group, observed differences in the experimental ^{2}H MAS NMR spectra for the α and γ polymorphs can be attributed directly to differences in the rate of reorientation of the $-N^+D_3$ group. The measured line widths and relative intensities of spinning sideband manifolds suggest that the rate of reorientation of the $-N^+D_3$ group is much faster for the α polymorph than the γ polymorph, in agreement with results from previous studies[6] and the suggestion that the $-N^+H_3$ group is engaged in stronger hydrogen bonding in the γ polymorph. Spectral simulations show significant broadening of the ^{2}H MAS NMR signal in the intermediate motion regime, suggesting that deuterons undergoing reorientation at rates in the range $\kappa \approx 10^4 - 10^6$ s^{-1} are likely to be undetectable in ^{2}H MAS NMR spectra for materials with natural isotopic abundances. Isotropic line widths in simulated ^{2}H MAS NMR spectra exhibit a significant dependence on the reorientational jump frequency across the range $\kappa \approx 10^2 - 10^9$ s^{-1}, which is significantly wider than the range of motional frequencies ($\kappa \approx 10^4 - 10^8$ s^{-1}) that are accessible *via* analysis of wideline ^{2}H NMR quadrupole echo lineshapes.[5]

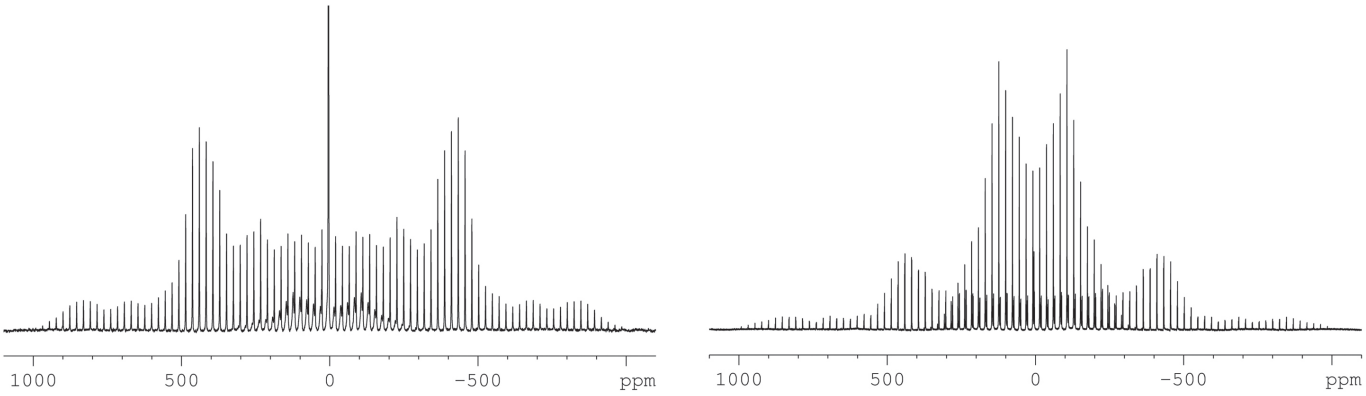

Figure 1. ^{2}H MAS NMR spectra of the α (bottom) and γ (top) polymorphs of glycine-d_5 (130.51 MHz; MAS frequency, 3 kHz; 298 K).

^{1}H and ^{2}H NMR Parameters from ^{2}H MAS NMR Spectra and First-Principles Calculations

The ^{1}H NMR chemical shifts for the α and γ polymorphs of glycine were determined from the ^{2}H MAS NMR spectra, taking into account the known second-order shift. We have investigated the opportunity to exploit quantum-mechanical (QM) calculations of ^{2}H quadrupole interaction parameters and ^{1}H chemical shifts in order to reveal the structural dependence of these parameters. Our results suggest that the existence of two short intermolecular C–H···O contacts for one of the H atoms of the $>CH_2$ group in the α polymorph of glycine has a significant influence on the ^{2}H quadrupole coupling and ^{1}H chemical shift for this site.

The advantages provided by QM natural bond orbital analysis for identifying relatively strong intermolecular interactions in the solid state have also been explored. In particular, we have found that for one H atom in the $>CH_2$ group of the α polymorph, three intermolecular $n_O \rightarrow \sigma^*$(C–H) delocalizations from lone pairs on oxygen atoms of neighbouring molecules are associated with stabilization energies greater than 0.5 kcal mol^{-1}, while in contrast, the intermolecular delocalization is significantly weaker for the other H site in the α polymorph and for both H atoms in the $>CH_2$ group of the γ polymorph.

References

1. Maricq, M.; Waugh, J. S. *Chem. Phys. Lett.* **1977**, *47*, 327.
2. Aliev, A. E.; Harris, K. D. M.; Apperley, D. C. *Chem. Phys. Lett.* **1994**, *226*, 193.
3. Mizuno, T.; Nemoto, T.; Tansho, M.; Shimizu, T.; Ishii, H.; Takegoshi, K. *J. Am. Chem. Soc.* **2006**, *128*, 9683.
4. Aliev, A. E.; Mann, S. E.; Iuga, D.; Hughes, C. E.; Harris, K. D. M. *J. Phys. Chem. A* **2011**, *115*, 5568.
5. Aliev, A. E.; Mann, S. E.; Rahman, A. S.; McMillan, P. F.; Corà, F.; Iuga, D.; Hughes, C. E.; Harris, K. D. M. *J. Phys. Chem. A* **2011**, *115*, 12201.
6. Gu, Z.; Ebisawa, K.; McDermott, A. *Solid State Nucl. Magn. Reson.* **1996**, *7*, 161.

Exploring Secondary Structures in Polymorphic Alzheimer's $A\beta_{(11-25)}$ Fibrils Using $^{15}N\{^{17}O\}$ REAPDOR NMR

Oleg N. Antzutkin,[1,2] Andrei V. Filippov,[2] Dinu Iuga,[1] Steven P. Brown,[1] and Ray Dupree[1]

[1]*Department of Physics, University of Warwick,*
[2]*Chemistry of Interfaces, Luleå University of Technology, Luleå, Sweden*

Overview

Recently Härd and co-workers have identified β-sheet-rich oligomers of cysteine-cysteine (CC) cross-linked model Alzheimer's $A\beta_{(1-42)}$CC peptide which are 100-fold more likely to cause apoptotic cell death of nerve cell cultures *in vitro* than amyloid fibrils.[1] Therefore, oligomers of amyloidogenic peptides may be the key toxic species for brain neurons, causing a variety of neurodegenerative diseases. It has also been suggested that toxic oligomers are rich in different types of β-sheet or/and β-hairpin structures, having different inter- or/and intramolecular hydrogen bonding patterns.[2] Their structure could be a target for development of inhibitors or monoclonal antibodies for future treatment of amyloid-related neurodegenerative diseases. Using a variety of ^{13}C and ^{15}N solid-state NMR methods extended sets of structural constraints can be obtained and molecular level models for toxic oligomers can be developed, as has been already successfully achieved for amyloid fibrils.[3,4] However, our preliminary studies have indicated that NMR spectral resolution for some of key molecular fragments of oligomers of U-^{13}C,^{15}N-$A\beta_{(1-42)}$CC is not sufficient for an unambiguous assignment of ^{13}C,^{15}N resonances and for the extraction of structural constraints needed for modelling of the structure of oligomers. In particular, $^{13}C\ldots{}^{13}C$ distances in the range 5-6 Å and $^{15}N\ldots{}^{13}C$ distances in the range 4-5 Å are not necessarily direct evidence of the presence of intramolecular hydrogen bonds in β-hairpin structures. A more direct approach to determining hydrogen bonding contacts would be to measure the ^{15}N-^{17}O dipolar coupling, since a value of *ca.* 75 Hz corresponds to a $^{15}N\ldots{}^{17}O$ internuclear distance of *ca.* 2.8 Å which indicates a N-H … O=C hydrogen bond. Recently $^{15}N\{^{17}O\}$ REAPDOR NMR has been successfully employed to measure ^{15}N-^{17}O dipolar couplings in hydrogen-bonded model compounds, namely the selectively labelled amino acid glycine and nucleic acid uracil.[5] Aiming at future studies on toxic oligomers of full-length Aβ peptides, in this work we validate further this novel approach for two polymorphs of amyloid fibrils of the Alzheimer's Aβ peptide.

$^{15}N\{^{17}O\}$ REAPDOR NMR probes hydrogen bonding in $A\beta_{(11-25)}$ fibrils

We have validated the utility of $^{15}N\{^{17}O\}$ (^{1}H-decoupled, ^{15}N-detected, ^{17}O-adiabatic pulse) REAPDOR on fibrils of amyloid-β peptide $A\beta_{(11-25)}$, Asp-Val-His-His-Gln-Lys-Leu-Val_{18}(^{17}O)-Phe-Phe-Ala_{21}(U-^{13}C,^{15}N)-Glu-Asp-Val-Glu, which includes the "key" amyloidogenic central fragment of the full-length Alzheimer's β-amyloid peptides. As previously suggested by Petkova *et al.*, depending on pH of the incubated solution this peptide adopts either 17 + k ⇔ 22 – k (at pH 2.4) or 17 + k ⇔ 20 – k (at pH 7.4) registry antiparallel β-sheet structures with intermolecular hydrogen bonds (see Figure 1).[6] However, the model for $A\beta_{(11-25)}$ fibrils formed at pH 2.4 (Figure 1a) is less certain; it has been developed using only a small number of structural constraints and some $^{13}C\{^{15}N\}$ REDOR data (for example, the intermolecular distances between Leu17/Ala21 ^{15}N-^{13}C pairs) did not fit well to simulations corresponding to ^{13}C … ^{15}N distances in the suggested idealized models.[6] Thus, by selective ^{17}O and ^{15}N labeling of $A\beta_{(11-25)}$ we aim to detect the specific hydrogen bonding between Val18 and Ala21 suggested by the putative model for $A\beta_{(11-25)}$ (pH 2.4) fibrils (Figure 1a). Note that no 2.8 Å $^{15}N\ldots{}^{17}O$ contacts between these amino acid residues are expected in $A\beta_{(11-25)}$ (pH 7.4) fibrils, which adopt an almost in-registry antiparallel β-sheet structure (Figure 1b).[6] Therefore, these real biological systems are ideal for validating the $^{15}N\{^{17}O\}$ REAPDOR NMR methodology in cases for which $^{13}C\{^{15}N\}$ REDOR provided ambiguous structural constraints.

Figure 2 compares ^{15}N spectra recorded using the $^{15}N\{^{17}O\}$ REAPDOR experiment with 7 ms of dephasing (red lines) and without the ^{17}O adiabatic pulse (blue lines). For the $A\beta_{(11-25)}$ (pH 2.4) sample (a) a narrow resonance is observed at *ca* 127 ppm due to amyloid fibrils together with a broad peak at 120 ppm due to amorphous aggregates. For the narrow resonance, a dephasing of 8% observed. For this sample REAPDOR dephasing at different times was successfully simulated using ^{15}N-^{17}O dipolar coupling of 75 Hz and 13% of ^{17}O enrichment (Figure 2c). No dephasing was observed for $A\beta_{(11-25)}$ (pH 7.4) fibrils (see Figures 2b and 2c), thus proving the utility of this method for direct probing of hydrogen bonds fibrils. It should be possible to achieve higher degrees of ^{17}O enrichment starting with 90%-^{17}O labelled $H_2{}^{17}O$ in order to increase the amplitude of REAPDOR dephasing. Using these high levels of ^{17}O enrichment, $^{15}N\{^{17}O\}$ REAPDOR could be applied to study hydrogen bonding in "key" fragments of toxic oligomers of the full length $A\beta_{(1-40)}$ & $A\beta_{(1-42)}$ and their mutations and work along these lines is currently in progress.

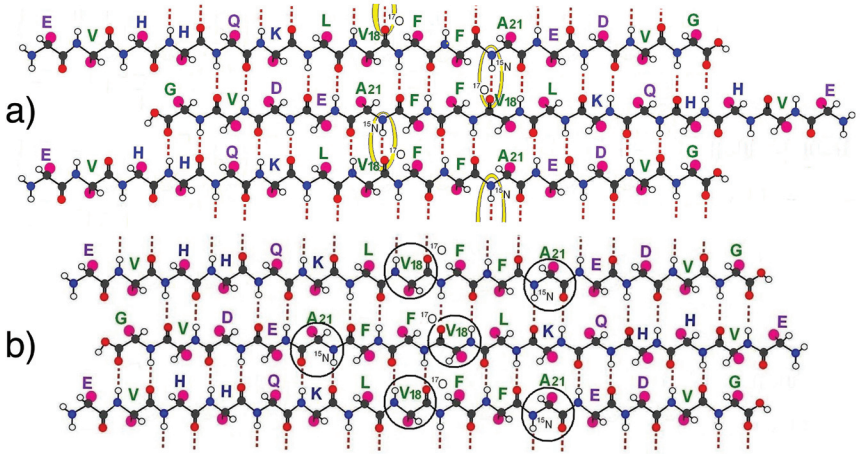

Figure 1. Schematic representation of hydrogen bonding in putative models of amyloid fibrils of $A\beta_{(11-25)}$ incubated in an aqueous solution at pH 2.4 for 80 days with seeding, 17 + k ⇔ 22 – k registry (a) and at pH 7.4 for 20 days without seeding, 17 + k ⇔ 20 – k registry (b).[6] Selectively isotopically labelled fragments involved in C=^{17}O…H-^{15}N hydrogen bonds are highlighted by yellow ellipsoids in (a) and are absent in (b) (black circles).

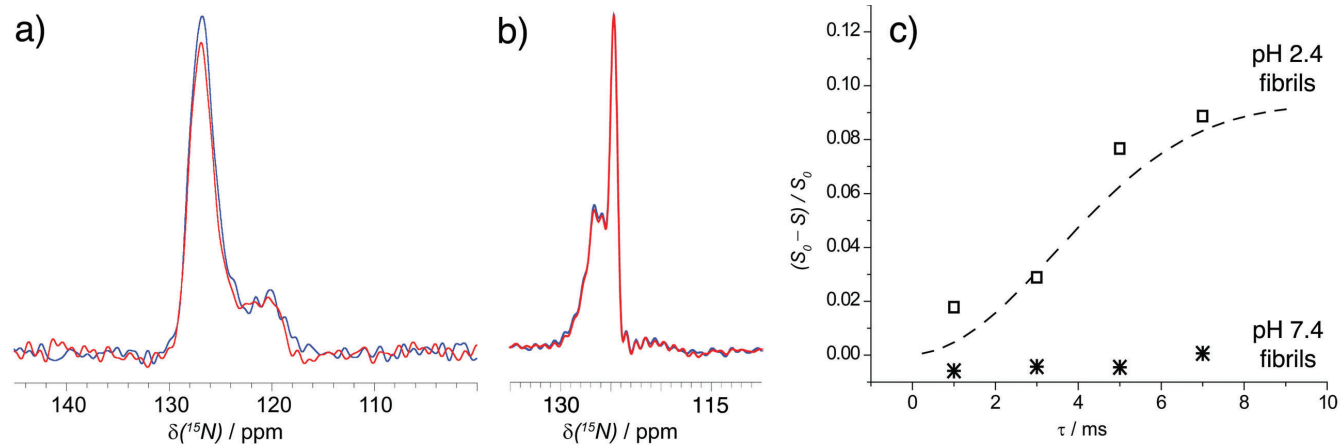

Figure 2. ^{15}N{^{17}O} REAPDOR NMR (850 MHz, 8 kHz MAS) spectra of ca. 10 mg amyloid fibrils formed by a selectively Val18-^{17}O (enrichment 15 ± 5 %) and Ala21-U-^{15}N,^{13}C (enrichment 98-99%) labelled fragment of Alzheimer's peptide Aβ(11-25) incubated in an aqueous solution at pH 2.4 for 80 days with seeding (a) and at pH 7.4 for 20 days without seeding (b). Spectra correspond to the experiment with adiabatic 0.48 τ_r ^{17}O pulse and mixing time 7 ms (S, red lines) and without the ^{17}O pulse (S_0, blue lines). (c) REAPDOR dephasing ($(S_0-S)/S_0$) at different mixing times is shown for pH 2.4 fibrils (□) together with SIMPSON simulations with ^{15}N-^{17}O dipolar coupling of 75 Hz and 13% of ^{17}O enrichment. No REAPDOR dephasing was observed for pH 7.4 fibrils (∗).

References

1. Sandberg, A.; Luheshi, L. M.; Söllvander, S.; Pereira de Barros, T.; Macao, B.; Knowles, T. P. J.; Biverstål, H.; Lendel, C.; Ekholm-Petterson, F.; Dubnovitsky, A.; Lannfelt, L.; Dobson, C. M.; Härd, T. *Proc. Natl. Acad. Sc. U.S.A.* **2010**, *107*, 15595.
2. Ahmed, M.; Davis, J.; Aucoin, D.; Sato, T.; Ahuja, S.; Aimoto, S.; Elliot, J. I.; Van Nostrand, W. E.; Smith, S. O. *Nat. Str. Mol. Biol.* **2010**, *17*, 561.
3. Petkova, A. T.; Ishii, Y.; Balbach, J. J.; Antzutkin, O. N.; Leapman, R. D.; Delagio, F.; Tycko, R. *Proc. Natl. Acad. Sc. USA* **2002**, *99*, 16742.
4. Wasmer, C.; Lange, A.; Van Melckebeke, H.; Siemer, A. B.; Riek, R.; Meier, B. H. *Science* **2008**, *319*, 1523.
5. Hung, I.; Uldry A.-C.; Becker-Baldus, J.; Webber, A. L.; Wong, A.; Smith, M. E.; Joyce, S. A.; Yates, J. R.; Pickard, C. J.; Dupree, R.; Brown, S. P. *J. Am. Chem. Soc.* **2009**, *131*, 1820.
6. Petkova, A. T.; Buntkowsky, G.; Dyda, F.; Leapman, R. D.; Yau, W.-M.; Tycko, R. *J. Mol. Biol.* **2004**, *335*, 247.

High-Field ^{45}Sc Solid-State NMR for the Study of Scandium-containing Framework Materials

Valerie R. Seymour, Daniel M. Dawson, John M. Griffin and Sharon E. Ashbrook

School of Chemistry and EaStCHEM, University of St Andrews

Overview

The trivalent terephthalate metal organic frameworks (MOFs) MIL-53, MIL-68, MIL-88 and MIL-101 are some of the most important types of microporous materials in terms of their porosity, flexibility and thermal stability.[1] This combination of properties has led to the investigation of their performance in hydrogen storage, adsorption and separation, catalysis and drug delivery. However, their physical properties and adsorption behaviour can be strongly dependent on the metal cation, and Al^{3+}, V^{3+}, Cr^{3+}, Fe^{3+} Ga^{3+} and In^{3+} variants have been reported in considerable detail. We have extended this exploration to scandium analogues of these and similar materials, and also demonstrated the formation of a new material, Sc_2BDC_3 (BDC = benzene-1,4-dicarboxylate), which has promising properties for the adsorption of small molecules.[2] Alongside conventional diffraction approaches, solid-state NMR provides valuable information about the local structure and disorder in these materials, and the incorporation of solvent or water molecules into the pores. ^{45}Sc MAS NMR has been shown to be a sensitive probe of the local environment of scandium in framework structures.

As ^{45}Sc is a quadrupolar nucleus (I = 7/2), and there is an inverse dependence of the second-order quadrupolar interaction upon magnetic field strength, sensitivity can be significantly enhanced by the use of high-field spectrometers. Furthermore, the increase in resolution provided by high-field MQMAS experiments may allow similar but crystallographically-distinct Sc species to be resolved. High-field NMR enables lineshapes with larger quadrupolar couplings to be acquired accurately, and provides additional information on the distributions of quadrupolar and shielding parameters that are present.

^{45}Sc Multiple-Quantum MAS NMR of Scandium Framework Materials

^{45}Sc MAS and MQMAS NMR spectra were obtained for a range of scandium framework materials including Sc-MIL-100, Sc-MIL-88, Sc-MIL-53 (dehydrated), Sc-MIL-53 (hydrated) and Sc-ABTC. For Sc_2BDC_3, which exhibits a narrow lineshape, only MAS spectra were obtained. For the two Sc-MIL-53 samples, dried and hydrated, two distinct lineshapes were resolved in the MQMAS NMR spectra, as shown in Figure 1.

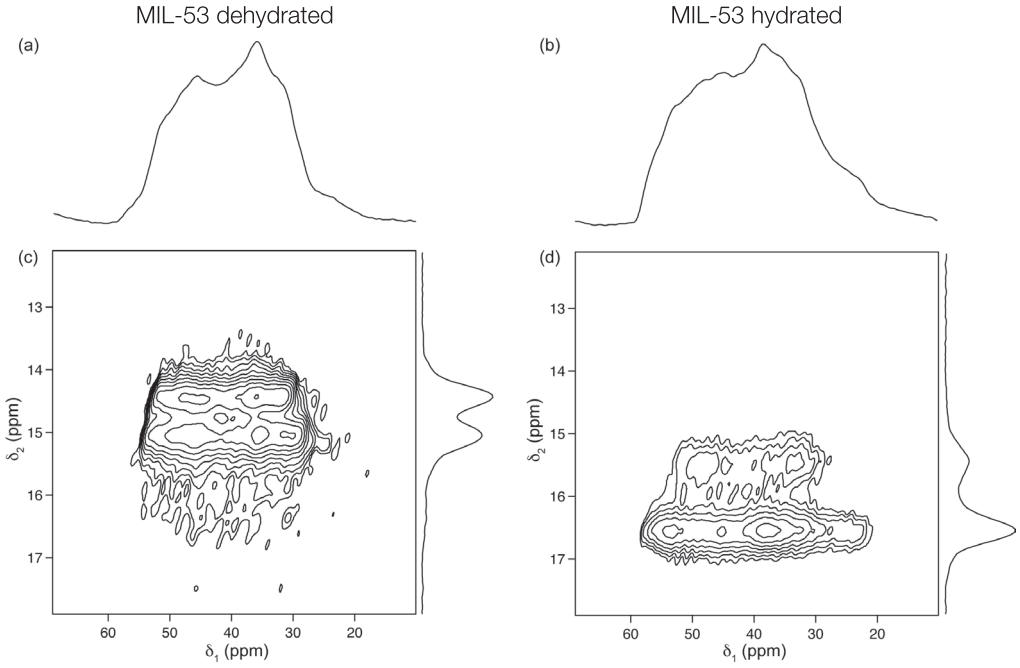

Figure 1. 20.0 T (a) ^{45}Sc MAS NMR spectra and (b) ^{45}Sc MQMAS NMR spectra of MIL-53 dried and rehydrated. Spectra were recorded using a split-t_1 shifted-echo experiment, with an MAS rate of 30 kHz.

The structural changes of MIL-53 on dehydration or hydration can be followed using ^{45}Sc NMR, with changes in both chemical shift and quadrupolar broadening. For dehydrated Sc-MIL-53, the two ^{45}Sc resonances are clearly resolved, with isotropic chemical shifts of 55.1 and 56.9 ppm, and quadrupolar products P_Q (= $C_Q(1 + \eta_Q^2/3)^{1/2}$) of 14.7 and 15.6 MHz, respectively. For rehydrated Sc-MIL-53, the two resonances have an intensity ratio of 1 : 3, consistent with the presence of four ^{45}Sc species, three of which are coincident in δ_1, as expected when the symmetry is lowered. It is difficult to extract accurate NMR parameters from this spectrum due to the overlap of the resonances but, generally, the Sc species have higher C_Q values and higher isotropic chemical shifts than observed for the dehydrated material.

To help interpret the MAS spectra, NMR parameters were calculated using the periodic planewave DFT code CASTEP.[3] The structures obtained from diffraction were geometry optimised (minimising the forces upon the atoms) with the atomic coordinates varied and the unit cell size and shape retained. For the dehydrated material there is good agreement between experimental and calculated NMR parameters, with C_Q values for the two ^{45}Sc species of 15.2 (Sc1) and 14.1 MHz (Sc2), although the difference in isotropic chemical shift between the two is slightly overestimated (~ 4 ppm cf 1 ppm). The agreement is sufficient to enable the two ^{45}Sc resonances in the experimental spectrum to be assigned as Sc2 (δ_1 = 14.6 ppm) and Sc1 (δ_1 = 15.2 ppm). For the dehydrated material, the calculated parameters are in broad agreement with those determined experimentally, with C_Q values between 16.5 and 17.3 MHz (and P_Q values between 16.8 and 17.6 MHz), and generally higher isotropic chemical shifts. The agreement between calculation and experiment for this rehydrated material is perhaps not expected to be as good as that observed for dehydrated MIL-53(Sc), owing to the presence of water molecules within the pores and, consequently, possible disorder and dynamics. For the ^{13}C NMR spectra (not shown), good agreement is also obtained between experiment and calculation for the resonances in the carboxylate region (those in the aromatic region are too overlapped for detailed analysis). For dehydrated MIL-53(Sc) four carboxyl species are expected, but the calculation shows these are present in two resonances (each containing two species), separated by ~5.3 ppm. In the rehydrated material eight resonances are predicted within ~4 ppm, again in good agreement with the experimental spectrum. This part of the work has now been published as part of a more extensive structural investigation of MIL-53.[4]

References

1. Llewellyn, P. L.; Bourrelly, S.; Serre, C.; Vimont, A.; Daturi, M.; Hamon, L.; De Weireld, G.; Chang, J. S.; Hong, D. Y.; Hwang, Y. K.; Jhung, S. H.; Ferey, G. *Langmuir* **2008**, *24*, 7245.
2. Mowat, J. P. S.; Miller, S. R.; Slawin, A. M. Z.; Seymour, V. R.; Ashbrook, S. E.; Wright, P. A. *Micro. Meso. Mater.* **2011**, 142, 322.
3. Segall, M. D.; Lindan, P. J. D.; Probert, M. J.; Pickard, C. J.; Hasnip, P. J.; Clark, S. J.; Payne, M. C. *J. Phys. Condens. Matter* **2002**, *14*, 2717.
4. Mowat, J. P. S.; Seymour, V. R.; Griffin, J. M.; Thompson, S. P.; Slawin, A. M. Z.; Fairen-Jimenez, D.; Düren, T.; Ashbrook, S. E.; Wright, P. A. *Dalton Trans.* **2012**, Advance article.

Structural Analysis of Mersacidin-Lipid II Complexes

Judicaël Parisot,[1] Dinu Iuga,[2] David C. Griffin,[1] Eefjan Breukink,[3] Hans-Georg Sahl,[4] Gabrielle Bierbaum[4] and Boyan B. Bonev[1]

[1]*School of Biomedical Sciences, University of Nottingham,*
[2]*Department of Physics, University of Warwick,*
[3]*Biochemistry, Utrecht University, The Netherlands,*
[4]*Microbiologie, Universität Bonn, Germany*

Overview

Bacterial resistance to all classes of antibiotics, currently in use, has been reported. Lanthionine antibiotics are one class of target-specific antimicrobial peptides with high activity against Gram-positive pathogens and low cytotoxicity. This stems from their unique mode of action, which relies on recognition of lipid II, the mature bacterial cell wall intermediate.[1-3] Mersacidin/lipid II complex-formation inhibits transglycosylation and involves a unique recognition site, most likely residing on the disaccharide-pentapeptide moiety of lipid II. We seek a description of this antibiotic/target interface from membrane-embedded complexes to create a template for computational screening of synthetic macrocyclic antibiotics.[4]

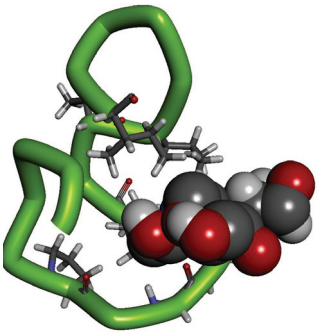

Figure 1. Solution NMR structure of mersacidin (1MQZ)[5] with N-acetyl-muramic acid from lipid II (this work).

Correlation spectroscopy of mersacidin/lipid II membrane complexes

Uniformly ^{13}C,^{15}N-labelled mersacidin and ^{13}C,^{15}N-labelled lipid II were investigated by proton-driven spin diffusion (PDSD)[6] to probe molecular connectivity within the complex. To facilitate spectral assignment, we combined the PDSD data with HNCA and HNCO[7] from ^{15}N labelled antibiotic/target complexes. We have completed a significant part of the spectral assignment of mersacidin. One particular difficulty arises from a sequential tetra-Gly region, part of which is in contact with the target. Clear internal connectivity within aminoacid residues is observed with good separation across peptide bonds. Weaker interresidue couplings facilitate sequential assignment.

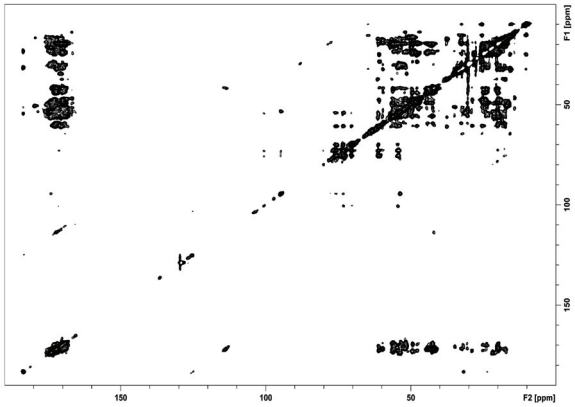

Figure 2. PDSD spectrum from ^{13}C,^{15}N-mersacidin / ^{13}C,^{15}N-lipid II in bilayer lipid membrane.

Previously suggested involvement of 17E [5] was confirmed, which is now shown to engage lipid II at murein NAc. In addition, 6P and 19I are proximal to GlcNAc-1 and MurNAc ring carbons. The pentapeptide in lipid II remains relatively mobile and does not appear to interact directly with the antibiotic.

References

1. Breukink, E.; Wiedemann, I.; van Kraaij, C.; Kuipers, O. P.; Sahl, H. G.; de Kruijff, B. *Science* **1999**, *286*, 2361.
2. Bonev, B. B.; Breukink, E.; Swiezewska, E.; De Kruijff, B.; Watts, A. *FASEB J.* **2004**, *18*, 1862.
3. Parisot, J. L.; Carey, S.; Breukink, E.; Chan, W. C.; Narbad, A.; Bonev, B. *Antimic. Agents Chemoth.* **2008**, *52*, 612.
4. Turpin, E. R.; Bonev, B. B.; Hirst, J. D. *Biochemistry* **2010**, *49*, 9594.
5. Hsu, S. T. D.; Breukink, E.; Bierbaum, G.; Sahl, H. G.; de Kruijff, B.; Kaptein, R.; van Nuland, N. A. J.; Bonvin, A. *J. Biol. Chem.* **2003**, *278*, 13110.
6. Grommek, A.; Meier, B. H.; Ernst, M. *Chem. Phys. Lett.* **2006**, *427*, 404.
7. van Rossum, B. J.; Castellani, F.; Pauli, J.; Rehbein, K.; Hollander, J.; de Groot, H. J. M.; Oschkinat, H. *J. Biomol. NMR* **2003**, *25*, 217.

Fast MAS ^{1}H Spectroscopy of ^{1}H-Diluted Systems: Subtilin/Target Membrane Complexes

David C. Griffin,[1] Dinu Iuga,[2] Filip Ciesielski[1] and Boyan B. Bonev[1]

[1]*School of Biomedical Sciences, University of Nottingham,* [2]*Department of Physics, University of Warwick*

Overview

Subtilin is a 3353 Da Class I lanthionine antibiotic, which acts *via* lipid II-mediated membrane poration[1] to inhibit cell wall biosynthesis, deregulate bacterial division and cell wall formation, akin to nisin.[2] High specificity in bacterial target recognition by both subtilin and nisin is conferred by pyrophosphate recognition of mature peptidoglycan intermediates lipid II and undecaprenyl pyrophosphate found in the outer leaflets of bacterial membranes.[3]

Fast MAS in deuterated peptides in bilayer membranes

The linewidth in proton spectra from peptides in lipid membranes is dominated by field-independent isotropic line broadening, which results from strong interproton dipolar couplings. Such isotropic broadening is approximately inversely proportional to the MAS frequency[4] and responds to multipulse homonuclear decoupling.[5]

We combine high ^{1}H dispersion at the UK 850 MHz Solid-State NMR Facility with fast MAS averaging of interproton dipolar interactions, the strength of which was reduced by random ^{2}H isomorphic substitutions. For this study, subtilin, deuterated randomly at 70% proton replacement along with the protonated target, undecaprenyl pyrophosphate (11PP) in hydrated membranes, was investigated under fast MAS or under homonuclear proton decoupling.

Undecoupled fast MAS ^{1}H NMR spectra, acquired between 13 and 60 kHz, revealed little improvement in spectral resolution, which suggests that 70% deuteration reduces interproton dipolar couplings to values, that permit mechanical averaging at as low as 15 kHz MAS.

We also acquired ^{1}H NOESY spectra to assess the intensity of proton cross-peaks at high levels of deuteration. We conclude that 70% deuteration, which leads to cross-peak intensity diminution to 9% of the predicted intensity in fully protonated samples, allowed sufficient residual intensity to observe low-intensity well-resolved resonances.

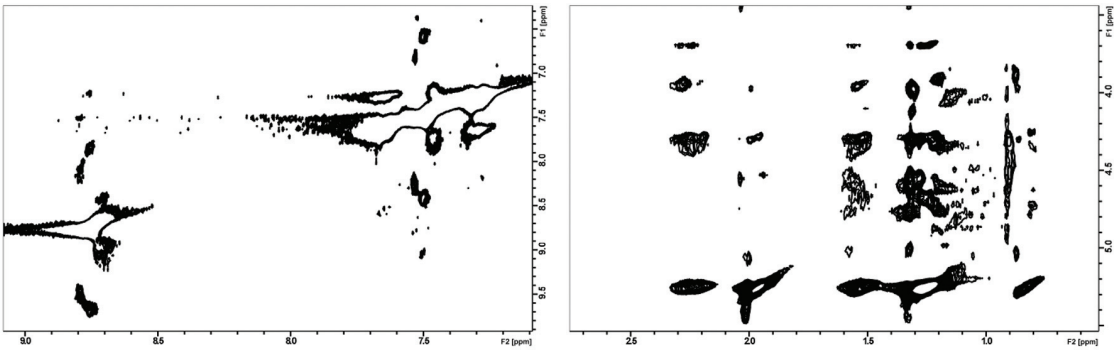

Figure 1. Proton NOESY from hydrated membranes at 20°C and 60 kHz MAS: 0.7 ^{2}H-subtilin, protonated 11PP and DOPC hydrated in D_2O.

References

1. Parisot, J. L.; Carey, S.; Breukink, E.; Chan, W. C.; Narbad, A.; Bonev, B. *Antimicrob. Agents Chemother.* **2008,** *52*, 612.
2. Hyde, A. J.; Parisot, J.; McNichol, A.; Bonev, B. B. *Proc. Natl. Acad. Sci. U.S.A.* **2006,** *103*, 19896.
3. Bonev, B. B.; Breukink, E.; Swiezewska, E.; De Kruijff, B.; Watts, A. *FASEB J.* **2004,** *18*, 1862.
4. Maricq, M. M.; Waugh J. S. *J. Chem. Phys.* **1979,** *70*, 3300.
5. Lesage, A.; Sakellariou, D.; Hediger, S.; Elena, B.; Charmont, P.; Steuernagel, S.; Emsley, L. *J. Magn. Reson.* **2003,** *163*, 105.

^{14}N-^{1}H Correlation Spectra of a Pharmaceutical and a Co-crystal

Andrew Tatton,[1] Dinu Iuga,[1] Tran N. Pham,[2] Fred G. Vogt[2] and Steven P. Brown[1]

[1]*Department of Physics, University of Warwick,*
[2]*GlaxoSmithKline*

Overview

^{14}N-^{1}H solid-state NMR experiments offer the opportunity to probe N-H correlations for organic solids without recourse to isotopic labelling.[1,2] Brown and co-workers have recently shown, for the case of a synthetic guanosine derivative, how ^{14}N-^{1}H spectra identify intermolecular contacts across N…H hydrogen bonds.[3] We show here further applications of the ^{14}N-^{1}H method. ^{14}N-^{1}H experiments were recorded using a HMQC pulse sequence with R^3 recoupling of the ^{14}N-^{1}H dipolar coupling,[1] employing the UK 850 MHz Solid-state NMR Facility's 1.3 mm probe that allows MAS at 60 kHz and a ^{14}N nutation frequency of 120 kHz.

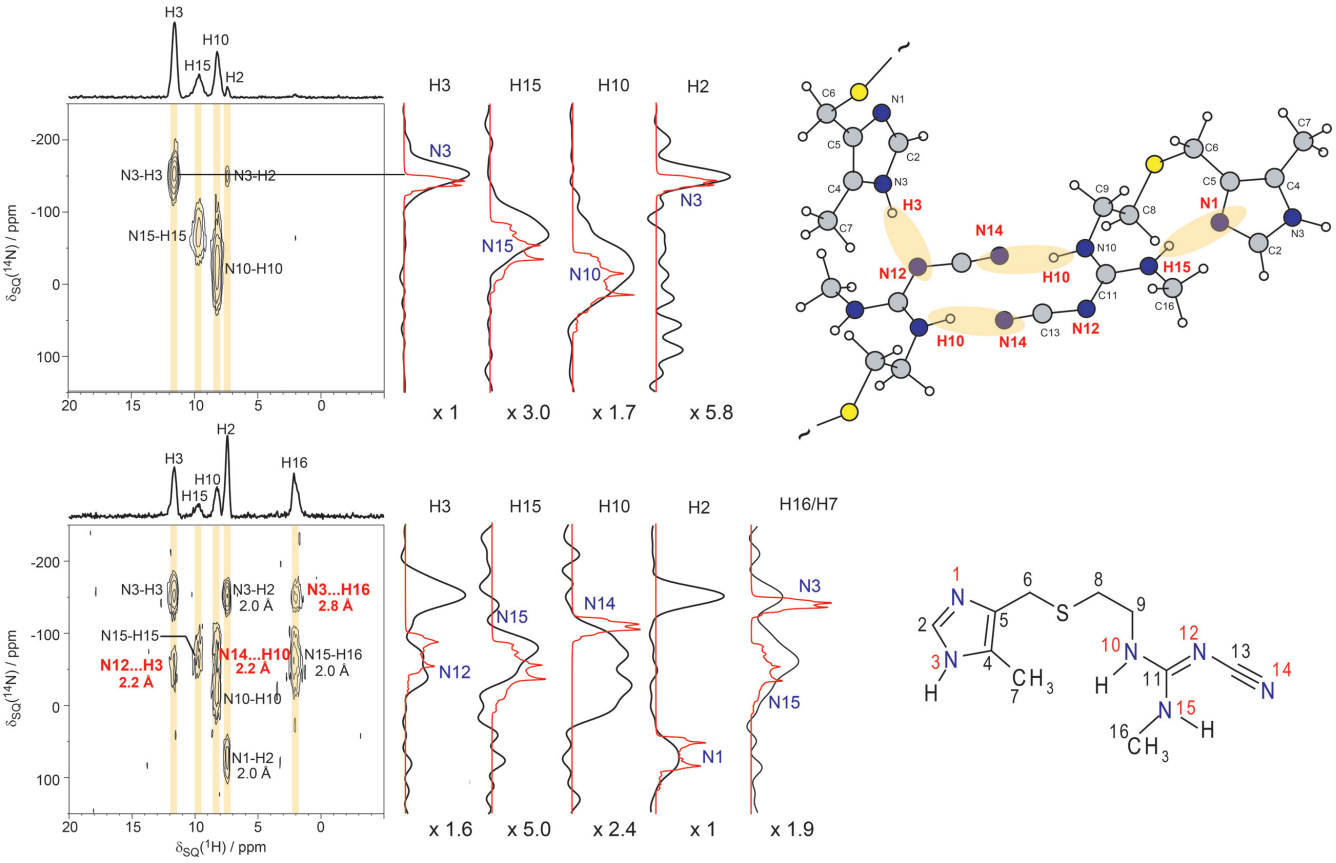

Figure 1. ^{14}N–^{1}H HMQC (850 MHz, 60 kHz MAS, 6 hours experimental time) spectra with ^{1}H skyline projections of cimetidine recorded using n=2 rotary resonance (R^3) recoupling of ^{14}N-^{1}H heteronuclear dipolar couplings for (top) τ_{RCPL} = 200 μs and (bottom) τ_{RCPL} = 600 μs. For peaks corresponding to longer-range N…H proximities, the nearest distance as extracted from the geometry-optimised (CASTEP) crystal structure is stated. Intermolecular hydrogen-bonding correlations are shown in red. On the right-hand side, individual ^{14}N subspectra taken through each ^{1}H resonance (black trace) are overlaid with spectra simulated for each ^{14}N site using SPINEVOLUTION[5] (red trace). ^{14}N isotropic chemical shift parameters used in the simulations were found experimentally using ^{15}N CPMAS, while the corresponding ^{14}N quadrupolar parameters were calculated using the GIPAW method within CASTEP – a consistent scaling by a factor of 0.95 was applied to the calculated C_Q values to give best agreement between the centres of gravity of the experimental and simulated lineshapes.

^{14}N-^{1}H spectra

Figure 1 presents ^{14}N-^{1}H spectra of the pharmaceutical molecule, cimetidine, recorded with two different recoupling times.[4] For the shorter recoupling time (top row, τ_{RCPL} = 200 μs), predominantly only one-bond NH correlation peaks are observed (N3-H3, N10-H10, N15-H15). For the longer recoupling time (bottom row, τ_{RCPL} = 600 μs), longer-range N...H correlations are additionally observed. Of particular interest are the two longer-range intermolecular N...H correlations. These arise from intermolecular N...H-N hydrogen-bonding motifs, namely N14...H10-N10 and N12...H3-N3. Additionally, longer-range intramolecular through-space correlations are seen for N15 to the H16 methyl protons, N3 to the H7 methyl protons and N1 to the aromatic H2 proton. On the right-hand side, experimental ^{14}N spectra (black lines) as extracted for the distinct ^{1}H resonances are compared to simulated spectra (red lines) that use the isotropic ^{15}N chemical shifts and the ^{14}N quadrupolar coupling constants, C_Q, that have been calculated using CASTEP.

Figure 2 presents a ^{14}N-^{1}H spectrum of the co-crystal formed between nicotinamide and palmitic acid, recorded for a recoupling time of 667 μs, for which cross peaks corresponding to longer-range distances can be expected in addition to one-bond NH correlations. Importantly, a correlation peak corresponding to the intermolecular N...HO hydrogen bond between the nicotinamide N1 nitrogen and the palmitic acid carboxylic acid group is observed. This is in addition to the NH one-bond connectivities in the nicotinamide NH_2 group (N2-H37/H38), as well as the intramolecular two-bond proximities of the nicotinamide N1 nitrogen to the neighbouring aromatic protons (H33 & H36).

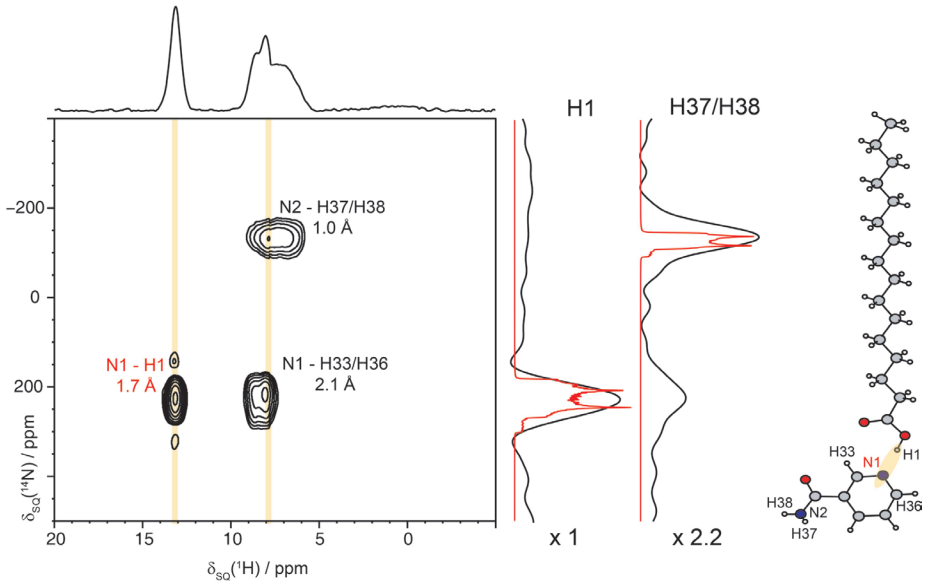

Figure 2. ^{14}N–^{1}H HMQC (850 MHz, 60 kHz MAS) spectrum with a ^{1}H skyline projection of a co-crystal of nicotinamide and palmitic acid, recorded using n=2 rotary resonance (R^3) recoupling of ^{14}N-^{1}H heteronuclear dipolar couplings for τ_{RCPL} = 667 μs. On the right-hand side, individual ^{14}N subspectra taken through each ^{1}H resonance (black trace) are overlaid with spectra simulated for each ^{14}N site using SPINEVOLUTION[5] (red trace). ^{14}N isotropic chemical shift parameters used in simulation were found experimentally using ^{15}N CPMAS, while the corresponding ^{14}N quadrupolar parameters were calculated using the GIPAW method within CASTEP.

References

1. Gan, Z. H.; Amoureux, J. P.; Trebosc, J. *Chem. Phys. Lett.* **2007**, *435*, 163.
2. Cavadini, S.; Abraham, A.; Bodenhausen, G. *Chem. Phys. Lett.* **2007**, *445*, 1.
3. Webber, A. L.; Masiero, S.; Pieraccini, S.; Burley, J. C.; Tatton, A. S.; Iuga, D.; Pham, T. N.; Spada, G. P.; Brown, S. P. *J. Am. Chem. Soc.* **2011**, *133*, 19777.
4. Tatton, A. S.; Pham, T. N.; Vogt, F. G.; Iuga, D.; Edwards, A. J.; Brown, S. P. *CrystEngComm* **2012** (published online).
5. Griffin, R. G.; Veshtort, M. *J. Magn. Reson.* **2006**, *178*, 248.

^{17}O NMR of Bone and Biomimetic Materials

Sharon E. Ashbrook,[1] Erika Davies,[2] Melinda J. Duer[2] and David G. Reid[2]

[1]*School of Chemistry and EaStCHEM, University of St Andrews,*
[2]*Department of Chemistry, University of Cambridge*

Overview

Bone is a complex organic-inorganic composite, consisting primarily of a protein network (collagen type I) deposited onto nanocrystalline mineral platelets. While the mineral phase in bone can be described as a non-stoichiometric carbonatoapatite, model calcium phosphate systems such as hydroxyapatite (HA) and octacalcium phosphate (OCP) provide a well-defined starting point for any structural investigation.

These basic models can be extended by including biologically-relevant organic species, e.g., chondroitin sulphate or citric acid. Hydroxyapatite composites are prepared by precipitating the hydroxyapatite in a solution containing the target biomolecule. OCP-citrate, a particularly intriguing material, is formed when citrate is incorporated into the hydrated layer of OCP during hydrolysis from α-tricalcium phosphate.[1] While it is not clear how or where the biomolecules are incorporated into the hydroxyapatite composites, OCP-citrate is a (comparatively well-defined) model system in which the organic molecules are known to play a key role in determining structure and stability.

New Insights from ^{17}O NMR at 850 MHz

Density functional theory (DFT) calculations were performed using CASTEP to determine the NMR parameters associated with the oxygen environments in OCP found at the interface between the hydrated and apatitic regions of this material (this region serves as a useful model of the mineral surface in bone).[2-5] The calculations indicated that these oxygen environments should appear in the 30-100 ppm region of the ^{17}O NMR spectrum, with stronger association with hydrogen (*i.e.,* HPO_4 or PO_4 hydrogen bonded to water) resulting in signals at lower frequency. Bearing these results in mind when considering the 1D ^{17}O double frequency sweep (DFS) MAS NMR spectra presented in Figure 1, it is clear that none of the synthetic HA materials model bone well, either in the presence or absence of an organic coprecipitate. OCP, a layered structure lacking organic inclusions, exhibits the expected range of low frequency environments, but the intensity is considerably weaker than observed in the case of bone. When we consider OCP-citrate, however, a layered material in which citrate molecules span the hydrated region and can be considered the structural equivalent of "buttresses", an excellent correspondence with the spectrum of bone is found. An exciting new model of bone mineral therefore emerges, in which citrate plays a crucial role in controlling the size and stability of the nanocrystals from *within*. This model contrasts sharply with that recently proposed by Hu *et al.*, in which the high levels of citrate in bone were attributed to citrate molecules adsorbed on the mineral surface.[6]

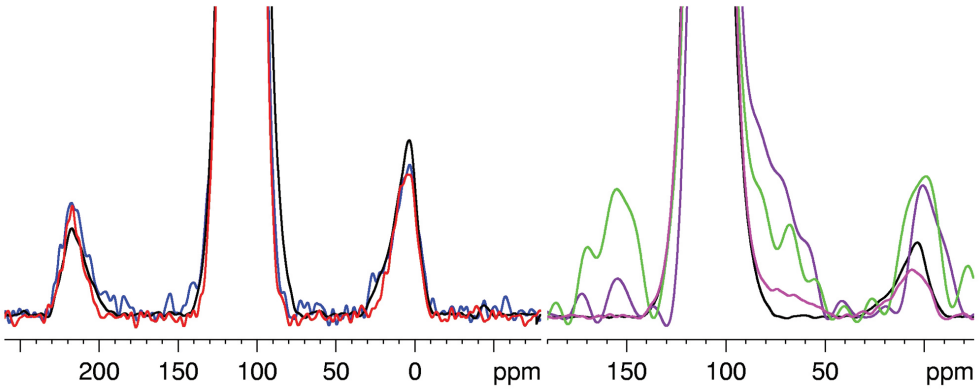

Figure 1. ^{17}O DFS MAS NMR spectra of ^{17}O-enriched HA (black), HA coprecipitated with chondroitin sulphate (blue), HA coprecipitated with $^{13}C_6$-labelled citric acid (red), OCP (pink), natural abundance OCP-citrate (purple) and adult horse bone (green). Note the low-frequency "foot" present in the spectra on the RHS (pure HA is also included on the RHS for comparison).

While the synthetic HA composites are unsuitable for investigations of the surface structure of bone mineral, the 2D ^{17}O MQMAS spectra presented in Figure 2 reveal an interesting distinction between the pure HA and the composite materials. There are two isotropic peaks evident in the projection to the left of the figure (116 and 123 ppm).[7] The small protrusion at the top of the contour for pure HA corresponds to an oxygen environment at 108 ppm (C_Q = 4.1 MHz, consistent with Wu *et al.*). This environment is barely evident in the chondroitin sulphate composite, and completely absent in the citrate composite. Once again DFT calculations have guided our understanding, revealing that these low frequency environments correspond to orthophosphate oxygen atoms directed (in a pair-wise fashion) towards the hydroxyl channels found in the hexagonal form of hydroxyapatite. The MQMAS data therefore indicates that the presence of the organic material is somehow disrupting these channels, but how and in what precise manner remains unclear.

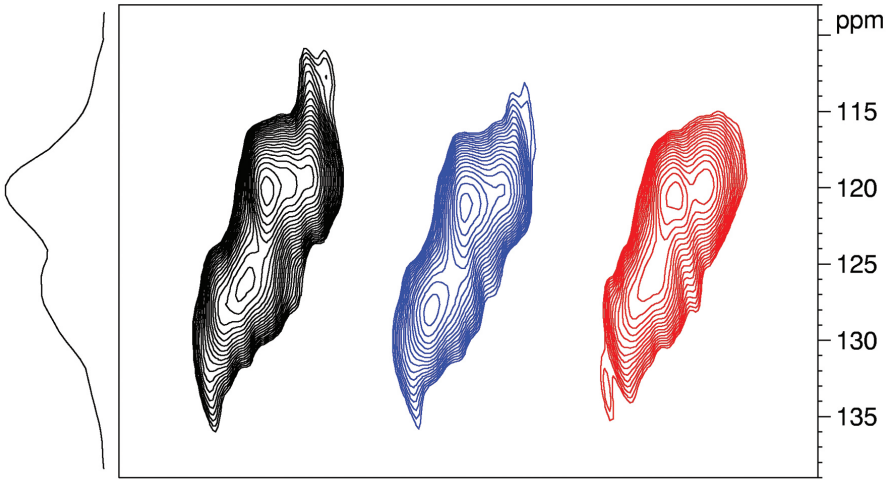

Figure 2. ^{17}O MQMAS spectra of ^{17}O-enriched HA (black), HA coprecipitated with chondroitin sulphate (blue) and HA coprecipitated with $^{13}C_6$-labelled citric acid (red). Note the prominent low-frequency feature present in the pure HA.

Summary

By combining ^{17}O NMR investigations at high field with DFT calculations performed on model calcium phosphate systems, we have identified a material that mimics bone mineral more accurately than pure HA. This discovery forms the basis of an exciting new model of the structure of bone mineral, and provides an intuitively-appealing explanation of the role of citrate in bone.

We have also found that precipitating hydroxyapatite in the presence of chondroitin sulphate or citric acid results in disruption of the hydroxyl channels within the structure, however further work will be required to determine the underlying mechanism.

References

1. Markovic, M.; Fowler, B. O.; Brown, W. E. *Chem. Mater.* **1993**, *5*, 1401.
2. Clark, S. J.; Segall, M. D.; Pickard, C. J.; Hasnip, P. J.; Probert, M. I.; Refson, K.; Payne, M. C. *Z. Kristallogr.* **2005**, *220*, 567.
3. Pickard, C.; Mauri, F. *Phys. Rev. B* **2001**, *63*, 245101.
4. Yates, J.; Pickard, C.; Mauri, F. *Phys. Rev. B* **2007**, *76*, 024401.
5. McNellis, E. R.; Meyer, J.; Reuter, K. *Phys. Rev. B* **2009**, *80*, 205414.
6. Hu, Y. Y.; Rawal, A.; Schmidt-Rohr, K. *Proc. Natl. Acad. Sci. USA* **2010**, *107*, 22425.
7. Wu G.; Rovnyak, D.; Huang, P. C.; Griffin, R. G. *Chem. Phys. Lett.* **1997**, *277*, 79.

Studying the Ca Environment in α-Tricalcium Phosphate Using High-Field ^{43}Ca MAS and DOR NMR

James F. MacDonald,[1] Iain Gibson,[2] and John V. Hanna[1]

[1]*Department of Physics, University of Warwick,*
[2]*Department of Chemistry, University of Aberdeen*

Overview

Calcium phosphate ceramics generate great interest in the field of biomaterials due to the mineral component of bone and teeth being an analogue of the mineral hydroxyapatite (HA).[1] It is essential to understand how these materials contribute to the mineralization of teeth and bone, while also understanding how they can be used as bone replacement material in the body. One such viable material is tricalcium phosphate ($Ca_3(PO_4)_2$, TCP); the α-phase of TCP has been shown to be a suitable material due to it being almost completely resorbable under physiological conditions, unlike HA which has poor solubility in the body. Unfortunately the higher solubility of α-TCP results in lower structural stability and implant strength when its performance is measured against materials such as HA. It has been found that the solubility of α-TCP can be modified by substituting silicon into the lattice. This silicon-substituted system possesses the added advantage of the silicon component being osteoconductive, thus stimulating bone growth through the introduced implant material.[2]

To complement the current program of study we are presently undertaking on α-TCP (DFT calculations, diffraction techniques and ^{31}P MAS NMR), we performed ^{43}Ca MAS NMR and DOR measurements on ~33 % ^{43}Ca enriched samples of α-TCP and silicon substituted α-TCP ($Ca_3(PO_4)_{2-x}(SiO_4)_x$, Si-α-TCP), to determine the invoked changes to the Ca-O environments in the substituted system. The substitution of silicon into the α-TCP structure produces vacancies; ^{31}P-^{29}Si heteronuclear correlation and ^{29}Si MAS NMR measurements on these systems suggests that the Si- α -TCP structure is characterised by specific silicon-rich regions in the unit cell. Comparison of the differences of the Ca-O bonding between the structures will help to determine what Ca site or sites are being affected by the silicon.

Experimental

All ^{43}Ca MAS and DOR NMR measurements were performed on a Bruker Avance III-850 (20.0 T) operating at a characteristic ^{43}Ca frequency of 57.2 MHz. The ^{43}Ca MAS experiments were performed on a Bruker 4 mm triple channel MAS probe utilising MAS frequencies of 10 kHz. Non-selective (or 'solution') pulse times of 12 μs were measured on a $CaCl_2$ solution, from which a selective (or 'solid') pulse time of 3 μs was calibrated for the ^{43}Ca (I=7/2) nucleus. All ^{43}Ca MAS measurements were undertaken with a flip angle of π/3 (2 μs) and a recycle delay of 5 s. The associated ^{43}Ca DOR measurements were undertaken using a Samoson designed DOR probe which enabled an inner rotor speed of ~ 6 kHz and outer rotor speed of ~1.3 kHz. For the DOR probe measurements non-selective (or 'solution') pulse times of 16 μs were measured on a $CaCl_2$ solution from which a selective (or 'solid') pulse time of 4 μs was calibrated. The subsequent DOR experiments utilised a flip angle of ~ π/4 (4 μs) and a recycle delay of 2.5 s. All measured ^{43}Ca chemical shifts from the MAS and DOR techniques were directly referenced to the primary reference of 1.0 M $CaCl_2$ (aq).

Results

Figure 1(a)

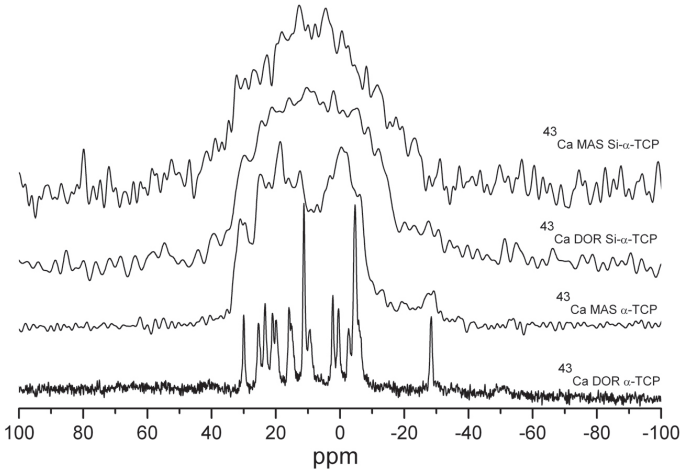

Figure 1(b)

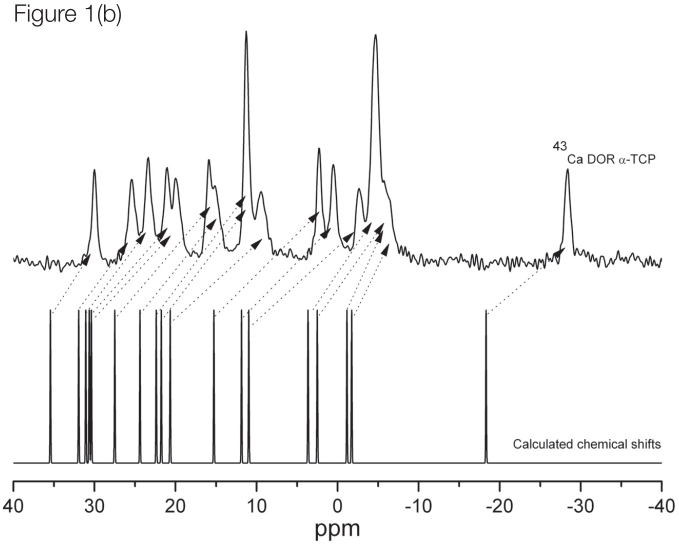

Figure 1. (a) ^{43}Ca MAS and DOR data acquired at 20.0 T for α-TCP and Si-α-TCP, and (b) a direct comparison of the GIPAW DFT calculated ^{43}Ca isotropic chemical shifts derived using the NMR-CASTEP package and the 'apparent' uncorrected ^{43}Ca shifts as measured from the 20.0 T DOR data.

Previous lower field ^{31}P and ^{29}Si MAS NMR studies on α-TCP have demonstrated that very high quality samples with exceptionally high short range order can be produced from the high temperature quench preparations. The large and highly complex monoclinic unit cell (space group $P2_1/a$) is composed of 12 P and 18 Ca positions;[3] the ^{31}P MAS study unambiguously corroborates this structural analysis, although other previous studies have proposed alternative structural models involving 15 P positions.[4] The lower two ^{43}Ca MAS and DOR spectra shown in Figure 1a also provide evidence for the monoclinic $P2_1/a$ model. It can be observed that the ^{43}Ca MAS data are a superposition of many partially resolved and partially averaged lineshapes which are presumably attributed to the 18 Ca sites described in this model. However the corresponding DOR data show that the residual second order quadrupolar broadening is removed thus facilitating clear resolution of these ^{43}Ca resonances. These data are further supported by the GIPAW DFT calculated ^{43}Ca isotropic chemical shifts obtained using NMR-CASTEP. Their correlation with the apparent shifts at 20.0 T (Figure 1b) is quite reasonable, and further DOR studies at lower B_0 field strengths will permit a direct comparison of the measured and calculated isotropic chemical shifts to be undertaken.

Similar ^{43}Ca MAS and DOR measurements from the Si-α-TCP system demonstrate that Si substitution into the α-TCP structure introduces enormous chemical shift dispersion, even at a dopant level of ~1%. This system is being further investigated with ^{29}Si-^{31}P heteronuclear correlation techniques to investigate the Si siting within this structure.[5]

References

1. Mow, V. C.; Huiskes, R. *Basic Orthopaedic Biomechanics and Mechano-Biology,* Lippincott Williams & Wilkins, 2005.
2. Rawl, A.; Wei, X.; Akinc, M.; Schmidt-Rohr, K. *Chem. Mater.* **2008**, 20, 2583.
3. Mathew, M.; Schroeder, L. W.; Dickens, B.; Brown, W. E. *Acta Cryst.,* B **1977**, 33, 1325.
4. Bohner, M.; Lemaitre, J,; Legrand, A. P.; De La Caillerie, J.-D.; Belgrand, P. *J. Mat. Sci., Mater. Med.* **1996**, 7, 457.
5. MacDonald, J. F., *et al. manuscript in preparation.*

^{89}Y and ^{1}H NMR Studies of the Defects in Y Doped Perovskites

Frédéric Blanc,[1] Luke Sperrin,[1] Lucienne Buannic[2] and Clare P. Grey[1,2]

[1]*Department of Chemistry, University of Cambridge, UK,*
[2]*Department of Chemistry, State University of New York, NY, USA*

Overview

Perovskites have been proposed as good electrolytes materials for solid oxide fuel cells (SOFC) devices as they present very high protonic conductivity when hydrated. Observation of the mobile species (the protons of the hydroxyl groups) is challenging (if possible) by diffraction-based techniques, but ^{1}H solid state NMR spectroscopy is a powerful method to probe the proton environment and thus understand the mechanism of protonic conduction in these perovskites materials.[1] Hydroxyl sites in oxides are often created by dissociative absorption of water on oxide ion vacancies – obtained by cation doping – at high temperatures.[2] Among all the perovskites that have been proposed as electrolytes, we have focused on Y doped $BaZrO_3$ as this material is particularly suited due to high protonic conductivity and tolerance to CO_2 and alkanes gases.[2] This report highlights the observation of 1. the oxygen ion vacancies near the yttrium sites by ^{89}Y NMR and 2. the protonic hydroxyl defects by ^{1}H NMR.

Observation of Crystallographic Oxygen Defects in Y doped $BaZrO_3$ by ^{89}Y NMR

The ^{89}Y NMR spectra of a series of Y doped $BaZrO_3$ (with Y contents of 10, 30 and 50 %) obtained at 20 T using both ZrO_2 and Si_3N_4 rotors are given in Figure 1. Firstly, comparison of the ^{89}Y spectra obtained with ZrO_2 and Si_3N_4 rotor clearly demonstrates that the 105 ppm peaks obtained with ZrO_2 rotors (Figure 1a) arise from an Y containing material in ZrO_2. Small amount of yttrium stabilized zirconia (YSZ) is always present in ZrO_2 (and in ZrO_2 rotor) for mechanical strength and the recent work by various groups showed that 12 coordinated Y at about 100 ppm exists in YSZ.[3,4] Thus, we assigned this 105 ppm peak to YSZ and not to any yttrium environment in Y doped $BaZrO_3$. The signal at isotropic shift of 256 ppm here suggests the presence of yttrium in 12 coordination[5] arising from small amount of Y doping into the A = Ba site of $BaZrO_3$ as proposed recently from synchrotron X ray diffraction measurements.[6,7] The use of Si3N4 rotor was crucial here to observe 12 coordinated Y as the peak at 105 ppm for 12 coordinated Y in YSZ could have been misleading for a large amount of 12 coordinated Y in contradiction with the recent findings.[6,7] Secondly, all the spectra of the Y doped $BaZrO_3$ materials are dominated with a signal at 410 ppm (typical of Y in 6 fold symmetry) in agreement with Y doping in the B = Zr site of $BaZrO_3$ (Figure 1b). We note that the linewidth of these peaks is much broader than when ZrO_2 rotors are used for reasons that are not entirely clear to us. Finally and most importantly, we note that the spectra seem to show significant amount of Y in 5 fold symmetry (at about 470 ppm), for Y sites bearing oxide ion vacancies, suggesting a composition of the type $Ba_{1-x-2b}Y_{2b}(Zr_{1-x+b}Y_{x-b})O_{3-x+1.5b}$, where x is the nominal content of Y (x = 0.1 – 0.5) and b the content of Y (estimated 0.1) in doping into the A site.

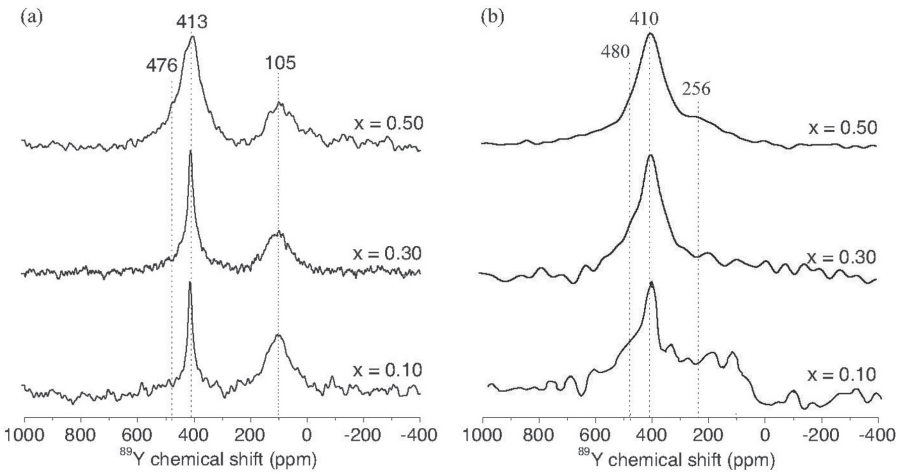

Figure 1. ^{89}Y NMR spectra of Y doped $BaZrO_3$ at various Y contents (x = 10, 30 and 50 %) obtained at 20.0 T using a 7mm single channel probe using (a) conventional ZrO_2 rotor at a MAS of 1 kHz or (b) Si_3N_4 rotor at a MAS of 4 kHz.

Observation of Protonic Defects in hydrated Y doped $BaZrO_3$ by ^1H NMR

As stated on the overview, observation of the proton mobile species in protonic conductors is crucial and extremely informative but often challenging. Nevertheless, ^1H NMR is very well suited to detect protonic defect sites as shown recently on hydrated Sc doped $BaZrO_3$,[1] and we present here ^1H NMR initial results on hydrated $BaZrO_3$ doped with yttrium level at 10 and 50 %. The variable temperature ^1H MAS NMR spectra of $BaZr_{0.5}Y_{0.5}O_{2.75}(OH)_{0.25}$ is shown in Figure 2a. At room temperature, we observe one narrow resonance at 5.0 ppm while at -80 °C three peaks might be present which could be assigned to the three possible sites Y-(OH)-Y (at 6.8 ppm), Zr-(OH)-Y (5 ppm) and Zr-(OH)-Zr (3.8 ppm) based on the crystal structure and a random distribution of hydroxyl groups. Another possibility is the presence of the same site having different hydrogen bond with nearby oxygens without hydrogen. The main mechanism of the line broadening at low temperature is probably inhomogeneous broadening (rather than homonuclear dipolar coupling) in this weakly dense protonic material making the use of fast MAS and dipolar decoupling techniques not suitable for line narrowing. At the coalescence temperature (around 20 °C), rate constants for exchange of about 200 Hz could be extracted from the ^1H chemical shift.[8] This could be used to simulate the spectra at all temperature and access an "NMR" activation energy for the proton motion.

The room temperature ^1H MAS NMR spectra (top Figure 2b) of a sample containing less Y, *e.g.* $BaZr_{0.9}Y_{0.1}O_{2.95}(OH)_{0.05}$ presents two sites at 4.3 and 5.3 ppm assigned to Zr-(OH)-Zr and Zr-(OH)-Y, respectively. It is interesting to note that in this sample, that contains less yttrium and thus less protonic sites (as observed by TGA measurements, data not shown), we did not observe a single resonance corresponding to the motional average of all the individual sites. This suggests slower protonic motion in $BaZr_{0.9}Y_{0.1}O_{2.95}(OH)_{0.05}$ *vs.* $BaZr_{0.5}Y_{0.5}O_{2.75}(OH)_{0.25}$, which is in agreement with the proposal that lower protonic conductivity is usually observed when the concentration of mobile proton sites decreases.[2,9] In an attempt to observe chemical exchange, a series of ^1H 2D NOESY spectra was performed on $BaZr_{0.9}Y_{0.1}O_{2.95}(OH)_{0.05}$ which does not reveal cross peaks (Figure 2b) and is in agreement with exchange at a rate slower than 100 Hz.

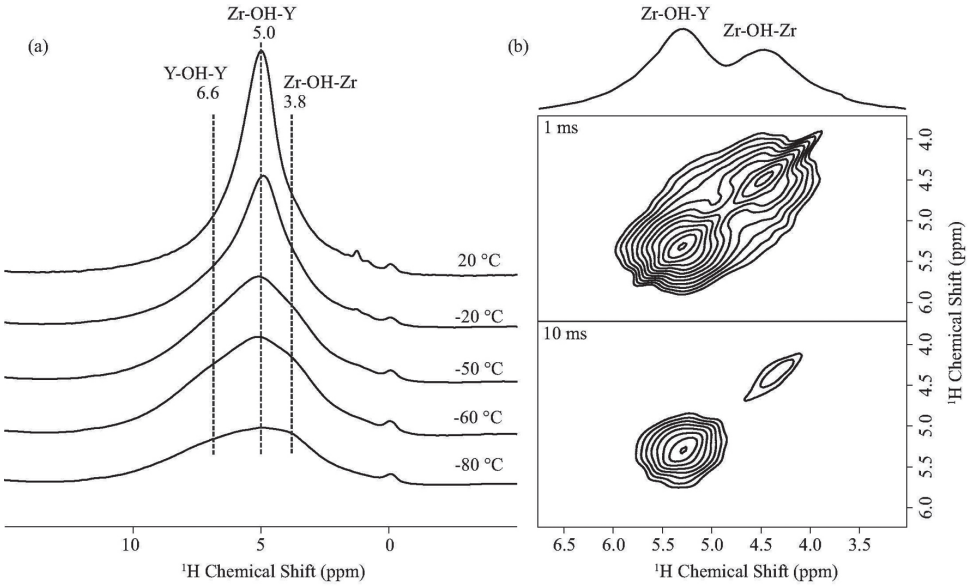

Figure 2. (a) Variable temperature ^1H NMR spectra of $BaZr_{0.5}Y_{0.5}O_{2.75}(OH)_y$ obtained at 20.0 T using a 4mm HX at a MAS frequency of 10 kHz. (b) Room temperature ^1H NOESY spectra of $BaZr_{0.9}Y_{0.1}O_{2.95}(OH)_y$ at a MAS frequency of 14 kHz.

References

1. Buannic, L.; Blanc, F.; Hung, I.; Gan, Z.; Grey, C. P. *J. Mat. Chem.* **2010**, *20*, 6322.
2. Kreuer, K. D. *Ann. Rev. Mat. Res.* **2003**, *33*, 333.
3. Kawata, K.; Maekawa, H.; Nemoto, T.; Yamamura, T. *Solid State Ionics* **2006**, *177*, 1687.
4. Henson, L. J.; Darby, R. J.; Kumar, R. V.; Farnan, I. *In* MRS Fall Meeting Boston, MA, USA, **2006**.
5. MacKenzie, K. J. D.; Smith, M. E. Multinuclear Solid-State NMR of Inorganic Materials; Elsevier: Oxford, 2002; Vol. 6.
6. Yamazaki, Y.; Babilo, P.; Haile, S. M. *Chem. Mater.* **2008**, *20*, 6352.
7. Yamazaki, Y.; Hernandez-Sanchez, R.; Haile, S. M. *J. Mat. Chem.* **2010**, *20*, 8158.
8. Levitt, M. H. Spin dynamics; Wiley: Chichester, 2000.
9. Kreuer, K. D. *Chem. Mater.* **1996**, *8*, 610.

^{17}O Solid State NMR Study of Electrochemical Products in Lithium-Oxygen Batteries

Michal Leskes[1], Gillian R. Goward[2] and Clare P. Grey[1]

[1]*Department of Chemistry, University of Cambridge, Cambridge, UK,*
[2]*Department of Chemistry, McMaster University, Hamilton, Ontario, Canada*

Overview

Lithium-oxygen batteries are promising energy storage systems due to the leap in specific energy they offer compared to standard lithium ion batteries. If successfully developed they can be integrated as the power supply of electric transportation.[1] To fulfill this promise, however, several challenges have to be addressed.[2] One of these involves the development of a practical electrolyte, the ion conducting medium connecting the lithium anode and the oxygen cathode. With increasing research in the past year it became evident that the electrolyte solvent plays a critical role in the fate of the battery.[3,4] Recent results suggest that with the common carbonate based electrolytes the reactive oxygen species formed during discharge of the battery react with the solvent leading to electrolyte decomposition and a complicated mixture of organo-lithium salts rather than the desired lithium peroxide or oxide. Currently most of the physical characterization techniques applied for the study of this system are limited in their capabilities to distinguish the different electrochemical products or in their depth of sensing into the pores of the cathode. Here we utilize for the first time ^{17}O solid state NMR which allows detection of reaction products formed in the bulk of the cathode material. Combined with density functional theory (DFT) calculations we can uniquely identify the main products formed in the battery in two electrolytes systems: the desired product lithium peroxide, formed in the first discharge with ether type electrolytes, and lithium carbonate which is the result of electrolyte decomposition. Due to the low natural abundance of the ^{17}O isotope (0.038%), its low NMR sensitivity and the small sample sizes, practical NMR measurements can only be performed at very high fields. The approach taken here is an initial characterization of the main discharge products the peroxide and carbonate followed by acquisition of the ^{17}O spectra from discharged cathodes extracted from lithium-oxygen batteries.

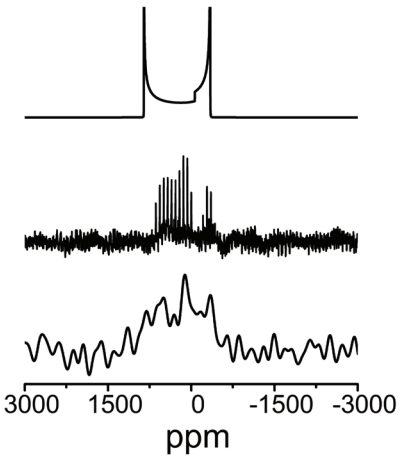

Figure 1. ^{17}O static spectrum of lithium peroxide acquired with a solid echo sequence (bottom) and QCPMG sequence (middle). The simulated spectrum, based on the calculated NMR parameters, is shown on top. The additional intensity in the centre of the pattern is due to carbonate impurity.

^{17}O Solid State NMR Study of lithium peroxide

Lithium peroxide is the main product expected to form in a rechargeable lithium-oxygen battery on which its high theoretical specific energy is based on. In the absence of an efficient way to enrich the peroxide with ^{17}O isotope we acquired the natural abundance spectrum at the 850 MHz. This high field is necessary to obtain ^{17}O signal especially due to the very large quadrupole interaction predicted by DFT calculation. The static natural abundance ^{17}O spectrum is shown in Figure 1 along with the simulated spectrum based on the calculated NMR parameters. This initial result demonstrate the unique quadrupole coupling constant (18 MHz) of the peroxide which is at least twice larger than most of the ^{17}O couplings reported in the literature thus making it clearly distinguishable. For comparison the calculated quadrupole coupling constant of the two oxygen species in lithium carbonate is of the order of 7 MHz.

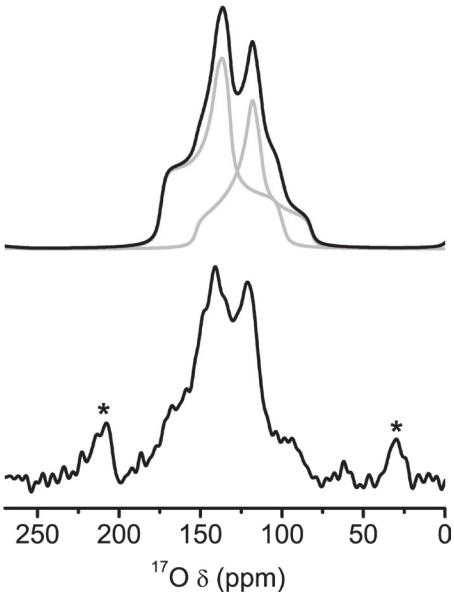

Figure 2. ^{17}O MAS spectrum of discharged cathode cycled with EC/DMC electrolyte (bottom). The MAS frequency is 20 kHz and the asterisks label background peaks from the zirconia rotor. The simulated spectrum on top is based on the calculated NMR parameters of lithium carbonate (C_q=7.7, 7.4 MHz, η=0.9, 0.9 for the two sites).

Identifying the main discharge products in lithium-oxygen cells

In order to compare the discharge products formed with different electrolyte solvents two cells were assembled: Cell A discharged in a mixture of ethylene carbonate (EC) and dimethyl carbonate (DMC) and cell B in dimethoxyethane (DME). The two cells were cycled under oxygen environment enriched with ^{17}O isotope (about 20%). The discharged cathodes were then extracted from the cells and studied by ^{17}O solid state NMR. The spectrum acquired from cell A and the simulated spectrum are plotted in Figure 2. The simulation is based on the calculated NMR parameters of the two oxygen sites in lithium carbonate and the good fit clearly demonstrates that this is the main product formed in cells cycled with carbonate electrolytes.

The spectrum of cell B is shown in Figure 3 and on top of it the fit based on the calculated NMR parameters of the single oxygen site in lithium peroxide. The main features, the two horns at the edge of the line shape, are those expected based on the natural abundance spectrum in Figure 1 and despite the substantial intensity in the center of the spectrum we can identify the peroxide specie as the main product formed in the first discharge with DME electrolyte. The additional contribution is due to zirconia from the NMR rotor (despite its natural abundance the ^{17}O isotope in about 1 gram of rotor has a significant signal compared to the cathode sample weighing about 1mg with only 20% enrichment).

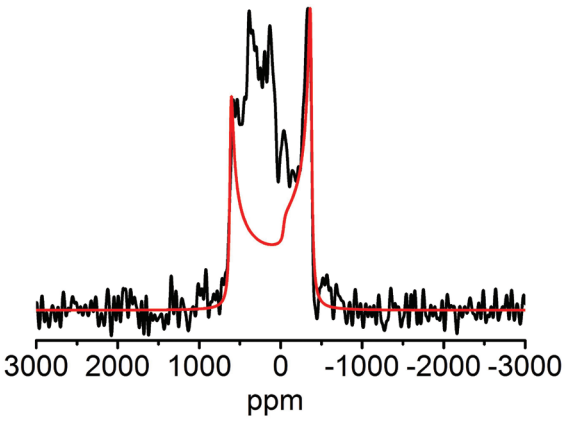

Figure 3. ^{17}O spectrum of discharged cathode cycled with DME electrolyte (black). The best fit simulated based on the calculated NMR parameters with C_q=18 MHz, η=0 and σ_{CSA}=–250 ppm, η=0 is plotted on top (red).

Comparing these two model cells we expect ^{17}O solid state NMR to be a valuable tool in the development of practical lithium-oxygen cells in which identifying electrochemical products is a key step.

References

1. Bruce, P. G.; Freunberger, S. A.; Hardwick, L. J.; Tarascon, J.-M. *Nature* **2012**, *11*, 19.
2. Girishkumar, G.; McCloskey, B.; Luntz, a. C.; Swanson, S.; Wilcke, W. *J. Phys. Chem. Lett.* **2010**, *1*, 2193.
3. Freunberger, S. A; Chen, Y.; Peng, Z.; Griffin, J. M.; Hardwick, L. J.; Bardé, F.; Novák, P.; Bruce, P. G. *J. Am. Chem. Soc.* **2011**, *133*, 8040.
4. Mccloskey, B. D.; Bethune, D. S.; Shelby, R. M.; Girishkumar, G.; Luntz, A. C. *J. Phys. Chem. Lett.* **2011**, *2*, 1161.

A ^{65}Cu Static NMR Study of Copper Thiocyanate-Based Materials Employed in Dye-Sensitized Solar Cell (IR) Absorber Devices

John V. Hanna

Department of Physics, University of Warwick

Overview

The development of devices for sensing IR radiation and solar energy absorption continues to be an important area of investigation because of the practical utilizations in a diverse variety of applications. Most widely used IR detectors depend on electron–hole generation in low band-gap semiconductor structures by incident radiation. These detectors exhibit good signal-to-noise performance and very fast response. However in order to achieve this, the semiconductor components of the detector need cryogenic or thermoelectric cooling. Thermal generation of carriers in a low band-gap semiconductor, impurity and defect mediated recombination, or thermally activated inter-sub-band transitions (i.e., in quantum well detectors) are limitations of conventional semiconductor photon detectors. The possibilities of using high band-gap semiconductors insensitive to background thermal noise and the flexibility of spectral response by choice of the dye are advantages of dye-sensitized devices (DSN). Furthermore, DSN produces only one type of carrier in the semiconductor volume. Therefore the dye-sensitized photocurrent remains insensitive to recombination at the grain boundaries or impurity sites. These attractive features of DSN have been exploited to construct solar cells using nanocrystalline films of oxide semiconductors and polymeric CuSCN to construct heterojunctions of the *n*-type semiconductor/dye/*p*-type semiconductor. Detector devices based on nanocrystalline TiO_2 (band gap=3.1 eV) film as the dye coated *n*-type substrate, and *p*-CuSCN (band gap 3.6 eV) as the hole collector have been fabricated and tested. Further research seeks to test variants of the *p*-CuSCN, particularly where the three dimensional CuSCN network has been selectively functionalised/terminated to produce partially reduced connectivity in the form of two-dimensional and one-dimensional polymers. A formal solid state NMR characterisation of these types of Cu(I) systems has been lacking as recent work[1,2] has demonstrated the difficulties of studying this nucleus, and GIPAW-DFT characterisation involving the $^{63/65}$Cu nucleus is largely unexplored.

Experimental

These ^{65}Cu static broadline NMR data measured for these Cu(I) systems were acquired at ambient temperatures using a Bruker Avance III 850 MHz spectrometer (20.0 T) and at a series of lower B_0 field strengths. All experiments were performed using a Bruker 5/7.5 mm static horizontal solenoid design probe and the reported ^{65}Cu static NMR data were acquired with the solid echo θ - τ - θ - τ - (acquire) ($\theta \approx \pi/3$ - $\pi/2$) experiment with an extended phase cycle to capture undistorted echoes with minimal influences from residual echo tails and finite pulse width effects.[3-6] 'Non-selective' (solution) $\pi/2$ pulse widths of 2 – 2.5 μs were calibrated on a secondary standard of solid CuCl from which 'selective' (solid) θ pulses of ~1.0 μs were employed in all solid echo measurements. The τ delay was 30 μs and the relaxation delay between transients was 0.5 - 2 s. All ^{65}Cu isotropic chemical shifts (δ_{iso}) were referenced directly to the primary IUPAC standard of saturated $[Cu(CH_3CN)_4]ClO_4$ in dry CH_3CN which was assigned to δ 0.0 ppm. The ^{65}Cu static broadline spectra acquired at all fields were simulated with the Bruker TOPSPIN solids package and the QUASAR solid state NMR data simulation program to deconvolute the nuclear quadrupole and chemical shift anisotropy contributions to these lineshapes. This treatment facilitated an accurate measurement of the isotropic chemical shift (δ_{iso}), quadrupole coupling constant (C_Q), nuclear quadrupole asymmetry parameter (η_Q), chemical shift anisotropy ($\Delta\delta$)/chemical shift span (Ω) and asymmetry (η_δ)/skew (κ), and the Euler angles (α, β, γ) relating the nuclear quadrupole and chemical shift tensor frames.

Results

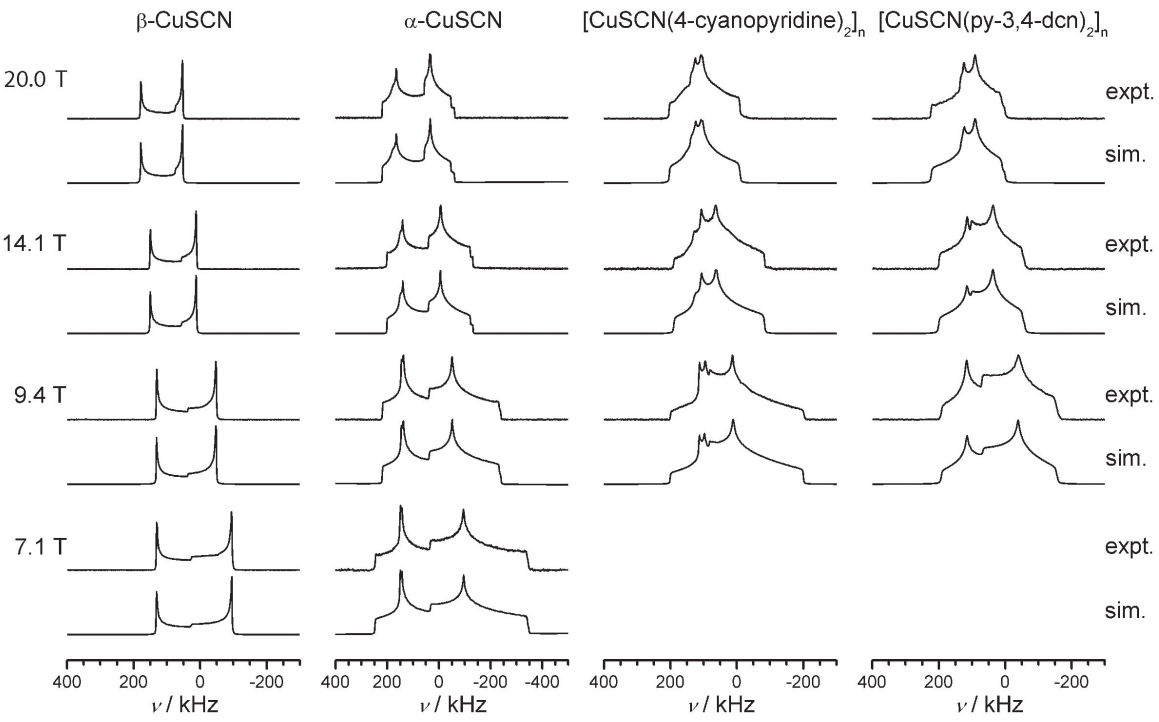

Figure 1. ^{65}Cu static NMR results for polymeric α-CuSCN, β-CuSCN, [CuSCN(4-CNpy)$_2$] and [CuSCN(py-3,4-dcn)$_2$] systems acquired at external magnetic fields of 7.1, 9.4, 14.1 and 20.0 T.

In similar fashion to other NMR active transition metal nuclei, the $^{63/65}$Cu (I = 3/2) linewidth is characterised by substantial quadrupole (C_Q) and chemical shift anisotropy/span contributions ($\Delta\delta/\Omega$). Given that the Cu metal site is directly coordinated to soft-donor ligands (involving N, S etc.) the covalent character of the bonding arrangement involving the metal centre is high. The termination of particular bonds in the network is achieved with N-based adducts such as pyridine, cyanopyridine, pyrazine, piperazine, bipyridine, phenanthroline etc. with increasing degrees of cyclic conjugation influencing the N coordination. Hence, the $\Delta\delta/\Omega$ contribution to the $^{63/65}$Cu static linewidth can vary markedly, and the only way to effectively deconvolute these contributions is to study these materials over a very wide range of magnetic field strengths.

Some typical ^{65}Cu broadline results for polymeric CuSCN systems such as α-CuSCN, β-CuSCN, [CuSCN(4-CNpy)$_2$] and [CuSCN(py-3,4-dcn)$_2$] are shown above in Figure 1. The appearance and linewidth of these data alter markedly with B_0 field, although the change in linewidth is not consistently proportional to 1/ B_0. Hence, in addition to the dominant quadrupole interaction another contribution must be influencing the linewidth and lineshape. The C_Q values for these systems fall within the ~12 – 16 MHz range, while the spans (Ω) show more substantial variation ranging over ~200 – 500 ppm.

References

1. Tang, J. A.; Ellis, B. D.; Warren, T. H.; Hanna, J. V.; Macdonald, C. L. B.; Schurko, R. W. *J. Am. Chem.* Soc. **2007**, *129*, 13049
2. Lucier, B. E.; Tang, J. A.; Schurko, R. W.; Healy, P. C.; Bowmaker, G. A.; Hanna, J. V. *J. Phys. Chem. C* **2010**, *114*, 7949.
3. Kunwar A. C.; Turner G. L.; Oldfield E. *J. Magn. Reson.* **1986**, *69*, 124.
4. Hirschinger J.; Granger P.; Rose J. *J. Phys. Chem.* **1992**, *96*, 4815.
5. Dumazy Y., Amoureux J. P., Fernandez C., *Mol. Phys.* **1997**, *90*, 959.
6. Bodart P. R., Amoureux J. P., Dumazy Y., Lefort R., *Mol. Phys.* **2000**, *98*, 1545.

New Insights into the Crystallization of Organic Materials by Combined *In-Situ* Solid-State and Solution-State NMR

Colan E. Hughes, P. Andrew Williams and Kenneth D. M. Harris

School of Chemistry, Cardiff University

Overview

We are focusing on the development and application of a new *in-situ* solid-state NMR strategy for exploring the evolution of crystallization processes from solution, with particular interest in monitoring the different solid phases (particularly different polymorphs) formed as a function of time during crystallization. The 850 MHz Facility has proven to be essential for this research, particularly in view of the advantages that it provides for maximizing resolution and sensitivity. An important recent development in our *in-situ* strategy has been to carry out combined measurements of both solid-state and solution-state NMR spectra, yielding complementary insights on the changes that occur in both the solid and liquid phases during the crystallization process.

Polymorphism in m-Aminobenzoic Acid

m-Aminobenzoic acid (*m*-ABA), which has five known polymorphs, undergoes various different crystallization pathways depending upon the solvent and experimental conditions. We have focused on crystallization experiments involving methanol or DMSO as the solvent. Preliminary solid-state ^{13}C NMR measurements on the individual polymorphs revealed that Forms II and V have very long relaxation times compared to the other forms (attributed to the fact that the *m*-ABA molecules in Forms II and V are present in a different tautomeric form), restricting the ability to observe Forms II and V in our *in-situ* solid-state ^{13}C NMR studies.

Crystallization of *m*-ABA from methanol in an incubator leads to concomitant crystallization of Forms I and III. Our *in-situ* solid-state ^{13}C NMR study focused on establishing the order in which these two polymorphs appear and whether any transition occurs between these polymorphs. As evident from Figure 1, the peak due to the carboxylate carbon allows the two polymorphs present to be distinguished. Initially, Form I is formed, but after about 2½ hours, Form I is observed to transform to Form III. These observations suggest that, under the conditions of the crystallization experiment, Form III has greater thermodynamic stability than Form I (from other experiments, Form III is believed to be the most stable of all the known forms). However, the formation of Form I is kinetically favoured, resulting in its rapid formation at the beginning of the crystallization process.

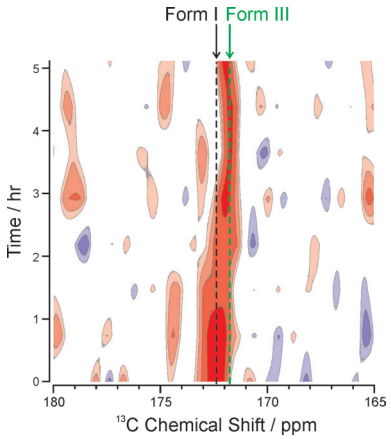

Figure 1. ^{1}H-^{13}C CP spectrum for m-ABA crystallizing from methanol, showing the carboxylate peak.

With DMSO as the solvent, crystallization experiments in the laboratory are found to give two different results. In some cases, Form I is obtained, while in other cases, no crystallization occurs. Our *in-situ* ^{13}C CPMAS NMR experiments for a sample of *m*-ABA in DMSO undergoing repeated crystallization and dissolution by cycles of cooling and heating also gave two distinct results. In some cases, no signal was observed, indicating that no solid phase is detected. However, as our measurements are unable to detect Forms II and V, solution-state ^{13}C NMR spectra were also acquired in order to explore possible changes in chemical shifts corresponding to changes in solution concentration. No such shifts were observed, leading to the conclusion that a supercooled solution was formed.

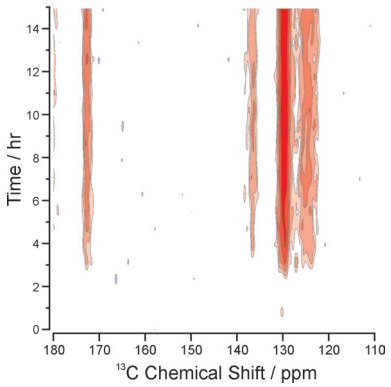

Figure 2. ^{1}H-^{13}C CP spectrum for m-ABA crystallizing from DMSO.

On other occasions, when the same solution was cooled, a solid-state ^{13}C NMR signal due to Form I was observed (in Figure 2, this signal appears after about 2½ hours) and no transition to any other polymorph was observed during the remaining 12 hours of the crystallization experiment. In this work, we also initiated a new strategy of interleaving direct-

excitation ^{13}C NMR measurements between successive CP measurements, allowing the chemical shifts of *both* the solution-state peaks and the solid-state peaks to be measured as a function of time during the crystallization process. After taking into account the effect of an overall shift due to slow cooling of the shims following dissolution at high temperature, our solution-state ^{13}C NMR results (Figure 3) reveal significant shifts of all peaks, commencing at the same time that the first peaks due to solid species appear in the CP spectra. These shifts are attributed to changes in the solution concentration (and perhaps changes in solution-state speciation) associated with the crystallization process. In support of this conclusion, the overall signal intensity of the direct-excitation spectra is constant for the first 2½ hours, then decreases as a function of time thereafter.

The signs and magnitudes of the changes in chemical shifts for different ^{13}C environments provide deeper insights on changes in interactions as a function of concentration (Figure 3). Specifically, the sign of the shift alternates around the aromatic ring (positive shifts for C-1, C-3, C-5; negative shifts for C-2, C-4, C-6 and the carboxylate carbon), suggesting that hydrogen bonding of the carboxylate and ammonium groups may become weaker as concentration decreases (with the greater change for C-3 compared to the carboxylate carbon suggesting that the ammonium group is affected more). These changes imply that the *m*-ABA molecules strongly self-associate, with a lesser extent of hydrogen bonding at lower concentrations.

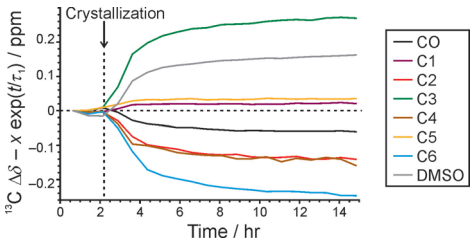

Figure 3. Solution-state ^{13}C chemical shifts for m-ABA during crystallization from DMSO.

Searching for New Polymorphs and Solvate Phases of Phenylalanine and Triphenylphosphine Oxide

In two other projects, our *in-situ* solid-state NMR strategy for studying crystallization has been used to explore the formation of new solid-state forms during the evolution of the crystallization process. Our study of phenylalanine was motivated by the fact that significant confusion exists in the literature concerning different solid forms, potentially involving both polymorphs and solvates. Our preliminary studies have discovered two hitherto unknown hydrate phases. Our *in-situ* solid-state ^{13}C NMR experiments examined crystallization of phenylalanine under the conditions found to produce these two hydrate phases. Working at the limit of sensitivity of the 850 MHz instrument, new peaks are observed in *in-situ* solid-state ^{13}C NMR spectra that are not due to any of the known forms of phenylalanine, providing the motivation to focus on isolating and determining the structures of these new solid forms.

Our study of triphenylphosphine oxide (TPPO) was motivated by its abundant polymorphism. There are four known forms (denoted MI, MII, MIII and O), of which only MI and O are readily prepared. Preliminary *in-situ* solid-state ^{31}P NMR results showed evidence for solid forms with ^{31}P resonances that do not correspond to either the MI or O phases, but which transform into MI or O on solvent removal. On the 850 MHz instrument, we have been successful in observing these new phases with greater resolution and exploring their formation in a time-resolved manner (Figure 4). Taking into account the initial shift of the peaks to lower chemical shift (due to the cooling of the shims), we observe the immediate formation of a phase with ^{31}P chemical shift similar to, but distinct from, the O phase. This new phase is then replaced gradually by two phases with ^{31}P chemical shifts close to the MI phase. Thus, our *in-situ* solid state ^{31}P NMR studies have identified three new phases of TPPO. In the solution-state ^{31}P NMR spectra, the intensity decreases gradually as a function of time, indicating that the amount of crystallized solid increases during the experiment, as solid phases of higher solubility are replaced by those of lower solubility. We are currently carrying out independent crystallization experiments in the laboratory in an effort to capture and identify these new forms of TPPO. Our X-ray diffraction studies of these new phases, which are currently ongoing, confirm that we do indeed observe new phases that do not correspond to either the MII or MIII polymorphs.

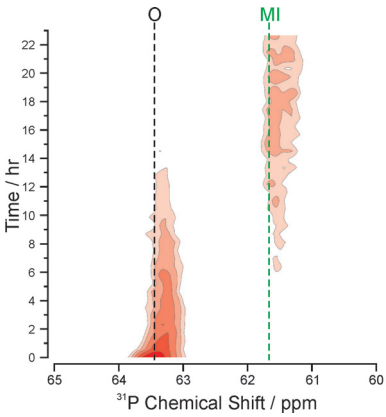

Figure 4. ^{1}H-^{31}P CP NMR spectrum of TPPO crystallizing from ethanol/cyclohexane.

References

1. Williams, P. A.; Hughes, C. E.; Lim, G. K.; Kariuki, B. M.; Harris, K. D. M. *paper submitted.*
2. Hughes, C. E.; Williams, P. A.; Harris, K. D. M. *paper submitted.*

Understanding ^{1}H Decoupling

Ilya Frantsuzov[1], Steven P. Brown[2] and Paul Hodgkinson[1]

[1]*Department of Chemistry, Durham University,*
[2]*Department of Physics, University of Warwick*

Overview

Resolution and sensitivity in solid-state NMR of organic compounds is limited by the relatively short decoherence times of ^{1}H and ^{13}C magnetisation. However, the relationship between radio-frequency (RF) ^{1}H decoupling sequences and achievable decoherence times is still poorly understood. We have previously shown that analysis[1] and efficient numerical simulation can be used to predict ^{1}H decoherence times under magic-angle spinning (MAS)[2] and have extended this work to multi-spin simulations involving time-dependent RF.[3] The goal of the current project is to understand how to efficiently decouple the abundant protons, for both homonuclear and heteronuclear decoupling, over the steadily widening parameter space (increasing static magnetic fields, RF powers, and MAS rates). Understanding how to decouple efficiently at high magnetic fields has obvious benefits for the wide range of Facility users who employ ^{1}H decoupling.

Methodology and preliminary results

It is generally difficult to achieve long ^{13}C decoherence times in CH_2 groups, owing to the strong dipolar coupling between the two ^{1}H nuclei. The time constant of the decay of the ^{13}C signal in glycine-2-^{13}C,^{15}N under a spin echo, usually termed T_2', was used as the primary metric of heteronuclear decoupling efficiency. T_2' has the advantage over the simple ^{13}C spectral linewidth of being unaffected by "inhomogeneous factors", improving both reproducibility and the sensitivity to small changes in decoupling efficiency. Using a labelled sample allows very detailed maps of decoupling performance to be obtained (taking 20 hours to record a map of ~2000 data points), which is particularly important at high MAS rates, where multiple "resonances" between RF and MAS cycle times are encountered.

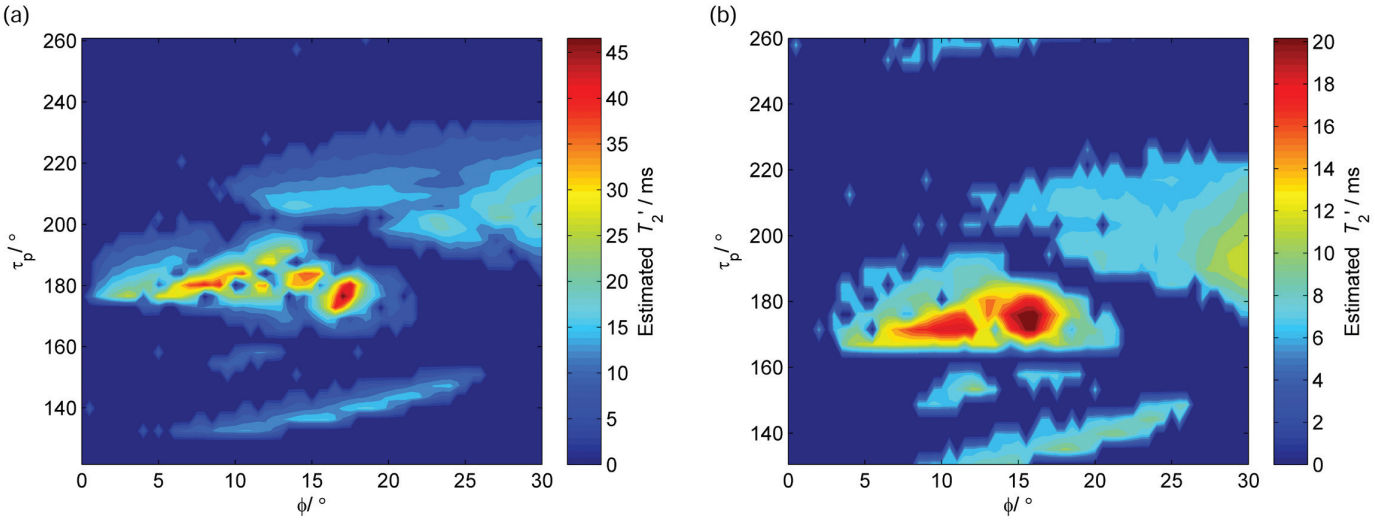

Figure 1. Parameter maps of T_2' as a function of pulse phase, ϕ, and pulse width, τ_p, for TPPM decoupling at 170 kHz RF nutation rate, 62.5 kHz MAS and two different magnetic fields: (a) 500 MHz (Durham) and (b) 850 MHz (Facility).

Figure 1 compares some of the results obtained at 850 MHz with results obtained under similar conditions, of high RF and ultra-fast sample spinning, at lower field (500 MHz). As predicted by theory and numerical simulations, the key term responsible for the features of these plots is a cross term between the ^{13}C,^{1}H dipolar coupling and the ^{1}H chemical shift anisotropy (CSA). The impact of these terms scales with the magnetic field, and correspondingly the decoherence times are significantly reduced at 850 MHz; although the overall shape and position of the decoupling optima are relatively insensitive to the magnetic field.

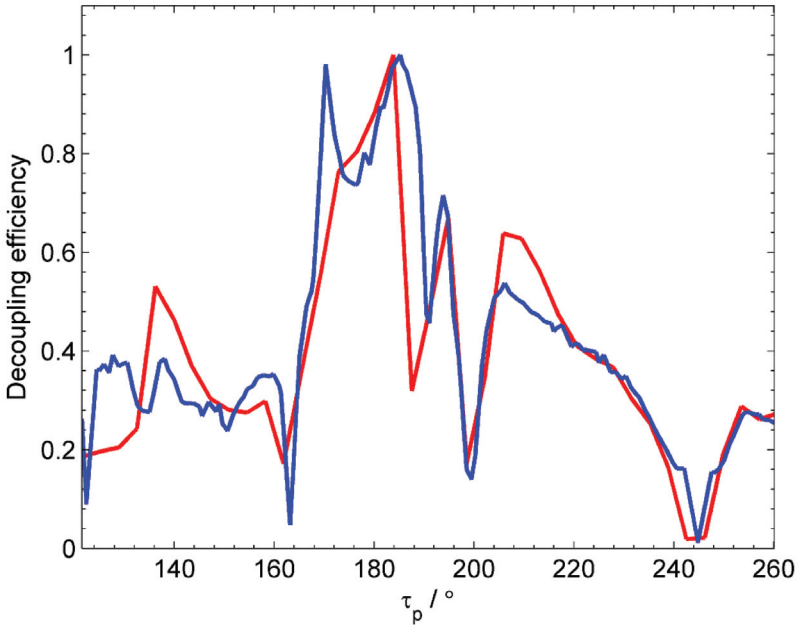

Figure 2. TPPM decoupling performance as a function of pulse width, τ_p (expressed as nutation angle) at 170 kHz RF, 62.5 kHz MAS and ϕ=15°: (blue) simulation and (red) experiment.

As shown in Figure 2, we have been able to reproduce the characteristic shape of the decoupling optima observed experimentally using numerical simulations of decoherence times under simultaneous magic-angle spinning and RF decoupling; the figure corresponds to a slice through the parameter map of Figure 1a at ϕ=15°. Similarly comparison of simulations at 850 MHz and 500 MHz show a factor of 1.8 difference in peak decoherence times, in agreement with the predictions above. Once we are confident that all the experimental variables, such as transient effects associated with switching RF phase, have been captured, the simulations will provide the robust predictive tool for decoupling performance that is currently missing. The next stage of the project is to identify novel decoupling sequences that are effective at high fields both from simulation and experimental optimisation.

References

1. Scholz, I.; Hodgkinson, P.; Meier, B.; Ernst, M. *J. Chem. Phys.* **2009**, *130*, 114510.
2. Zorin, V. E.; Brown, S. P.; Hodgkinson, P. *J. Chem. Phys.* **2006**, *125*, 144508.
3. Zorin, V. E.; Ernst, M.; Brown, S. P.; Hodgkinson, P. *J. Magn. Reson.* **2008**, *192*, 183.

Use of Double-Rotation (DOR) ^{11}B NMR to Identify Connectivity in Borate Crystals and Glasses

Diane Holland, Ray Dupree and Oliver Alderman

Department of Physics, University of Warwick

Overview

Borate crystals and glasses are remarkable for the variety of superstructural ring units making up their networks, in which boron can be present in both 3- and 4-coordinated states ([BO_3], B^{III} and [BO_4], B^{IV}). Crystalline $K_2B_4O_7$ (Figure 1) is an excellent example of their complexity, containing a combination of both single (ditriborate – 1 B^{III} and 2 B^{IV}) and fused (diborate – 2 B^{III} and 2 B^{IV}) rings which are connected to each other and also to non-ring [BO_3] planar triangle units (Figure 1). These complex arrangements are also thought to give rise to the unusual level of medium range order in borate glasses - the origin of our interest.

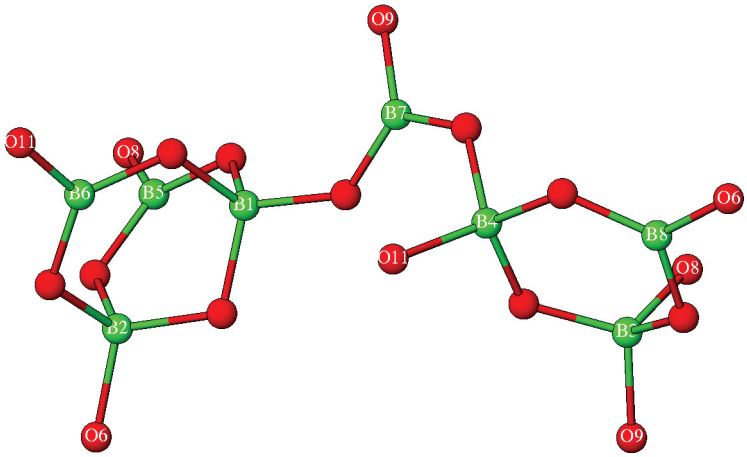

Figure 1. The superstructural unit found in c-$K_2B_4O_7$, containing (from left to right) a diborate unit; a non-ring [BO_3] unit; and a ditriborate unit. There are 8 crystallographically distinct B atoms and the unit is linked to others by the labelled O atoms.

(a) Superstructural units in borate crystals and glasses

In a previous 850 experiment, we demonstrated the increased resolution obtainable using Double Rotation (DOR) NMR for ^{11}B in both borate crystals and glasses (e.g. Pyrex[1]). More recently, both 1D and spin-diffusion (SD) ^{11}B DOR NMR were carried out on six crystalline borates to begin to establish a fingerprint database of the DOR shifts and to attempt assignment of the 1D peaks to crystallographically distinct B sites on the basis of the cross-peaks formed in SD. The MAS and 1D DOR spectra of some example borate crystals, shown in Figure 2, give an idea of the high resolution possible under DOR at 850 MHz, with linewidths as small as ~0.3 ppm and no overlap of the spinning sidebands with the main peaks. Figure 3a shows the improved resolution of the α-BaB_4O_7 ^{11}B DOR spectrum at 20 T compared with lower fields, whilst Figure 3b shows how the different quadrupole parameters , P_Q, for the B(III) sites, along with the isotropic shift, δ_{iso}, can be extracted from a multifield measurement.[2]

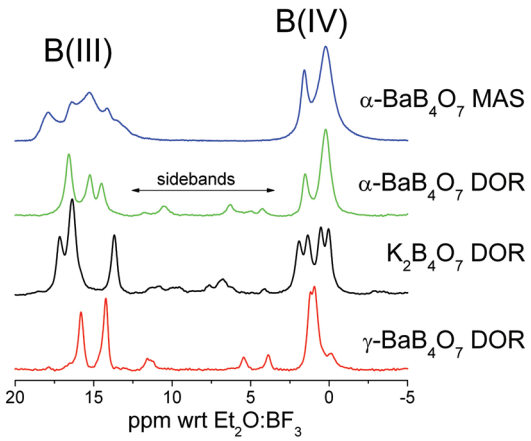

Figure 2. ^{11}B spectra from borate crystals:

- α-BaB_4O_7 MAS and DOR show the resolution of the B(III) sites under DOR where the second order quadrupole lineshape contribution is removed. This crystal contains di-triborate and di-pentaborate superstructural units.

-$K_2B_4O_7$ shows the resolution possible with DOR – peaks ~ 0.5 ppm wide. This crystal contains di-triborate and diborate superstructural units plus connecting [BO_3] units.

- γ-BaB_4O_7 is a BaB_4O_7 polymorph of unknown structure, showing clear differences from the α- form.

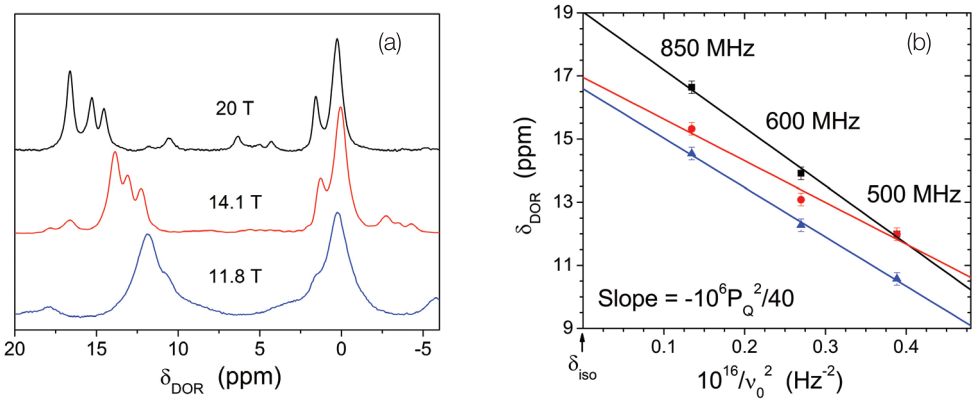

Figure 3. (a) DOR spectra of α-BaB_4O_7 obtained at different fields; (b) DOR shift plotted as a function of $10^{16}/\nu_0^2$ to obtain P_Q.

(b) Spin diffusion DOR ^{11}B NMR of $K_2B_4O_7$ and γ-BaB_4O_7 and identification of superstructural units

Figure 4a shows the 1D DOR spectrum from $K_2B_4O_7$ with the vertical lines representing the CASTEP calculated peak positions (after correction for the quadrupole induced shift) for the different boron sites in the structure. The SD spectrum (15 ms mixing time Figure 4b)) shows a cross-peak between B2 and B5,6 (as identified by CASTEP) which involves exchange within the diborate ring (Figure 1). The SD experiments sometimes showed *negative* cross-peaks (B8↔B3,B4 and B7↔B3,B4) as well as positive cross-peaks in the 2D spectra. At longer mixing time the intensity of these negative cross-peaks becomes increasingly positive and the full behaviour will be investigated further in a subsequent experiment.

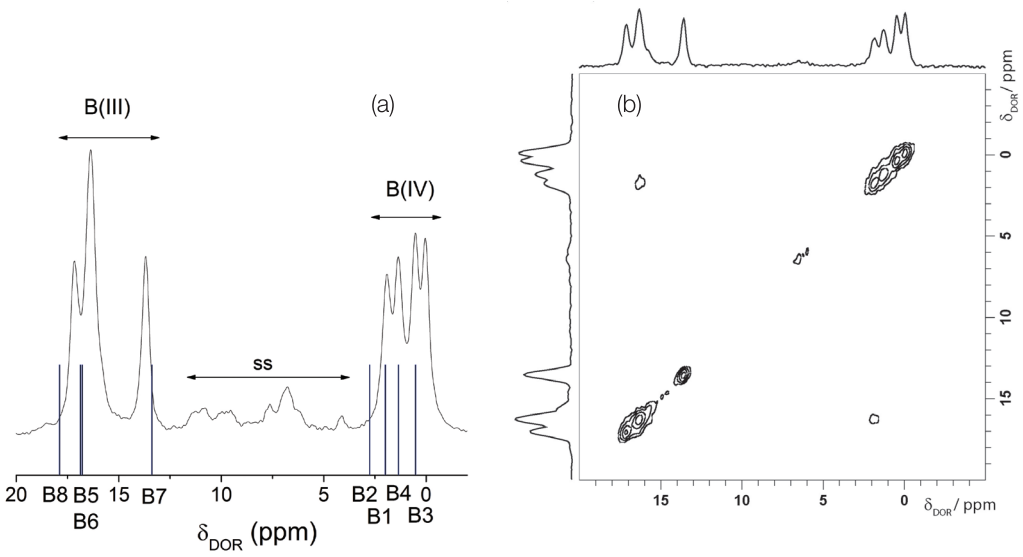

Figure 4. $K_2B_4O_7$ (a) 1D DOR spectrum and peak assignments from positions calculated using CASTEP; (b) SD DOR spectrum at 15 ms mixing time showing cross-peak between B2 and B5,6.

References

1. Howes, A. P.; Vedishcheva, N. M.; Samoson, A.; Hanna, J. V.; Smith, M. E.; Holland, D.; Dupree, R. *Phys. Chem. Chem. Phys.* **2011**, *13*, 11919.
2. Alderman, O. L. G.; Iuga, D.; Howes, A. P.; Holland, D.; Dupree, R. *Phys. Chem. Glasses* (in press)

Characterisation of Strontium and Magnesium Substituted Fluorapatite

Natalia Karpukhina[1], Robert V. Law[2], Dinu Iuga[3] and Robert G. Hill[1]

[1]*Barts and The London School of Medicine and Dentistry, Queen Mary University of London,*
[2]*Department of Chemistry, Imperial College London,*
[3]*Department of Physics, University of Warwick*

Overview

Strontium Sr^{2+} and magnesium Mg^{2+} cationic substitution in apatite $Ca_5(PO_4)_3OH$ are two particularly significant substitutions in the field of biomaterials and biominerals. Strontium promotes bone formation significantly improving osseointegration, which is used therapeutically for osteoporotic treatment. Strontium containing biomaterials, in particularly bioglasses where all calcium is replaced with strontium, react rapidly with body fluid producing a reactive apatite layer that integrates with biological tissue of bone. Magnesium Mg^{2+} ions are present the simulated body fluid (SBF), a buffer solution where bioactivity of a material is tested, and its inhibiting effect on apatite formation and remineralisation is often discussed. Thus, the effects of two cations substituting for Ca^{2+} on mineralisation of apatite are opposite to each other.

Two crystallographic calcium sites exist in the apatite lattice. As Sr^{2+} is slightly bigger than Ca^{2+} it is thought that Sr^{2+} would preferentially substitute on the Ca(I) site, the 9-fold coordinated Ca^{2+} ions. However, formation of mixed Ca/Sr coordination of the fluoride has been observed in the Ca/Sr substituted fluorapatites,[1,2] which indicates that Sr^{2+} also substitutes for the Ca(II) site. Mg^{2+} is smaller than Ca^{2+} and can go for the Ca(II) site[3] with the smaller coordination number 7. However, no significant changes in the Ca(II) site have been observed indirectly via ^{19}F MAS NMR in fluorapatite on Ca/Mg substitution from our own data.

Ultra high magnetic field (20T) of the UK National solid-state NMR facility together with recently developed sensitivity enhancing NMR techniques[4-7] offers a great opportunity to probe directly local environment of the low-gamma nuclei such as ^{43}Ca, ^{87}Sr, ^{25}Mg and obtain more structural information on Sr- or Mg- substituted fluorapatites in addition to the ^{31}P and ^{19}F MAS NMR data. Recent ^{43}Ca NMR study performed on hydroxyapatite[5,6] showed that two distinct calcium sites assigned to Ca(I) and Ca(II) can be resolved at natural abundance of the nucleus. Furthermore, with ^{43}Ca NMR a preference in cationic substitution for Ca(I) or Ca(II) specific sites can be investigated as was shown for the Pb^{2+} and Mg^{2+} substitutions in hydroxyapatite.[3,7] The aim of this project was to investigate type of strontium or magnesium cation substitution in fluorapatite by performing ^{43}Ca, ^{87}Sr and ^{25}Mg NMR at the 850MHz solid-state NMR facility.

Results

Figure 1 shows ^{43}Ca MAS NMR data for the fluorapatite and Sr- and Mg- substituted fluorapatites with different percentage 10-50% of substitution plotted in comparison with the hydroxyapatite spectrum.

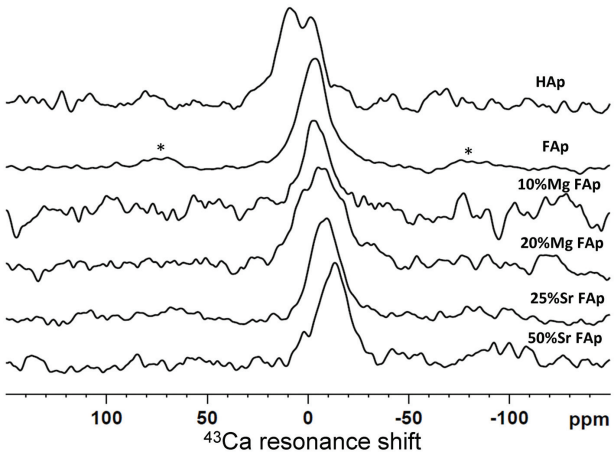

Figure 1. ^{43}Ca MAS NMR spectra of fluorapatites and hydroxyapatite (top) with the Sr- and Mg- substitution degree indicated in percentage.

At 20 T it has been reported previously that the ^{43}Ca NMR linewidth is dominated by chemical shift distribution. It is seen that ^{43}Ca NMR signal is different in fluorapatite compared to the previously reported hydroxyapatite; the two signals strongly overlap and a single broad non-resolved ^{43}Ca signal was observed here. Extensive ^{43}Ca NMR study for a broad range of inorganic compounds[8] revealed that ^{43}Ca chemical shift is sensitive to the small structural modifications. It is therefore possible that switch from OH^- to F^- should significantly alter the spectrum of apatite. The chemical shift of the Ca(II) site is therefore affected the most by the strongly electronegative F^- ion. To a much lesser extent the chemical shift of the Ca(I) site is also affected.

In Figure 2, ^{87}Sr NMR data of Sr-substituted fluorapatite are presented. Broadening of the signal is clearly observed until more than half of Ca is substituted with Sr. However, the width of the ^{87}Sr NMR static line of the 25%Sr FAp is significantly smaller compared to the recently observed in SrP_2O_6 and strontium malonate;[9] the estimated quadupolar coupling constant C_Q in FAp is not more than 20MHz. More accurate results will be obtained from the simulation.

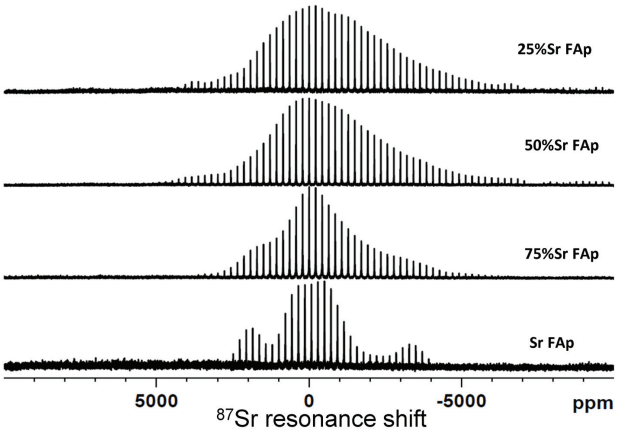

Figure 2. ^{87}Sr NMR spectra (static) of Sr-substituted fluorapatites. Percentage of Sr-substitution is indicated.

The ^{25}Mg MAS NMR spectra in Figure 3 showed complex magnesium environment in the fluorapatite with at least two different sites. These spectra differ from the data recently reported[1], though the data presented here were obtained at a higher spinning speed 14 kHz.

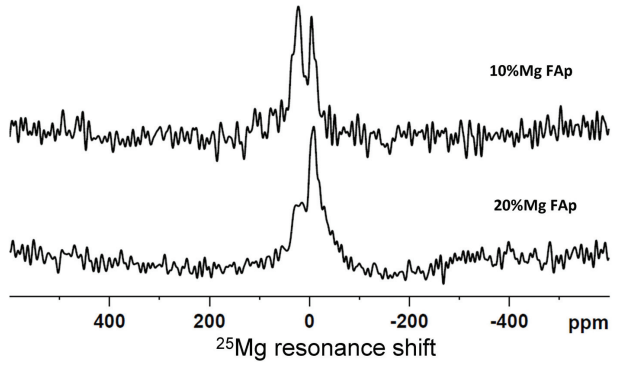

Figure 3. ^{25}Mg MAS NMR spectra of 10% and 20% Mg-substituted fluorapatites.

Further identification and interpretation of these ultra high field solid-state NMR results is aim of the ongoing investigation.

References

1. Cho, G.; Chau, C.-N; Yesinowski, J. P. *J. Phys. Chem. C* **2008**, *112*, 6165.
2. Hill, R.; Calver, A.; Skinner, S., Stamboulis, A.; Law, R. *Bioceramics 18, Key Engineering Materials* **2006**, *309-311*, 305.
3. Laurencin, D.; Almora-Barrios, N.; de Leeuw, N.; Gervais, C.; Bonhomme, C.; Mauri, F.; Chrzanowski, W.; Knowles, J. C.; Newport, R. J.; Wong, A.; Gan, Z.; Smith, M. E. *Biomaterials* **2011**, *32*, 1826.
4. Bowers, G. M.; Lipton, A. S.; Mueller, K. T. *Solid State Nucl. Magn. Reson.* **2006**, *29*, 95.
5. Laurencin, D.; Wong, A.; Dupree, R.; Smith, M. E. *Magn. Reson. Chem.* **2008**, *46*, 347.
6. Laurencin, D.; Wong, A.; Hanna, J. V.; Dupree, R., Smith, M. E. *J. Am. Chem. Soc.* **2008**, *130*, 2412.
7. Pizzala, H.; Caldarelli, S.; Eon, J.-G.; Malta Rossi, A.; Laurencin, D.; Smith, M. E. *J. Am. Chem. Soc.* **2009**, *131*, 5145.
8. Lin, Z.; Smith, M. E.; Sowrey, F. E.; Newport, R. J. *Phys. Rev. B* **2004** *69*, 224107.
9. Bonhomme, C.; Laurencin, D.; Hanna, J. V.; Smith, M. E. The UK 850 MHz Solid-State NMR Faciltiy Annual Report **2010**, 48.

^{43}Ca MQ MAS Investigation of Bioactive Glass

Richard A. Martin[1], Gregory J. Rees[2], Dinu Iuga[2], Mark E. Smith[2] and John V. Hanna[2]

[1]*Aston Research Centre for Healthy Ageing & School of Engineering, Aston University,*
[2]*Department of Physics, University of Warwick*

Overview

Bioactive CaO-Na_2O-SiO_2-P_2O_5 glasses are of great importance due to their ability to chemically bond to bone and stimulate new bone growth.[1] Under physiological conditions these materials release essential elements such as Ca and P, followed by Si, which promote the formation of hydroxyapatitie, HA, the naturally occurring mineral present in both teeth and bones. The release of calcium is thought to be the first step in the formation of new bone. As the glass dissolves Ca^{2+} and PO_4^{3-} groups then precipitate from the solution to form an amorphous calcium phosphate layer which then crystallizes to form hydroxyapatite.

In order to be able to model and predict the behaviour of these materials, and thereby optimise these glasses, it is necessary to understand the local structure of the glass, particularly the local calcium environment. However the local environment that calcium adopts within bioactive glasses is not well understood. Calcium can adopt a wide range of environments in its crystalline phases; for example, the number of oxygen atoms surrounding calcium varies from 6.67 in Wollastonite (CaO-SiO_2) to 8 in Pseudowollastonite (the high temperature phase of CaO-SiO_2), whilst calcium oxide and hydroxyapatite have 6 and 8.4 oxygen atoms per calcium respectively. The corresponding Ca–O bond lengths also vary over the range 2.28 - 2.72 Å.[2] It is anticipated therefore that calcium will have a complex local environment in amorphous bioactive glasses. Furthermore the Ca-O correlations overlap in real space with the Na-O, O-(Si)-O and O-(P)-O correlations making it difficult to unambiguously determine the Ca-O correlations from neutron and X-ray diffraction patterns.

The importance of strontium in bioactive glasses has also become of increasing interest in recent years due to its effect on bone. Strontium is known to stimulate the bone-forming osteoblast cells and inhibit the bone-resorbing osteoclasts as well as reducing bone desorption, and thus increase bone formation and mass, without having an effect on the mineralization of bone.

Experimental

Glassy $(SiO_2)_{49.46}(Na_2O)_{26.38}(P_2O_5)_{1.07}(CaO)_{23.08}$ and $(SiO_2)_{49.46}(Na_2O)_{26.38}(P_2O_5)_{1.07}(CaO)_{11.54}(SrO)_{11.54}$ samples were therefore investigated using ^{43}Ca (I = 7/2) NMR. Due to the low natural abundance of ^{43}Ca the samples were partially enriched (~ 5%).

A triple-quantum MAS (3QMAS) experiment was undertaken with a 3.2 mm double-resonance Bruker MAS probe at a spinning frequency of 10 kHz. MQMAS experiments were recorded using a Z-filter pulse sequence.[3] A non-selective 4.5 μs excitation and 1.25 μs conversion pulse was followed by two 25.00 μs central-transition selective π/2 pulse, collecting 96 transients for each of the 128 slices with a recycle interval of 5 s.

Results

Figure 1 presents the ^{43}Ca MQ MAS NMR spectra, recorded at B_0 = 20.0 T. As shown the Ca spectra are readily resolved at 57.55 MHz. Preliminary assignments have been made in line with results of Shimoda *et al.* [4] and indicate that calcium is predominately in a distorted octahedral environment. Molecular dynamics simulations are being conducted to assist with the interpretation.

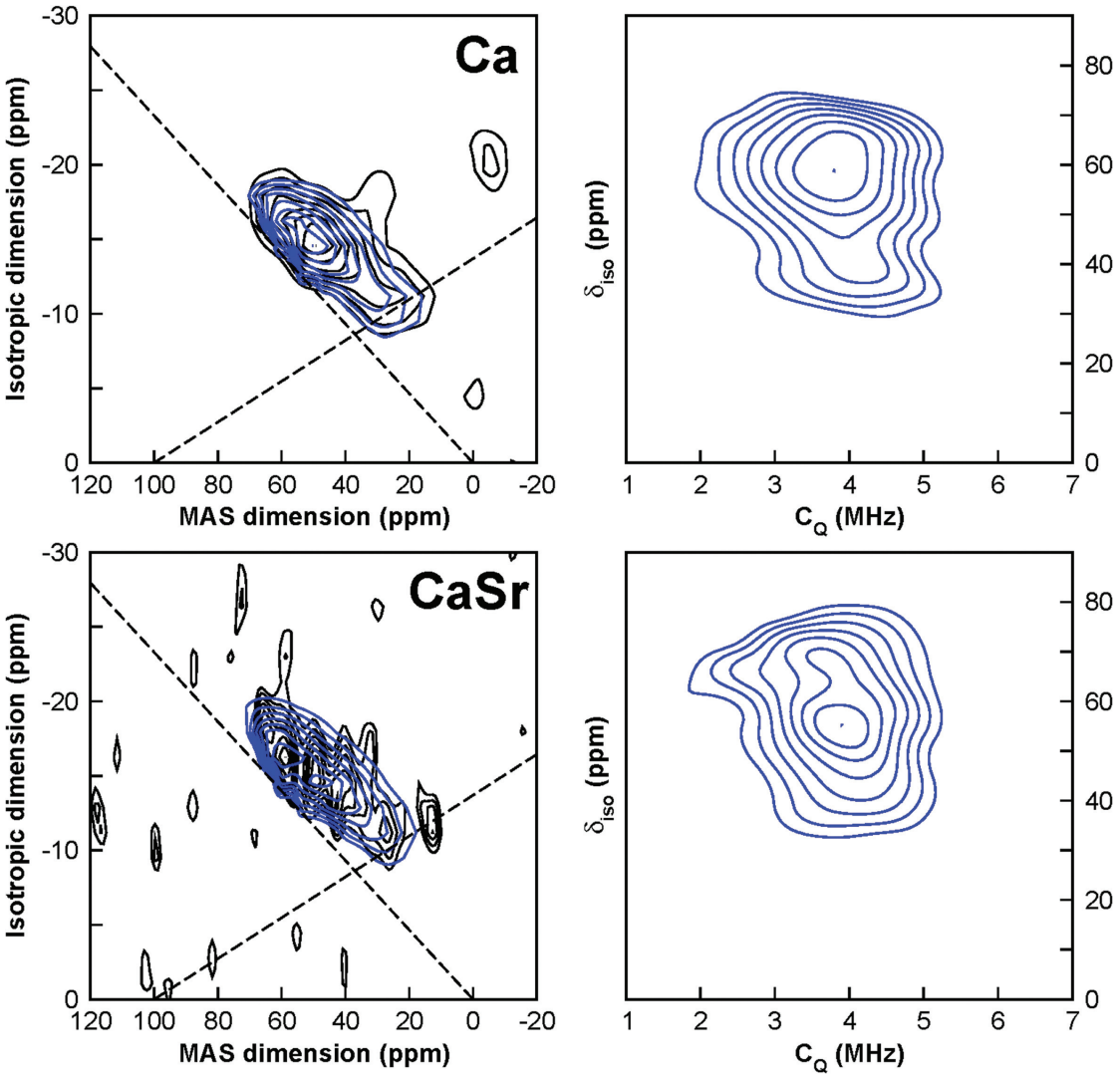

Figure 1. ^{43}Ca 3QMAS spectra of calcium bioglass (top left) and calcium / strontium bioglass (bottom left). Mathematical inversion of the 3QMAS spectra to give the quadrupolar coupling constant (C_Q) and isotropic shift (δ_{iso}) axis of the calcium bioglass (top-right) and calcium / strontium bioglass (bottom-right).

References

1. Hench, L. L. *J. Mater. Sci.: Mater. Med.* **2006**, *17*, 967.
2. Lin, Z.; Smith, M. E.; Sowrey, F. E.; Newport, R. J. *Phys. Rev. B* **2004**, *69*, 224107.
3. Amoureux, J.-P.; Fernandez, C.; Steuernagel, S *J. Mag. Reson. Series A* **1996**, *123*, 116.
4. Shimoda, K.; Tobu, Y.; Shimoikeda, Y.; Nemoto, T.:, Saito, K. J. *Magn. Reson.* **2007**, *186*, 1569.

Mapping the Glycosaminoglycan Binding Site in Alzheimer's Amyloid Fibrils and Prefibrillar Oligomers by High-Field ^{13}C Solid-State NMR

Jillian Madine,[1] Maya Pandya,[2] Sheena Radford[2] and David Middleton[1]

[1]*Institute of Integrative Biology, University of Liverpool,*
[2]*Astbury Centre for Structural Molecular Biology, University of Leeds*

Overview

Several proteins and peptides are known to assemble into micrometre-long amyloid fibrils that are the pathological hallmark of human disease. Various factors, including polysaccharides of the glycosaminoglycan (GAG) class, are ubiquitously associated with amyloid *in vivo* and can profoundly affect amyloid growth kinetics and pathogenicity. One of the most important challenges in developing a molecular understanding of amyloid pathogenicity is to structurally characterize the transitory oligomeric intermediates that are formed prior to the mature, insoluble fibrils in the assembly process.[1] There is mounting evidence that soluble oligomeric species, rather than mature insoluble fibrils, are the culprits of toxicity.[2-3]

The aim of this work is to use ^{13}C solid-state NMR at high field to provide the first insights into the GAG recognition sites within fibrils and oligomers of $A\beta_{1-40}$, one of the polypeptides famously associated with Alzheimer's disease.

Results

First, ^{13}C DARR solid-state NMR was used to monitor GAG binding to uniformly ^{13}C labelled $A\beta_{1-40}$ fibrils in two morphologies, with two-fold and three-fold molecular symmetry, reported by Tycko and co-workers.[4-5] The two fibril strains were obtained by seeding as reported elsewhere (seeds kindly provided by Dr R. Tycko). The excellent resolution and sensitivity of the high-field DARR spectra of seeded $A\beta_{1-40}$ fibrils permitted approximately 70 % of the spectra to be assigned with reference to the chemical shift values previously tabulated.[4-5]

For the 3-fold symmetry fibrils, several of the cross-peaks show movements and/or changes in intensity after the addition of the GAG analogue heparin (a 5 kDa fraction) in a 5-fold molar excess (Figure 1a). The same changes occur when the fibrils are grown in the presence of heparin. By contrast, little or no change in the spectrum for the two-fold fibrils occurs after adding heparin (Figure 1b). These results are supported by biochemical measurements of heparin binding to the two fibril strains. **The first key finding of this work is thus that GAG binding to $A\beta_{1-40}$ fibrils is highly strain-specific**.

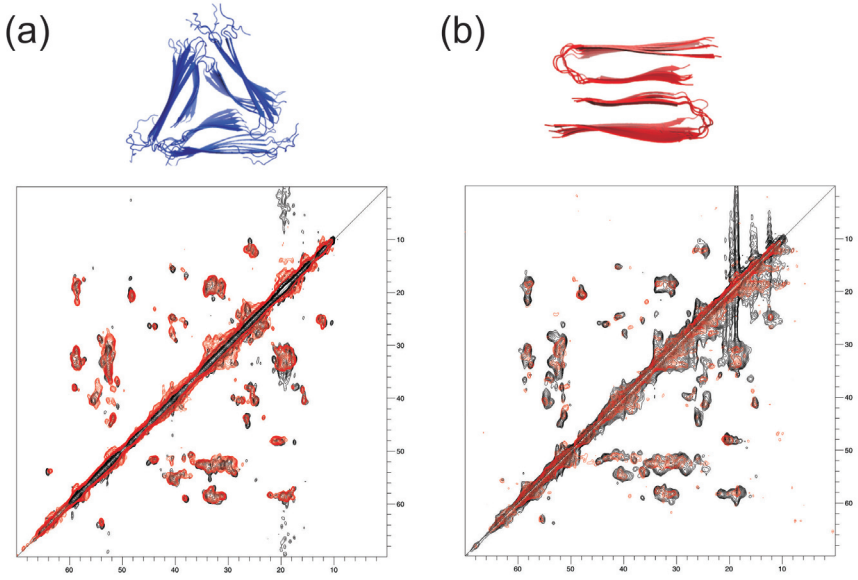

Figure 1. ^{13}C DARR spectra of $A\beta_{1-40}$ fibrils before (black) and after (red) addition of 5 kDa heparin. (a) Three-fold symmetry fibrils. (b) Two-fold symmetry fibrils.

With reference to the chemical shift changes, a model has been proposed for the interaction between heparin and the three-fold symmetry $A\beta_{1\text{-}40}$ fibrils. **The second key finding of this work is that the heparin binding sites lie at the junctions between neighbouring $A\beta_{1\text{-}40}$ molecules (Figure 2).**

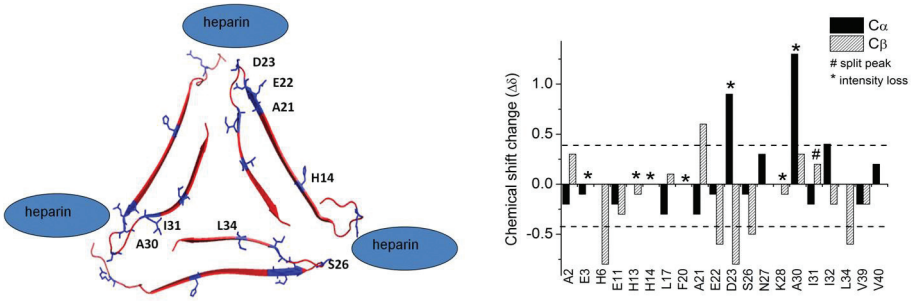

Figure 2. Model for the GAG binding site in the three-fold symmetry $A\beta_{1\text{-}40}$ fibrils based on chemical shift mapping.

The next stage of the work was to investigate the effect of GAG binding on the structure of soluble $A\beta_{1\text{-}40}$ oligomers. Preparation of oligomers by evaporation from hexafluoroisopropanol yields spherical species which are stable for the duration of the NMR experiments.[6] DARR spectra of the oligomers exhibit broad lines which indicate that the oligomers are less highly ordered (or more polydisperse) than the mature fibrils, and further experiments will be necessary to assign the spectrum. The unassigned spectrum nevertheless shows very interesting features which are related to heparin binding. Many of the cross peaks indicate large changes in ^{13}C chemical shifts after adding a 5-fold excess of heparin, much greater than seen for the fibrils. **The data are thus consistent with substantial remodelling of the oligomers by heparin.** Furthermore, a new set of cross-peaks appear in the presence on heparin, and these cannot be ascribed to any amino acid residues within the polypeptide. The cross-peaks have been observed reproducibly and appear to represent intermolecular heparin-Aβ dipolar couplings as all other interpretations have been ruled out.

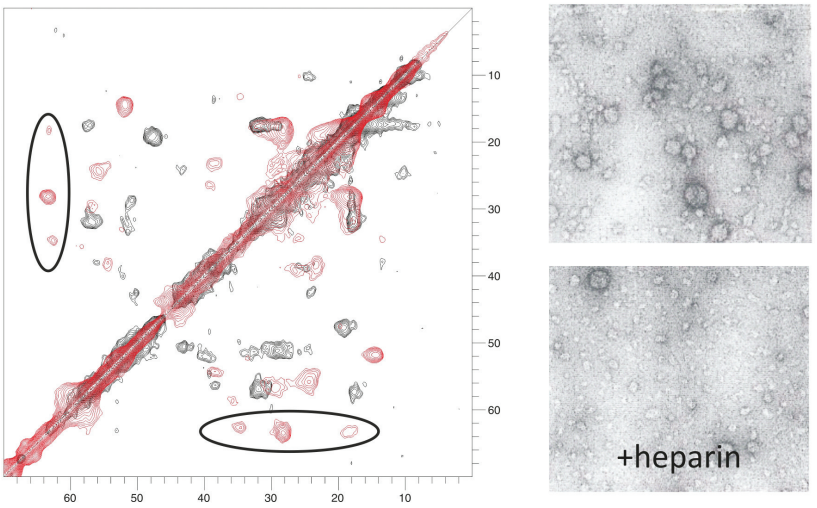

Figure 3. Transmission electron micrographs and ^{13}C DARR spectra of $A\beta_{1\text{-}40}$ oligomers before and after the addition of 5 kDa heparin. The circled area indicates new cross-peaks appearing after the addition of heparin.

References

1. Kirkitadze, M. D.; Condron, M. M.; Teplow, D. B. *J. Mol. Biol.* **2001**, *312*, 1103.
2. Shankar, G. M.; Li, S. M.; Mehta, T. H.; Garcia-Munoz, A.; Shepardson, N. E.; Smith, I.; Brett, F. M.; Farrell, M. A.; Rowan, M. J.; Lemere, C. A.; Regan, C. M.; Walsh, D. M.; Sabatini, B. L.; Selkoe, D. J. *Nature Medicine* **2008**, *14*, 837.
3. Orte, A.; Birkett, N. R.; Clarke, R. W.; Devlin, G. L.; Dobson, C. M.; Klenerman, D. *Proc. Natl. Acad. Sci. USA* **2008**, *105*, 14424.
4. Petkova, A. T.; Yau, W. M.; Tycko, R. *Biochemistry* **2006**, *45*, 498.
5. Paravastu, A. K.; Leapman, R. D.; Yau, W. M.; Tycko, R. *Proc. Natl. Acad. Sci. USA* **2008**, *105,* 18349.
6. Haupt, C.; Leppert, J.; Rönicke, R.; Meinhardt, J.; Yadav, J. K.; Ramachandran, R.; Ohlenschläger, O.; Reymann, K. G.; Görlach, M.; Fändrich, M. *Angew. Chem. Int. Ed.* **2012**, *51*, 1576.

^{17}O Solid-State NMR of the Aluminophosphate SIZ-4

John M. Griffin, Valerie R. Seymour, Daniel M. Dawson, Sharon E. Ashbrook and Russell E. Morris

School of Chemistry and EaStCHEM, University of St Andrews

Overview

Zeolites, including aluminosilicates and aluminophosphates (AlPOs), are an important class of microporous materials with applications in medicine, catalysis, separation and ion exchange. Solid-state NMR is a valuable tool for studying such materials, as the basic constituents of their frameworks are NMR-active nuclei: ^{29}Si, ^{27}Al, ^{31}P and ^{17}O. Whilst many of these nuclei are commonly studied, the exception is ^{17}O, for which there are few studies on framework materials. This is largely due to the low natural abundance (0.037%) and high spin quantum number (I = 5/2) of ^{17}O, meaning that more complex two-dimensional NMR experiments such as MQMAS are required to obtain high-resolution spectra. Although financially costly, zeolites may be enriched using either ^{17}O-enriched O_2 or H_2O. However, enrichment levels obtained using post-synthetic approaches are often low. This difficulty in enrichment with ^{17}O is a major obstacle to full characterisation of zeolites by NMR. In recent years we have developed the use of ionic liquids in the synthesis of zeolites. This method uses only microlitre quantities of water, allowing for a more cost-effective ^{17}O enrichment process. In this project, we demonstrate the use of high-field ^{17}O NMR to study as-prepared and calcined samples of the ionothermally-prepared AlPO framework, SIZ-4. Our results demonstrate the feasibility of this method for the study of ^{17}O-enriched AlPO and other zeolite frameworks, and this approach opens up many new possibilities for detailed studies of the materials themselves and how the structure is perturbed upon exposure to adsorbed species or catalytic substrates.

Results

The structure of as-prepared SIZ-4 consists of twelve distinct O species, and the calcined material contains four distinct bridging O species in Al-O-P linkages. First-principles DFT calculations predict ^{17}O quadrupolar coupling constants, C_Q, of 5.7-6.5 MHz for all O species in the as-prepared and calcined structures. To remove the second-order quadrupolar broadening of the ^{17}O resonances, ^{17}O DOR NMR spectra were recorded for the two materials. In these spectra, shown in Figures 1a and 1b, the broadened central transition lineshapes are split into a number of isotropic resonances surrounded by spinning sidebands. Simulated spectra based on the calculated NMR parameters (which show just isotropic resonances) are in good agreement with the experimental results. In principle, the ^{17}O DOR NMR spectra of SIZ-4 contain information relating to the magnitudes and relative orientations of both the quadrupolar and chemical shielding tensors. However, owing to the overlap of the resonances and spinning sidebands it is not straightforward to extract this information. In order to obtain further insight into the magnitudes of the quadrupolar interactions for the different sites, two-dimensional ^{17}O MQMAS NMR spectra were recorded in total times of 83 and 59 hours for as-prepared and calcined SIZ-4, respectively. In these spectra, shown in Figures 1c and 1d, distinct groups of resonances are resolved in the indirect δ_1 dimension.

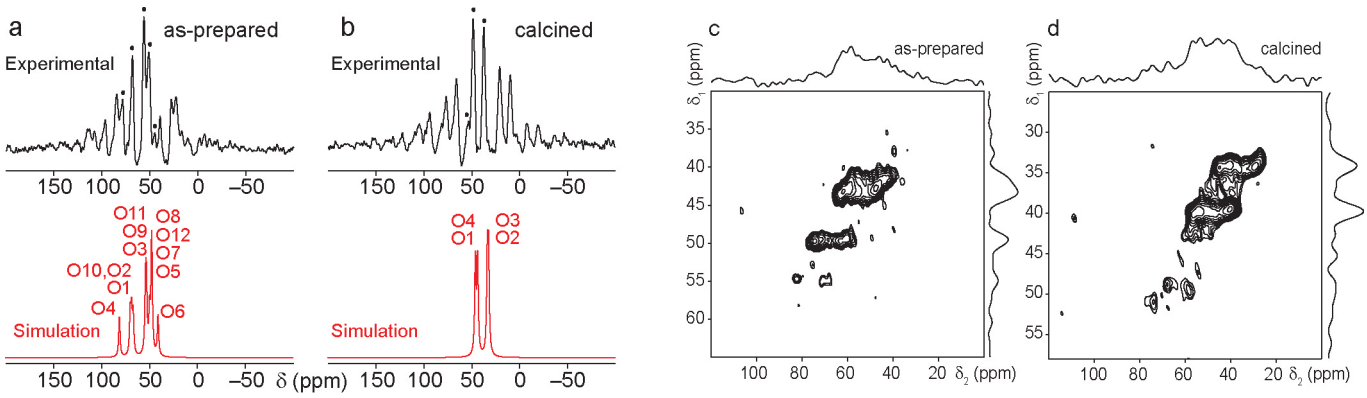

Figure 1. ^{17}O DOR (experimental and simulated) and MQMAS NMR of (a,c) as-prepared and (b,d) calcined SIZ-4. All spectra were recorded at 20.0 T, with a DOR outer rotor spinning frequency of 1.6 kHz or MAS frequency of 20 kHz.

High-Field Solid-State ^{13}C NMR Study of Cu(II)-Based MOFs

Daniel M. Dawson, Sharon E. Ashbrook and Russell E. Morris

School of Chemistry and EaStCHEM, University of St Andrews

Overview

Metal-organic frameworks (MOFs) are a class of microporous materials composed of metal-based units connected by organic "linkers". MOFs typically have > 50% free volume that may be used for gas storage, catalysis, *etc.* MOFs can be studied by X-ray diffraction, but this requires long-range order, which is not guaranteed for guest-loaded MOFs. Solid-state NMR does not require long-range order and can probe local structure and dynamics. However, many MOFs contain paramagnetic metal ions, which complicate acquisition and assignment of NMR spectra. Here, high-field ^{13}C NMR spectra of the Cu^{2+}-based MOFs, HKUST-1 and STAM-1, were acquired with the aim of using 1D spectra and T_1 values to aid assignment.

^{13}C MAS NMR of HKUST-1

HKUST-1 is a simple MOF containing Cu dimers linked by benzene-1,3,5-tricarboxylate (btc), leading to a large-pore structure. Its local structure is similar to STAM-1 (see below). The ^{13}C NMR spectrum contains three resonances at 850, 227 and –50 ppm, which move to 795, 228 and –78 ppm upon dehydration.

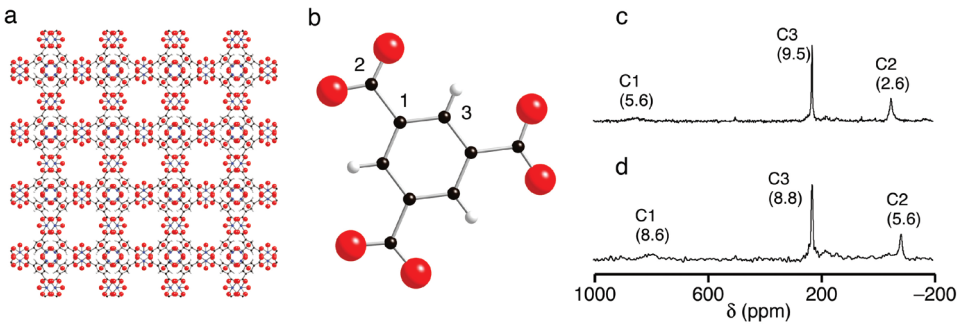

Figure 1. (a) Structure of HKUST-1. (b) Structure of btc and numbering scheme used in assignment. ^{13}C (58 kHz MAS, 20 T) NMR spectra of HKUST-1 (c) and dehydrated HKUST-1 (d). T_1 values measured at 20.0 T (in ms) are given in parentheses.

^{13}C MAS NMR of STAM-1

STAM-1 contains the same dimers as HKUST-1, linked by the methyl ester of btc (mmbtc). The mmbtc gives the MOF unusual properties, as both hydrophobic and hydrophilic pores are present. The ^{13}C NMR spectra contain resonances between 850 and –50 ppm in STAM-1 and 795 to –78 ppm upon dehydration. Assignment was attempted by measurement of T_1 relaxation constants, which depend on B_0 and C-Cu distance. However, T_1 values did not vary significantly with field, and were short (1-20 ms) for both MOFs. Therefore, assignment by T_1 values alone was not possible but, in combination with cross-polarisation and isotopic labeling, spectra were assigned as shown.

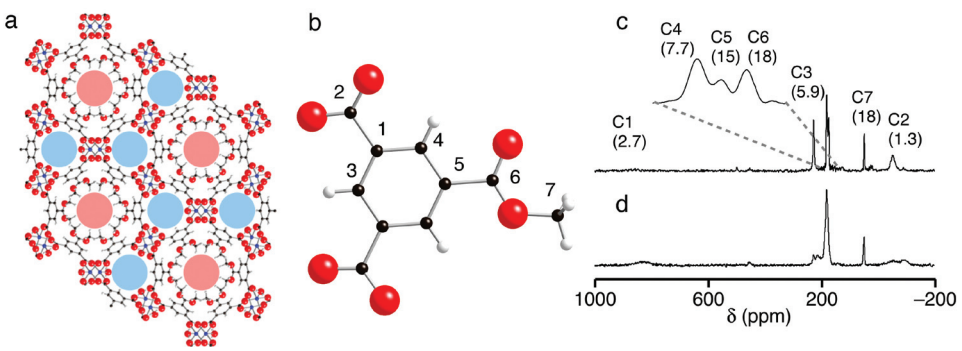

Figure 2. (a) Structure of STAM-1 with hydrophobic and hydrophilic pores coloured, respectively, pink and blue. (b) Structure of mmbtc and numbering scheme used in assignment. ^{13}C (58 kHz MAS, 20 T) NMR spectra of STAM-1 (c) and dehydrated STAM-1 (d). T_1 values at 20.0 T (in ms) are given in parentheses.

^{87}Sr Solid-State NMR of Biomaterials, and ^{43}Ca and ^{137}Ba Solid-State NMR of Organic-Inorganic Hybrid Materials

Danielle Laurencin,[1] Christel Gervais,[2] Christian Bonhomme,[2] John V. Hanna[3] and Mark E. Smith[3]

[1]*Institut Charles Gerhardt de Montpellier, France,*
[2]*Department of Chemistry, Pierre and Marie Curie University Paris 06, France,*
[3]*Department of Physics, University of Warwick*

Overview

Calcium and strontium are major components of natural and synthetic biomaterials. Indeed, calcium is the main cation in bone, whereas strontium has been shown to be an important element in the treatment of osteoporosis, and it is now incorporated in several bioceramics and bioglasses. It is important to understand the local structure around both of these cations in biomaterials, in order to be able to rationalize and improve their properties. The same questions can be raised for the characterization of Sr and Ca environments in organic/inorganic hybrid materials. However, both ^{43}Ca and ^{87}Sr solid-state NMR experiments are challenging: calcium-43 is a low-γ nucleus (ν_0 = 57.2 MHz at 19.9 T) with low natural abundance (0.14%), whereas strontium-87 has a strong nuclear quadrupole moment (~8 times higher than that of ^{43}Ca), a low-γ (ν_0 = 36.8 MHz at 19.9 T) and a moderate natural abundance (7.0%). In this work, calcium-containing hybrid materials, as well as Sr-doped bioglasses (CaO-SiO_2, SrO: 7 wt %) were successfully studied by ^{43}Ca RAPT MAS and ^{87}Sr DFS WURST QCPMG VOCS experiments, respectively. We demonstrate also that ^{87}Sr labelling opens new perspectives for the detection of ^{87}Sr sites strongly subjected to the quadrupolar interaction. Finally, the WURST QCPMG (VOCS) approach was successfully applied to ^{137}Ba NMR, and used to characterize barium carbonate and boronate phases. Barium-137 (ν_0 = 94.4 MHz at 19.9 T) has a strong nuclear quadrupole moment and a moderate natural abundance (11.0%), but exceptional sensitivity was demonstrated using WURST QCPMG.

^{87}Sr NMR spectroscopy of Sr-doped CaO-SiO2 bioglasses[1]

Our previous attempts to record ^{87}Sr NMR of Sr-doped CaO-SiO_2 bioglasses in natural abundance at ultra-high field were encouraging (DFS WURST QCPMG VOCS sequence). However, ~ 50 h of experimental time at ultra-high field was needed, with a very poor signal to noise ratio for the largest offsets. This particular point was an issue as very large C_Q(^{87}Sr) values can be expected (up to 65 MHz). Such contributions should correspond therefore to poorly defined broadened lines in the spectrum. In order to circumvent this problem, an ^{87}Sr labelled bioglass was synthesized (^{87}Sr content: ~ 90%, CortecNet, starting material: $SrCO_3$). The spectrum of the bioglass is presented in Figure 1 (8 offsets, 1 h per offset). The signal to noise ratio is now excellent and allows the full description of the Sr sites in the bioglass. Clearly, two main components are observed: a comparatively sharp one corresponding to C_Q(^{87}Sr) ~ 35 MHz and a much broader one (C_Q(^{87}Sr) ~ 65 MHz). It should be noted that it would have been impossible to readily detect this broad component from natural abundance experiments even at ultra-high field.

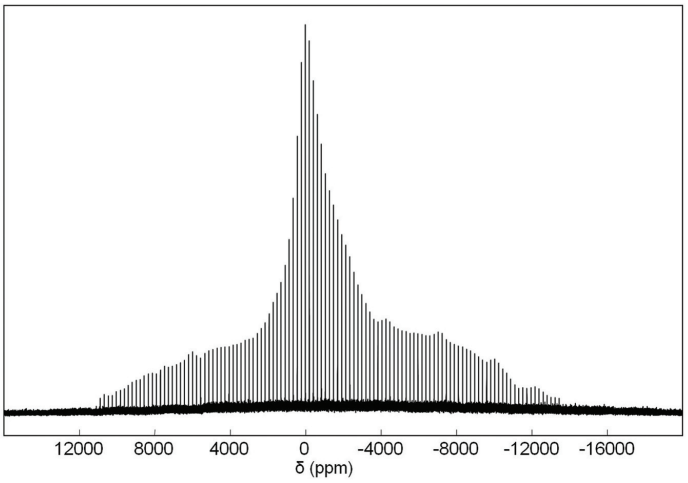

Figure 1. DFS WURST QCPMG VOCS spectrum of an ^{87}Sr-labeled CaO-SiO_2 bioglass.

^{43}Ca NMR spectroscopy of hybrid materials[2]

A new series of crystalline alkaline earth boronates has been prepared, to obtain a better understanding of the coordination chemistry of phenylboronate ligands.[2,3] For the calcium phenylboronate phase ($Ca(C_6H_5B(OH)_3)_2$), the structure has been determined by Rietveld refinement of the X-ray diffraction powder pattern. In order to determine the position of the hydroxyl protons, an NMR crystallography approach was used. Starting from the experimental crystal structure, different "reasonable" initial orientations were chosen the OH protons. The ^{1}H positions were then relaxed using DFT calculations, and the NMR parameters of the nuclei in each of the models tested (M1 to M4) were calculated using GIPAW. A comparison of the experimental (blue) and calculated ^{1}H, ^{13}C, ^{11}B and ^{43}Ca NMR data for the different models tested (red) is shown in Figure 2. This shows that the ^{43}Ca solid state NMR data, which was recorded at 850 MHz on a ~36% ^{43}Ca labeled sample, is crucial to discriminate between the models.

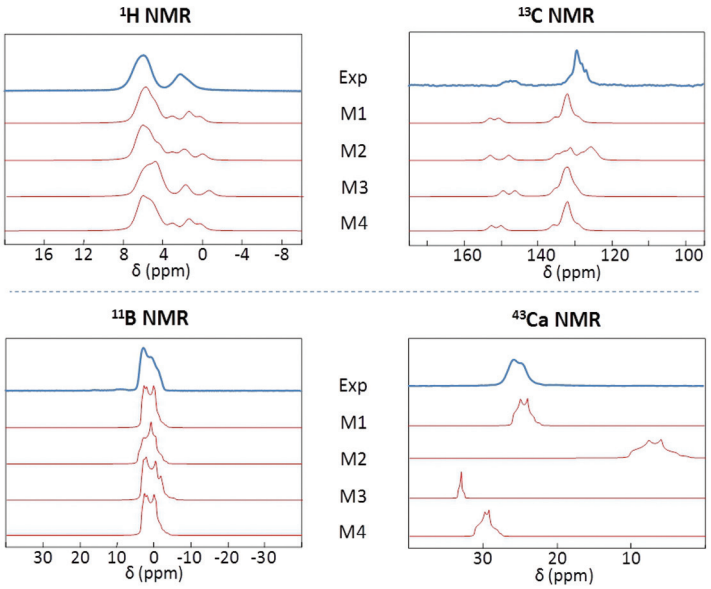

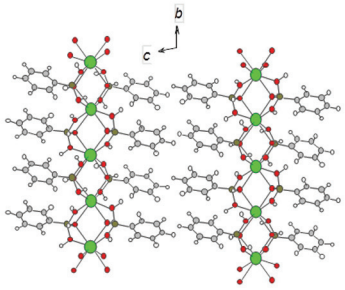

Figure 2. Experimental (blue) and modelled (red) solid-state MAS NMR spectra of $Ca(PhB(OH)_3)_2$.

^{137}Ba NMR spectroscopy[4]

The efficiency of the ^{137}Ba WURST QCPMG approach is demonstrated in Figure 3 (barium carbonate, C_Q ~ 17 MHz, η_Q ~ 0.3). Indeed, the bottom spectrum is obtained in 5 s (!) (16 scans, relaxation delay of 0.3 s, WURST excitation, 1 offset). The final spectrum (upper line in green) is obtained in 15 minutes with 7 offsets. The sequence was then applied to other materials, and the preliminary results concerning barium boronates are highly encouraging.

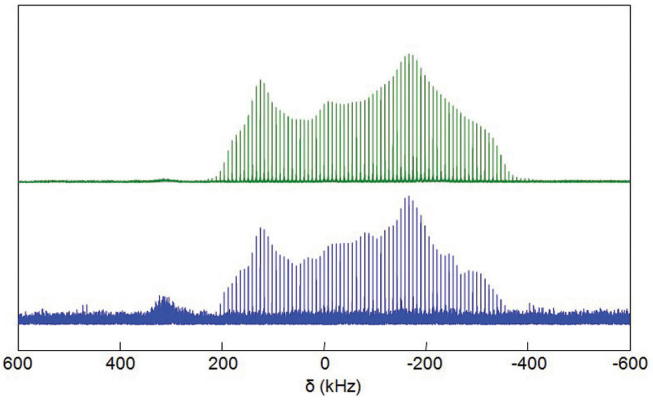

Figure 3. WURST QCPMG ^{137}Ba NMR spectra of $BaCO_3$, with 5 s (blue), and 15 min (green) acquisition.

References

1. Bonhomme, C.; Gervais, C.; Folliet, N.; Pourpoint, F.; Coelho Diogo, C.; Lao, J.; Jallot, E.; Lacroix, J.; Nedelec, J.-M.; Iuga, D.; Du, J.; Hanna, J. V.; Smith M. E.; Laurencin, D. *submitted*.
2. Reinholdt, M.; Croissant, J.; Di Carlo, L.; Granier, D.; Gaveau, P.; Bégu, S.; Devoisselle, J.-M.; Mutin, P. H.; Smith, M. E.; Bonhomme, C.; Gervais, C.; van der Lee, A.; Laurencin, D. *Inorg. Chem*. **2011**, *50*, 7802.
3. Li, A.; Wang, D.; Xiang, J.; Newport, R. J.; Reinholdt, M. X.; Mutin, P. H.; Vantelon, D.; Bonhomme, C.; Smith, M. E.; Laurencin, D.; Qiu D. *J. Non Cryst. Solids* **2011**, *357*, 3548.
4. Hamaed, H.; Ye, E.; Udachin, K.; Schurko, R. W. *J. Phys. Chem*. B **2010**, *114*, 6014.

NMR Studies of the Hydrogen Storage System $LiBH_4 + MgH_2$

Gregory Martin,[1] Jeremy Titman[1] and Gavin Walker[2]

[1]*School of Chemistry, University of Nottingham,*
[2]*Division of Energy and Sustainability Research, University of Nottingham*

Overview

$LiBH_4$ has a high theoretical gravimetric hydrogen density of 13.6 wt % with respect to its decomposition to LiH and B. However, its usefulness as a hydrogen storage material is limited by its high thermodynamic stability which means not all the available hydrogen is released even at 600 °C.[1] Many attempts have been made recently to reduce the dehydrogenation temperature by catalysis, thermodynamic destabilization and nano-engineering approaches, such as inclusion in mesoporous scaffolds and gels. Particular success has been achieved by the addition of MgH_2 which allows dehydrogenation and rehydrogenation at temperatures as low as 350 °C[2] according to the reversible reaction:

$$LiBH_4 + \tfrac{1}{2}MgH_2 \rightleftharpoons LiH + \tfrac{1}{2}MgB_2 + 2H_2$$

High-energy ball milling of mixtures of LiH and MgB_2 can reduce the required temperature to below the melting point of LiBH4, offering the prospect of reversible chemical hydrogen storage in the solid phase.[3] Multi-nuclear solid-state NMR spectroscopy has proved a useful tool to identify the amorphous or nano-crystalline intermediates in the dehydrogenation and rehydrogenation reactions, as well as the structural changes which occur on the nano-scale during ball milling. Recently, Hwang et al.[4] used ^{11}B MAS and $\{^1H\}$-^{11}B CPMAS NMR experiments to characterize the intermediates formed during the decomposition of $LiBH_4$. They concluded that these contain the hydrolytically stable closo-$[B_{12}H_{12}]^{2-}$ anion. Shaw *et al.*[5] studied the hydrogenation of ball-milled mixtures of LiH and MgB_2 (the reverse reaction) using a combination of ^6Li, ^{11}B and ^{25}Mg NMR at 21.1 T. Their results suggest that ball milling under an inert atmosphere produces a ternary $(Mg_{1-x}Li_{2x})B_2$ phase, which is an important intermediate. The reaction proceeds via two steps: the first produces $(Mg_{1-x}Li_{2x})B_2$ by Li^+/Mg^{2+} ion exchange, while the second involves the hydrogenation of $(Mg_{1-x}Li_{2x})B_2$ to $LiBH_4$ and MgH_2. In contrast to Hwang *et al.* who studied pure $LiBH_4$, these authors found no evidence for the formation of the $[B_{12}H_{12}]^{2-}$ anion.

Mechanism of dehydrogenation: multinuclear NMR studies

Partially and fully dehydrogenated samples of mixtures of $LiBH_4$ and MgH_2 with varying composition were prepared in order to investigate the mechanism. Ball-milled mixtures of $LiBH_4$ and MgH_2 were pressurized with H_2 inside in a reaction vessel and heated to a temperature of 670 K or 770 K. At constant temperature the H_2 over-pressure was slowly decreased, while the mass loss was measured. The resulting isotherm shows two plateaux which correspond to the initial decomposition of MgH_2 to Mg and H_2 followed by Mg-catalyzed dehydrogenation of $LiBH_4$ to LiH. For NMR measurements samples were quenched at several points along the second plateau. Powder neutron diffraction[6] on deuterated mixtures dehydrogenated at 770 K shows that $LiBD_4$ decomposition does not coincide with the formation of LiD indicating that $LiBD_4$ is converted into an undetected amorphous intermediate prior to the formation of the end products. The presence of Mg in Li-deficient compositions causes further dehydrogenation of LiD at the higher temperature, resulting in the generation of Li-Mg alloy phases detected via a shift in the lattice-spacing for Mg.

^{11}B, ^7Li and ^{25}Mg MAS NMR spectra of a 2:1 $LiBH_4$:MgH_2 mixture dehydrogenated at 670 K recorded at 7.0 T and 20.0 T using MAS rates of between 8 and 12 kHz are shown in Figure 1. In the 7.0 T ^{11}B MAS spectrum (left) of the fully hydrogenated ball-milled sample (top) shows the expected narrow –41 ppm (from BF_3OEt_2) central transition line due to $LiBH_4$ and the corresponding manifold of satellite transition sidebands. Both these features are almost completely absent from the ^{11}B MAS spectrum of the fully decomposed sample (bottom). The new resonance at +95 ppm which appears during the $LiBH_4$ decomposition plateau (middle two spectra) is close to the shift expected for MgB_2, but neutron diffraction suggests little crystalline MgB_2 is present until the dehydrogenation is complete. This suggests that amorphous MgB_2 is produced in the early stages of $LiBH_4$ decomposition. In the 7.0 T ^7Li MAS spectra (centre) a Knight-shifted peak at 134 ppm (from LiCl (aq)) which implies the presence of a metallic Li-containing species appears towards the end of the $LiBH_4$ decomposition plateau (bottom two spectra). This suggests the formation of small quantities of Li-Mg alloy.

A Knight-shifted peak at 1180 ppm (from $MgCl_2$(aq)) due to Mg metal is observed in the 20.0 T ^{25}Mg MAS spectrum (right) after ball milling (top), even before the dehydrogenation commences. Hence, ball milling alone initiates the decomposition of the more thermodynamically unstable MgH_2. A significant quantity of Mg metal remains in all samples until the dehydrogenation is complete. The peak due to MgB_2 at 255 ppm dominates the ^{25}Mg MAS spectrum of the fully decomposed sample (bottom).

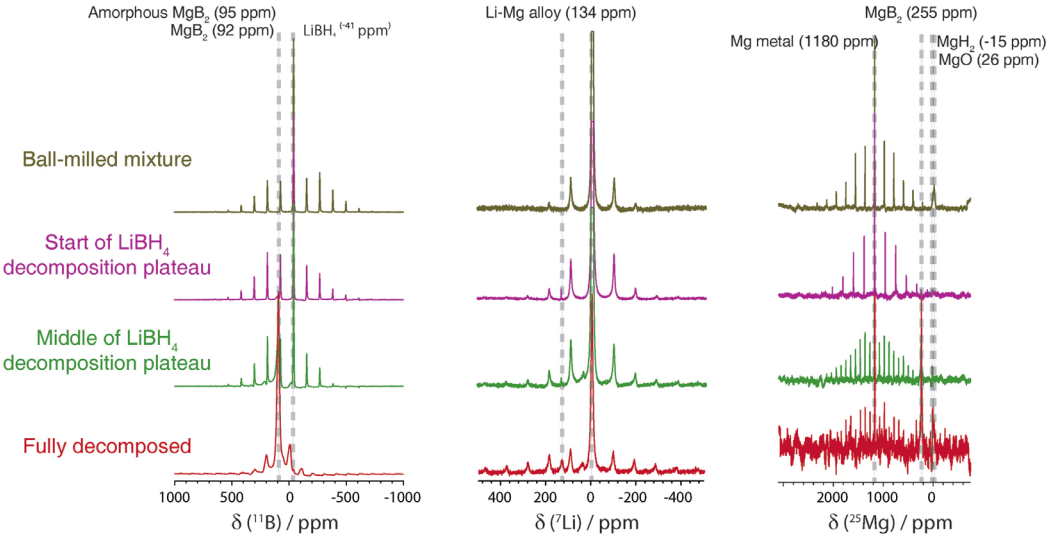

Figure 1. ^{11}B, ^{7}Li and ^{25}Mg MAS NMR spectra recorded at 7.0 T (^{11}B, ^{7}Li) and 20.0 T (^{25}Mg) for quenched samples of a 2:1 $LiBH_4$:MgH_2 mixture dehydrogenated at 670 K.

Broader lines are evident in the ^{11}B MAS spectrum of samples quenched towards the end of the $LiBH_4$ decomposition plateau, suggesting the presence of amorphous intermediates. ^{11}B MQMAS at 7.0 T and MAS rates 12-13 kHz was employed to resolve these lines for 2:1 and 0.3:1 $LiBH_4$:MgH_2 mixtures and the resulting spectra are shown in Figure 2. Note that only for decomposition at 670 K (left) does the expected MgB_2 end-product at +92 ppm dominate the spectrum and there is still a significant quantity of $LiBH_4$ starting material at –41 ppm in all cases. The remaining broad line dominates at 770 K (centre) and shifts from –2 ppm to –9 ppm as the mixture becomes increasingly Li-deficient (right). {^{1}H}-^{11}B CPMAS measurements show that this line arises from a combination of elemental B (+2 ppm) and the intermediate species $Li_2[B_{12}H_{12}]$ (–12 ppm) in varying amounts. The NMR results suggest that a lower dehydrogenation temperature favours the formation of Li-Mg alloy rather than $Li_2[B_{12}H_{12}]$ and this in turn promotes dehydrogenation.

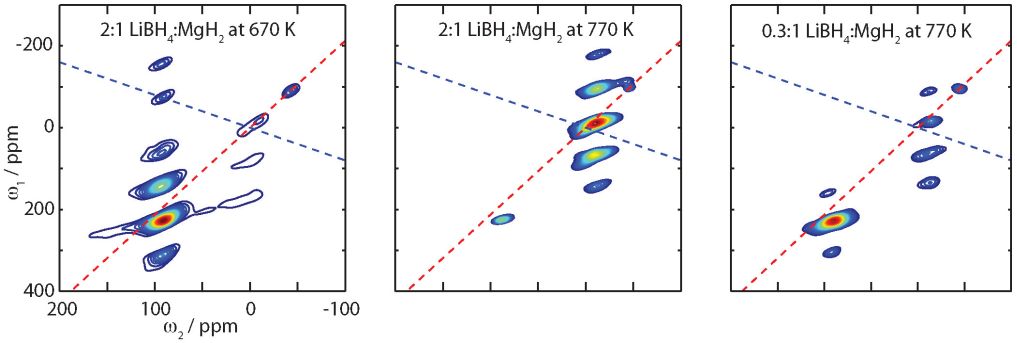

Figure 2. ^{11}B MQMAS spectra recorded at 7.0 T of fully decomposed mixtures of $LiBH_4$ and MgH_2 dehydrogenated at 670 K and 770 K.

References

Yu, X. B.; Grant, D. M.; Walker, G. S. *Chem. Commun.* **2006**, 3906.

Vajo, J. J.; Skeith, S. L.; Mertens, F. *J. Phys. Chem. B* **2005**, *109*, 3719.

Wan, X.; Markmaitree, T.; Osborn, W.; Shaw, L. *J. Phys. Chem. C* **2008**, *112*, 18232.

Hwang, S.; Bowman, R. C.; Reiter, J. W.; Rijssenbeek, J.; Soloveichik, G. L.; Zhao, J.; Kabbour, H.; Ahn, C. C. *J. Phys. Chem. C* **2008**, *112*, 3164.

Shaw, L. L.; Wan, X.; Hu, J. Z.; Kwak, J. H.; Yang, Z. *J. Phys. Chem. C* **2010**, *114*, 8089.

Price, T. E. C.; Grant, D. M.; Legrand, V.; Walker, G. S. *Int. J. Hydrogen Energy* **2010**, *35*, 4154.

High-Field $^{69/71}$Ga Solid-State NMR of Gallium Oxide Polymorphs

Martin R. Mitchell,[1] Sharon E. Ashbrook,[1] Helen Y. Playford[2] and Richard I. Walton[2]

[1]*School of Chemistry and EaStCHEM, University of St Andrews,*
[2]*Department of Chemistry, University of Warwick*

Overview

Gallium oxide, Ga_2O_3, is a semiconductor oxide with a large band gap (4.9 eV). It has attracted interest as a catalyst for the dehydrogenation of light hydrocarbons and the reduction of nitrogen oxides (NO_x) in car exhausts.[1] Ga_2O_3 also has potential applications in the fields of transparent conductors, high temperature gas sensors and photocatalysis.[2] Bulk Ga_2O_3 is often used as a precursor for the synthesis of various functional materials such as gallium nitride and zeolites.[3] The polymorphism of gallium oxide, however, is not well understood. The only major study on the subject was carried out by Roy *et al.* in 1952,[4] which suggested the existence of five polymorphs, designated α, β, γ, δ and ε. β-Ga_2O_3, shown in Figure 1b, has a monoclinic structure analogous to θ-Al_2O_3 and is the most thermodynamically stable, while the α polymorph, shown in Figure 1a is isostructural to α-Al_2O_3. We have recently made extensive studies of the chemistry of this system and have new routes to three uncharacterised polymorphs, γ-Ga_2O_3, ε-Ga_2O_3 and δ-Ga_2O_3. Conventional analysis of their diffraction patterns is complicated by the peak broadening caused by the small crystallite size and we have measured total neutron scattering data from all samples which is revealing details of the their local and long-range structures. To proceed with modelling the radial distributions thus produced, we need an independent probe of local structure: specifically to determine the proportion of octahedral and tetrahedral Ga in each polymorph. Previous work on gallium oxide using ^{71}Ga NMR used lower field[5] and we are not sure that the various samples were correctly identified.

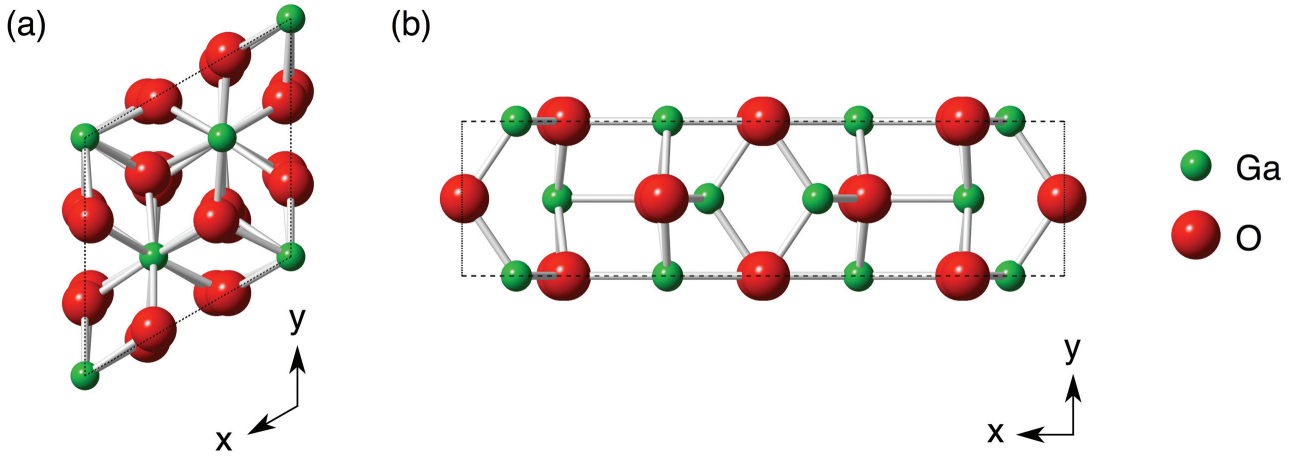

Figure 1. Structures of (a) α- and (b) β-Ga_2O_3

In this work, solid-state Ga NMR spectroscopy has been used to probe the local Ga coordination environment in the five polymorphs. Two isotopes, ^{69}Ga and ^{71}Ga, are NMR active and although both have relatively high sensitivity, they are both quadrupolar (I = 3/2), with relatively large quadrupole moments. As second-order quadrupolar broadening decreases with increasing B_0 field strength, high-field NMR experiments offer the best prospect for acquisition of undistorted MAS spectra, particularly when combined with rapid MAS.

Ga NMR of Ga_2O_3 polymorphs

^{71}Ga fast MAS NMR spectra were acquired, using a 1.3-mm probe, for the α and β polymorphs of Ga_2O_3, previously studied in the literature (as shown in Figure 2).[5,6] As expected, two quadrupolar lineshapes were observed for β-Ga_2O_3, corresponding to octahedral and tetrahedral Ga, with C_Q values of 8.3 and 11.2 MHz, respectively. For α-Ga_2O_3, a quadrupolar broadened lineshape is observed for the single octahedral site, with a C_Q of 8.2 MHz. In addition, however, broad lineshapes were also observed in the regions of the spectrum corresponding to both tetrahedral and octahedral Ga, indicating the presence of a disordered impurity phase, possibly arising from the GaOOH starting materials.

^{71}Ga MAS NMR spectra (see Figure 2) of the γ, δ and ε polymorphs reveal both tetrahedrally- and octahedrally-coordinated Ga in each case, with intensity ratios of 1 : 2, 1 : 2 and 1 : 3, respectively. The lineshapes are broad, with characteristic "tails" to low frequency, indicating some disorder in all three phases, and distributions of NMR parameters. Disorder in the bulk structure of these polymorphs is caused mainly by their small particle size, with additional contributions from the presence of multiple partially occupied crystallographic sites. The ^{71}Ga MAS NMR spectra provide confirmation of this disorder on a local scale and the ratios of tetrahedral and octahedral Ga are in good agreement with the neutron diffraction data. The spectrum of the δ-polymorph contains significant intensity *between* the regions characteristic of tetrahedral and octahedral Ga, which is evidence for greater disorder in the coordination environments in this polymorph. This may be caused by the large surface area of these very small (<2 nm) particles and the presence of a hydrated surface layer.

The spectra can be used alongside ongoing additional characterisation using diffraction to provide a complete structural description of the disordered Ga_2O_3 polymorphs on a range of length scales. Disordered nanomaterials are by nature complex, and a multidisciplinary approach, such as that undertaken here, is required to develop a full understanding of their structure and properties.

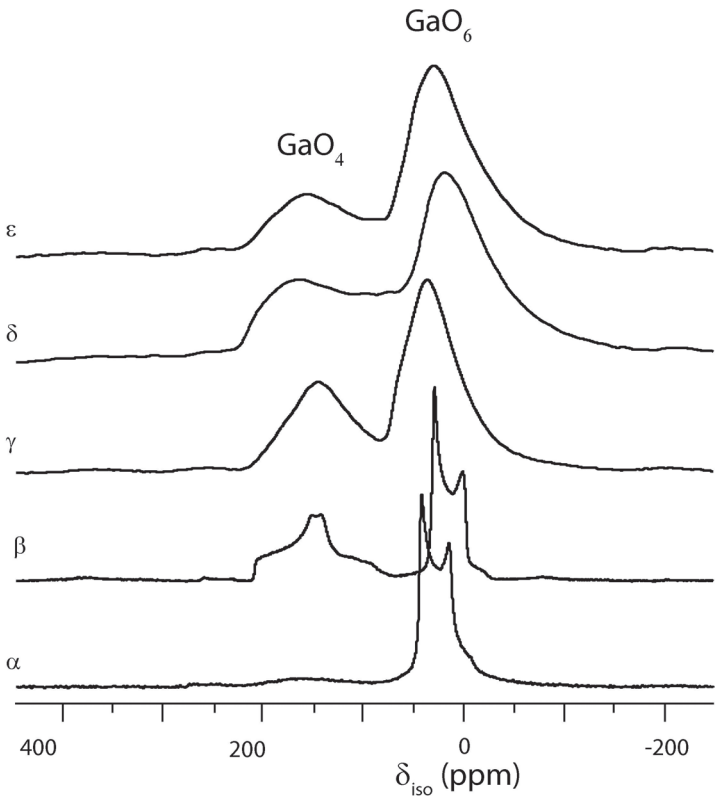

Figure 2. 20.0T ^{71}Ga MAS NMR Spectra of α, β, γ, δ and ε-Ga_2O_3, with an MAS rate of 60 kHz

References

1. Kim, S. W.; Iwamoto, S.; Inoue, M. *Ceram. Int.* **2009**, *35*, 1603.
2. Ge, S. X.; Zhang, L. Z.; Jia, H. M.; Zheng, Z. *J. Mater. Res.* **2009**, *24*, 2268.
3. Ifeacho, P.; Wiggers, H.; Schulz, C.; Schneider, L.; Bacher, G. *J. Nanopart. Res.* **2008**, *10*, 121.
4. Roy, R.; Hill, V. G.; Osborn, E. F. *J. Am. Chem. Soc.* **1952**, *74*, 719.
5. O'Dell, L. A.; Savin, S. L. P.; Chadwick, A. V.; Smith, M. E. *Appl. Magn. Reson.* **2007**, *32*, 527.
6. Massiot, D.; Farnan, I.; Gautier, N.; Trumeau, D.; Trokiner, A. and Coutures, J. P. *Solid State Nucl. Magn. Reson.* **1995**, *4*, 241.

Ultra-Fast Spinning Experiments on a 7-Helix Transmembrane Protein

Victoria A. Higman, Lubica Aslimovska, Peter J. Judge and Anthony Watts

Department of Biochemistry, University of Oxford

Overview

There is great interest in obtaining high-resolution structural data on 7-helix trans-membrane (7TM) proteins due to their importance as drug targets.[1] Solid-state NMR has the unique potential to provide high-resolution structural information within a native membrane environment and initial studies on 7TM proteins are showing that spectral assignment and structural characterisation is possible.[2-5] A key problem with all methods of protein structure determination is the large amount of protein required which contrasts with typically very low expression levels for membrane proteins. Recent solid-state MAS-NMR studies of fibrillar and microcrystalline proteins using ultra-fast spinning speeds (60-65 kHz) have shown that at the same field strength it is possible to obtain equally high-quality spectra using smaller amounts of protein sample than when using larger sample quantities at more conventional, lower (5-15 kHz) spinning speeds.[6-8] In principle, this method would be well suited to 7TM proteins. However, it is currently unknown whether membrane proteins are as robust as fibrillar and microcrystalline proteins and can withstand the high g-forces imposed on the sample by ultra-fast spinning. We have studied the behaviour of Bacteriorhodopsin (bR) under ultra-high spinning conditions to explore the use of ultra-fast spinning for the study of membrane proteins generally, and 7TM proteins in particular.

Results

The temperature behaviour of samples at high spinning speeds was investigated using ^{79}Br spectra in order to ensure that the protein sample would not be compromised by frictional heat created at high spinning speeds. The sample integrity of bR was monitored using ^{13}C spectra and found to remain constant up to spinning frequencies of 60 kHz (Figure 1).

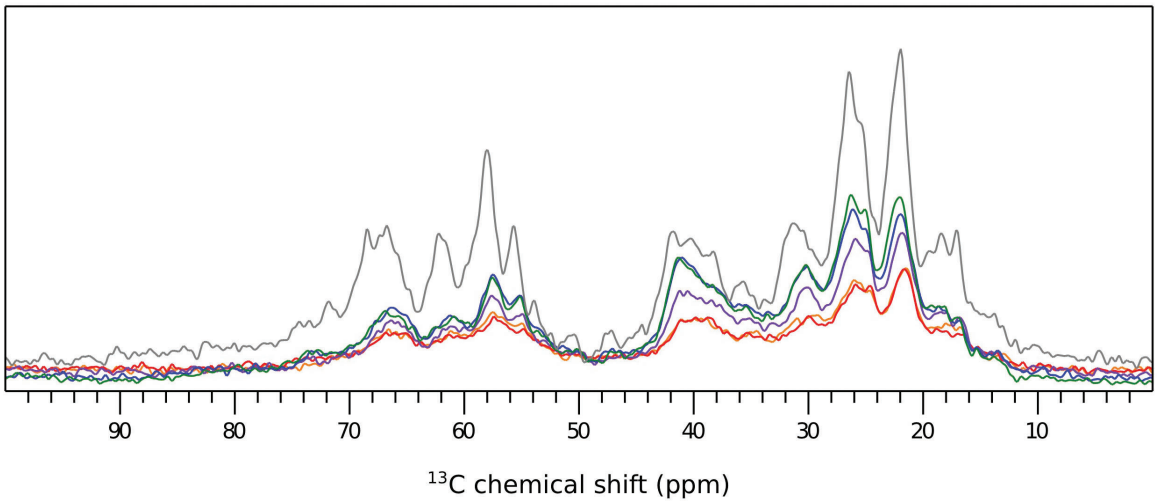

Figure 1. ^{13}C spectra of bR in purple membranes recorded at 850 MHz, a sample set temperature of -30°C and spinning frequencies of 12.2 kHz (green), 20 kHz (blue), 30 kHz (purple), 40 kHz (red), 50 kHz (orange) and 60 kHz (grey).

The change in chemical shift and intensity of the H_2O peak in ^{1}H spectra shows the gradual increase in sample temperature as the spinning speed is increased (Figure 2). It can be seen that upon moving from 50 to 60 kHz the ^{1}H linewidth improves dramatically due to improved averaging of the ^{1}H dipolar couplings. At a spinning frequency of 60 kHz low power band-selective cross-polarisation conditions were used[6] and decoupling was reduced to below 10 kHz. These low power conditions enabled the interscan delay to be lowered without causing increased sample heating and the signal-to-noise ratio per unit time was increased by more than double.

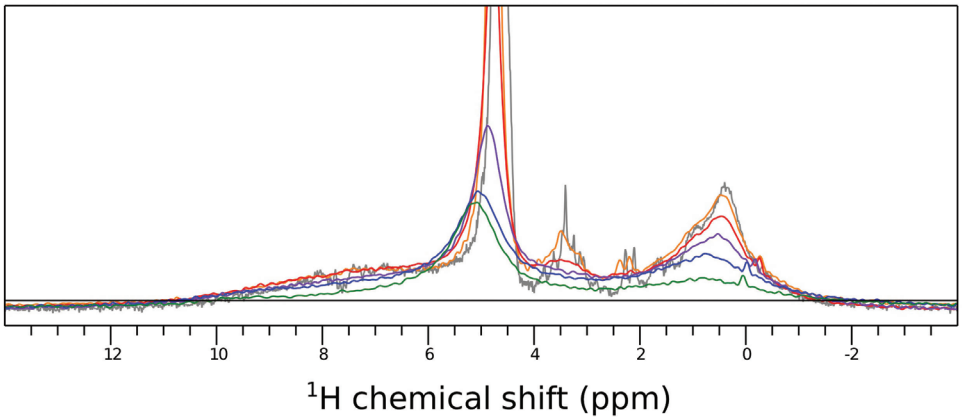

Figure 2. ^{1}H spectra of bR in purple membranes recorded at 850 MHz, a sample set temperature of -30°C and spinning frequencies of 12.2 kHz (green), 20 kHz (blue), 30 kHz (purple), 40 kHz (red), 50 kHz (orange) and 60 kHz (grey).

Conclusion and Outlook

The integrity of bR in purple membranes at ultra-high spinning speeds was established. Low radiofrequency power experimental conditions were determined which enabled good signal-to-noise ratios per unit time to be achieved. bR in purple membranes forms 2-dimensional crystalline arrays which may be more stable than some other membrane protein preparations. Nonetheless, these results indicate that ultra-fast MAS experiments of membrane proteins (and 7TM proteins in particular) using small amounts of sample are likely to be feasibly in future. The main limit may be the minimum sample temperature currently achievable at high spinning speeds (around +15-20°C).

References

1. Overington, J. P.; Al-Lazikani, B.; Hopkins, A. L. *Nat. Rev. Drug Discov.* **2006**, *5*, 993.
2. Etzkorn, M.; Martell, S.; Andronesi, O. C.; Seidel, K.; Engelhard, M.; Baldus, M. *Angew. Chem. Int. Ed.* **2007**, *46*, 459.
3. Shi, L. C.; Ahmed, M. A. M.; Zhang, W. R.; Whited, G.; Brown, L. S.; Ladizhansky, V. *J. Mol. Biol.* **2009**, *386*, 1078.
4. Yang, J.; Aslimovska, L.; Glaubitz, C. *J. Am. Chem. Soc.* **2011**, *133*, 4874.
5. Higman, V. A.; Varga, K.; Aslimovska, L.; Judge, P. J.; Sperling, L. J.; Rienstra, C. M.; Watts, A. *Angew. Chem. Int. Ed.* **2011**, *50*, 8432.
6. Laage, S.; Marchetti, A.; Sein, J.; Pierattelli, R.; Sass, H. J.; Grzesiek, S.; Lesage, A.; Pintacuda, G.; Emsley, L. *J. Am. Chem. Soc.* **2008**, *130*, 17216.
7. Vijayan, V.; Demers, J. P.; Biernat, J.; Mandelkow, E.; Becker, S.; Lange, A. *ChemPhysChem* **2009**, *10*, 2205.
8. Bertini, I.; Emsley, L.; Lelli, M.; Luchinat, C.; Mao, J. F.; Pintacuda, G. *J. Am. Chem. Soc.* **2010**, *132*, 5558.

Understanding the Role of Serum Amyloid P Component in the Stabilisation of Amyloid Deposits.

Garrick F. Taylor,[1] Joern M. Werner,[1] Stephen P. Wood[2] and Philip T. F. Williamson[1]

[1]*School of Biological Sciences, University of Southampton,*
[2]*Centre for Amyloidosis and Acute Phase Protein, Division of Medicine, University College London Medical School*

Overview

Amyloidosis is a family of pathological conditions characterised by the formation of insoluble deposits that lead to the disruption of local tissue. The formation of these deposits has been linked to the mis-folding of normally soluble proteins that results in the formation of large fibrillar structures. Over 30 such diseases have been identified and are linked to a number of socio-economically relevant diseases including Alzheimer's disease, Parkinson's disease, reactive systemic amyloidosis and dialysis related amyloidosis.[1] Although each of these diseases are characterised by the mis-folding of a particular protein, common to all amyloid deposits irrespective to the type of disease is the presence of the protein serum amyloid-P component (SAP). *In-vivo* the binding of SAP is thought to stabilise the fibrillar structures found in these amyloid deposits inhibiting the host's ability to clear them. Accordingly, SAP represents an attractive target for therapeutic intervention, with application across a broad spectrum of amyloid diseases.[2] Despite this the development of drugs that inhibit the binding of SAP to amyloid fibrils is challenging as although high-resolution crystal structures are readily available for the soluble SAP,[3] structural studies of amyloid fibrils and their interactions with other partners found *in-vivo* has been hindered by the intractability of these systems to modern methods in structure biology.

Identification of a serum amyloid-P component binding motif

To ascertain the structural motifs that are recognized by SAP we have undertaken a study to investigate the interaction of SAP with amyloid fibrils composed of the 99 residue β2-microglobulin at neutral pH which are similar to those found in patients suffering from dialysis related amyloidosis. Exploiting the excellent resolution afforded at 850 MHz we have employed chemical shift mapping studies that utilise the inherent sensitivity of the NMR resonances to the local electrostatic environment to determine residues on the surface of β2-microglobulin that are recognised by SAP upon binding. These studies revealed large changes in both intensity and position of resonances assigned to leucine, aspartate and glutamate sidechains, indicating a potential role for these residues in SAP binding (Figure 1). Subsequent biochemical studies have revealed that abolition of the negative charges suppressed SAP binding, confirming their role in the recognition of β2-microglobulin fibrils (Figure 2).[4] Interestingly, complementary chemical shift mapping and saturation difference NMR studies of monomeric β2-microglobulin and acidic amino acids reveal no specific interaction with SAP at the concentrations tested.[4] These studies indicate that not only is acidic charge necessary for SAP binding, but also the recognition of the amyloid fibril is highly dependent on the correct presentation of these acidic residues to the SAP.

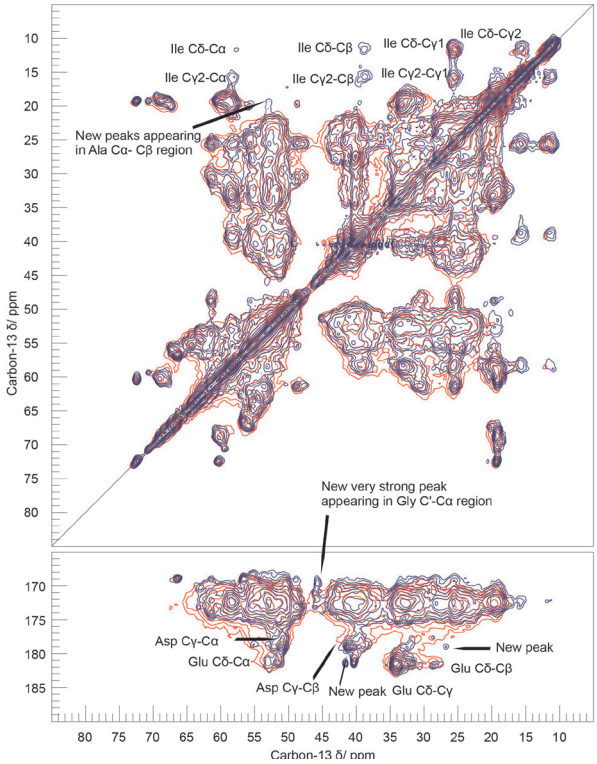

Figure 1. Comparison of β_2-microglobulin fibrils in with SAP bound (blue) and without SAP bound (red) with significant changes highlighted.

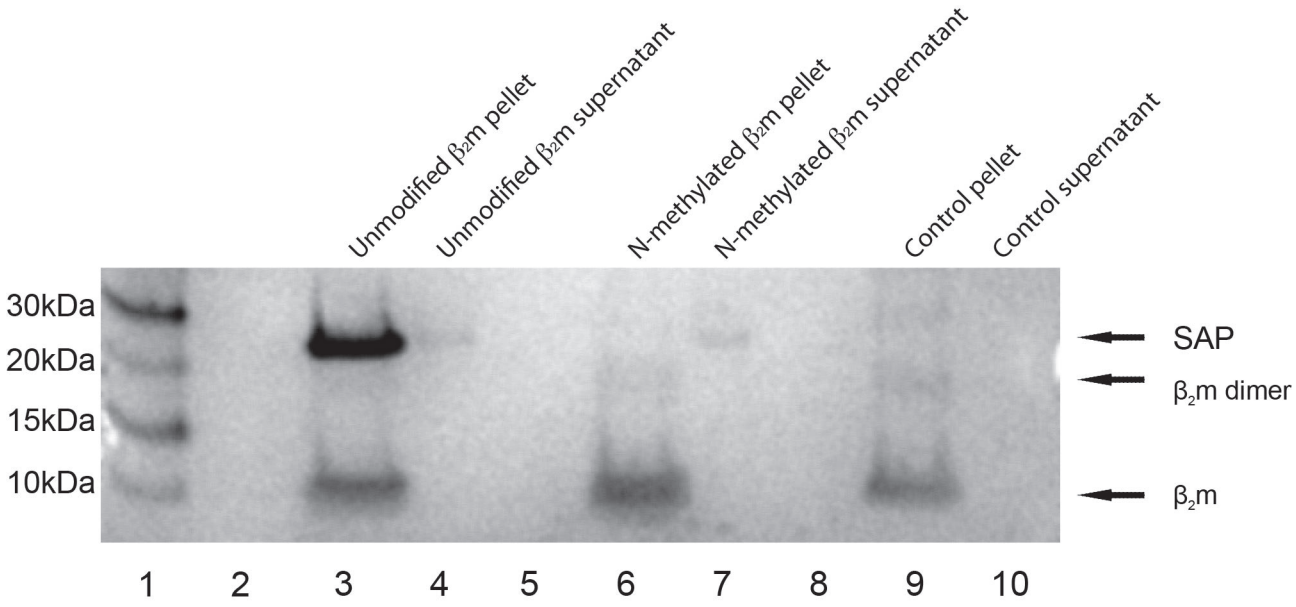

Figure 2. SDS-PAGE of SAP-fibril pull-down comparing unmodified with N-methylated β_2-microglobulin fibrils. Unmodified fibrils clearly associate with SAP resulting in the appearance of SAP in the pellet. In contrast N-methylated fibrils show no such affinity and the SAP is absent from the pellet.

Summary

These studies provide for the first time a molecular understanding of how SAP interacts with amyloid fibrils, highlighting an important role the highly repetitive fibrillar structure plays in presenting acidic residues in such a manner that they can be recognised by SAP, a property that may not be unique to β_2-microglobulin fibrils and which may account for SAP's ubiquitous affinity for amyloid fibrils. Work is underway to complete our assignment of β_2-microglobulin fibrils under physiological conditions that will enable us to uniquely identify which acidic and aliphatic residues within the β_2-microglobulin interact with SAP. We envisage that these studies will not only pave the way for the development of drugs to treat dialysis related amyloidosis but provide a generic route to the treatment of a wide range of amyloid diseases.

References

1. Chiti, F.; Dobson, C. M. Ann. Rev. Biochem. **2006**, *75*, 333.
2. Bodin, K.; Ellmerich, S.; Kahan, M. C.; Tennent, G. A.; Loesch, A.; Gilbertson, J. A.; Hutchinson, W. L.; Mangione, P. P.; Gallimore, J. R.; Millar, D. J.; Minogue, S.; Dhillon, A. P.; Taylor, G. W.; Bradwell, A. R.; Petrie, A.; Gillmore, J. D.; Bellotti, V.; Botto, M.; Hawkins, P. N.; Pepys, M. B. Nature **2010**, *468*, 93.
3. Emsley, J., White, H. E.; O'Hara, B. P.; Oliva, G.; Srinivasan, N.; Tickle, I. J.; Blundell, T. L.; Pepys, M. B.; Wood, S. P. Nature **1994**, *367*, 338.
4. Taylor, G. F., *The interaction between fibrillar beta-2-microglobulin and serum amyloid-P component*, in *Centre for Biological Sciences*. PhD. Thesis **2011**, University of Southampton: Southampton.

A High-Field Multinuclear Solid-State NMR Study of Hydrous Wadsleyite

John M. Griffin,[1] Andrew J. Berry,[2] Stephen Wimperis[3] and Sharon E. Ashbrook[1]

[1]*School of Chemistry and EaStCHEM, University of St Andrews,*
[2]*Department of Earth Sciences and Engineering, Imperial College London,*
[3]*School of Chemistry and WestCHEM, University of Glasgow*

Overview

Wadsleyite (β-Mg_2SiO_4) is a high-pressure silicate phase present in the so-called 'transition zone' between the upper and lower regions of the Earth's mantle. Although present in a relatively small quantity compared to other mantle silicate phases, wadsleyite has received considerable interest as a potential host for a large amount of hydrogen (colloquially termed 'water') within the mantle.[1,2] Indeed, the wadsleyite structure is thought to be capable of incorporating more hydrogen by weight than any other mantle silicate, with H_2O concentrations of up to 3.3 wt% having been reported.[3] If fully hydrated to this level, the mantle transition zone could contain an amount of H_2O equivalent to several oceans. However, the exact locations of hydrogen atoms in the structure of hydrous wadsleyite are not well understood. Hydrous wadsleyite can be synthesised in the laboratory, yet many standard techniques for structure determination then fail. Indeed, X-ray diffraction has yielded the structure of anhydrous wadsleyite but cannot tell us where low concentrations of H atoms are located in the hydrous form.

Solid-state NMR offers a powerful alternative technique for the study of inner-Earth minerals. Indeed, ^{1}H solid-state NMR can yield detailed information about proton chemical environments and hydrogen-bonding interactions. Furthermore, the ^{17}O nucleus (spin I = 5/2) also provides a highly sensitive probe of oxygen bonding geometry and coordination through changes in the chemical shift and second-order quadrupolar interactions. However, the low natural abundance of ^{17}O (0.037%) means that isotopic enrichment is usually required for observation of the NMR signal. In previous studies, we have successfully used this method to provide structural insight into a range of synthetic anhydrous silicate systems by ^{17}O solid-state NMR.[4,5] Nevertheless, characterisation of subtle structural changes upon hydration remains a challenge owing to the typically small sample volumes available. In the current work, we have attempted to address this problem by exploiting the significant signal enhancement achievable at a magnetic field strength of 20.0 T.

Results

The anhydrous wadsleyite structure, shown in Figure 1a, consists of pyrosilicate Si_2O_7 units (sites O2 – O4) and a five-coordinate O site (O1) surrounded by magnesium cations. A number of experimental and theoretical studies have identified the under-bonded crystallographic O1 site as a favourable location for protonation. In 1994, Smyth proposed that full hydration of the O1 site may be achieved through substitution of the Mg2 site.[2] Full hydration of the structure in this way gives a theoretical maximum hydration level of 3.3 wt%, in agreement with maximum hydration levels achieved in experimental studies.

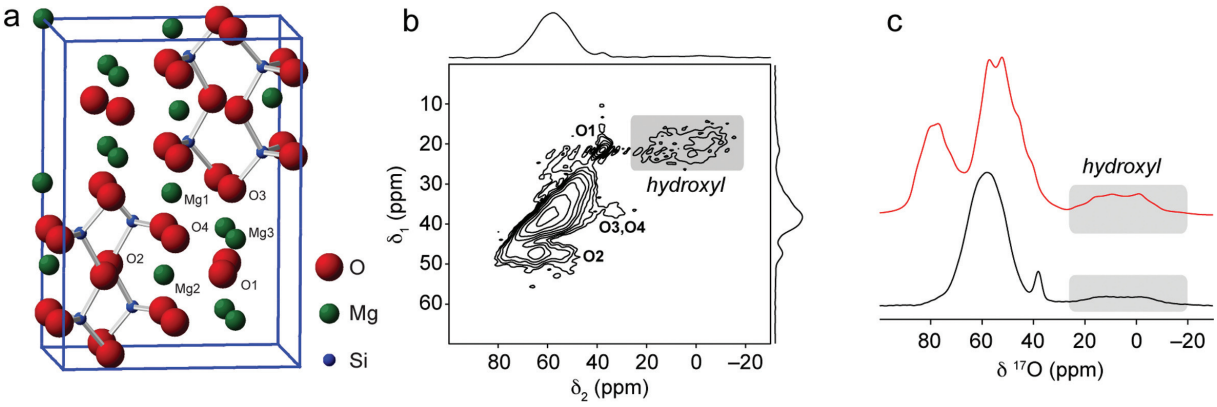

Figure 1. (a) Crystal structure of anhydrous wadsleyite. (b) ^{17}O STMAS NMR spectrum of hydrous wadsleyite. (c) Experimental ^{17}O MAS NMR spectrum of hydrous wadsleyite (black) and simulated spectrum (red) based on the Smyth model structure. Experimental spectra were recorded at 20.0 T with a MAS frequency of 30 kHz.

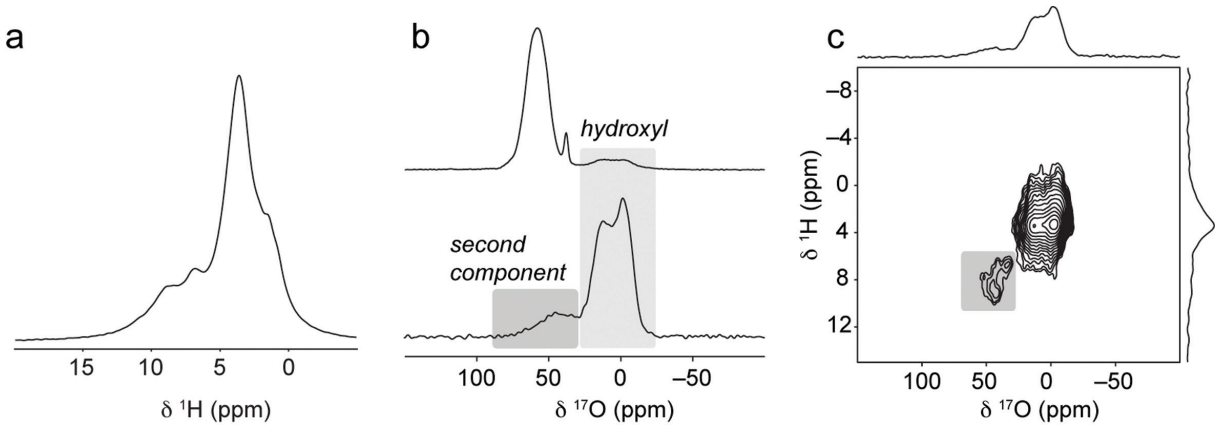

Figure 2. (a) ^{1}H MAS NMR spectrum of hydrous wadsleyite. (b) ^{17}O MAS (top) and CPMAS (below) NMR spectra of hydrous wadsleyite. A second component observed in addition to the hydroxyl resonance is highlighted in dark grey. (c) ^{1}H-^{17}O CP HETCOR NMR spectrum of hydrous wadsleyite showing the weaker component correlating to the higher chemical shift protons. All spectra were recorded at 20.0 T using a MAS frequency of 30 kHz.

In previous work at the 850 MHz facility, we have been able to observe OH hydroxyl oxygen sites in ^{17}O satellite transition (ST)MAS NMR spectra of hydrous wadsleyite, as shown in Figure 1b, confirming that protonation does indeed take place on O1. However, DFT calculations performed on the Smyth structure show poor agreement with the experimental ^{17}O MAS NMR spectrum, as shown in Figure 1c. Furthermore, a ^{1}H MAS NMR spectrum shown in Figure 2a of hydrous wadsleyite reveals several low intensity resonances at high chemical shifts (7-9 ppm) in addition to the OH hydroxyl protons at 4 ppm. Recently, a study by Deon *et al.*[6] combining Fourier-Transform Infrared spectroscopy and diffraction measurements suggested that protonation takes place on both the O1 and O3 sites through substitution of Mg3. Calculations on model structures protonated in this way indicate that the SiOH silanol protons should exhibit chemical shifts in the range 7-9 ppm, in agreement with the low intensity resonances observed in the ^{1}H MAS NMR spectrum. In the ^{17}O MAS NMR spectrum, resonances corresponding to the resulting SiOH silanol oxygen species should exhibit chemical shifts of approximately 60 ppm. Unfortunately, as shown in Figure 1b, the expected position of silanol oxygen species in the ^{17}O STMAS NMR spectrum is in the same region as the much higher intensity resonances corresponding to the non-protonated silicate oxygens. However, signal from the non-protonated oxygen species can be “filtered out” in a short-contact-time ^{1}H-^{17}O cross-polarisation (CP)MAS NMR experiment. A ^{1}H-^{17}O CPMAS NMR spectrum of hydrous wadsleyite recorded with a contact time of 500 μs is compared to a single-pulse ^{17}O MAS NMR spectrum in Figure 2b. In CPMAS NMR spectrum, the relative intensity of the OH hydroxyl oxygen resonance is magnified owing to the close proximity of the directly-bonded hydroxyl protons. However, an additional component is also observed at higher chemical shift. A ^{1}H-^{17}O heteronuclear correlation (HETCOR) spectrum, shown in Figure 2c, reveals that this resonance correlates to the protons observed at around 7-9 ppm. This is consistent with the presence of silanol oxygen groups in the structure of hydrous wadsleyite, for which oxygens with chemical shifts of ~60 ppm are in close proximity to the directly-bonded silanol hydrogens with chemical shifts of 7-9 ppm.

References

Bolfan-Casanova, N.; Keppler, H.; Rubie, D. C. *Earth Planetary Sci. Lett.* **2000**, *182*, 209.

Smyth, J. R. *Am. Mineral.* **1994**, *79*, 1021.

Kudoh, Y.; Inoue, T.; Arashi, H. *Phys. Chem. Min.* **1996**, *23*, 461.

Ashbrook, S. E.; Berry, A. J.; Hibberson, W. O.; Steuernagel, S.; Wimperis, S. *J. Am. Chem. Soc.* **2003**, *125*, 11824.

Ashbrook, S. E.; Berry, A. J.; Frost, D. J.; Gregorovic, A.; Pickard, C. J.; Readman, J. E.; Wimperis, S. *J. Am. Chem. Soc.* **2007**, *129*, 13213.

Deon, F.; Koch-Muller, M.; Rhede, D.; Gottschalk, M.; Wirth, R.; Thomas, S.-M. *Am. Mineral.* **2010**, *95*, 312.

^{43}Ca and ^{87}Sr Solid-State NMR Study of Pyrophosphates

Annabelle Baker,[1] Danielle Laurencin,[2] Christian Bonhomme,[3] Mark E. Smith[4] and Adrian Wright[1]

[1]*School of Chemistry, University of Birmingham,*
[2]*Institut Charles Gerhardt de Montpellier, France,*
[3]*LCMCP UMC CNRS 7574, University Paris 06, France,*
[4]*Department of Physics, University of Warwick*

Overview

A growing awareness of the existence and potential of amorphous inorganic materials has led to a rapid increase in their study in recent years. In particular, Yanabao et al.[1] have shown that amorphous calcium orthophosphates are present in much higher concentration in the early stages of tissue mineralisation than in samples taken later in development. Therefore, they must play an essential, although not fully understood, role in the bone mineralization process in mammals. The use of amorphous calcium phosphate phases as materials for bone substitution thus appears as particularly promising, because their relative instability suggests that they will be resorbable, meaning that they can be progressively replaced by natural bone tissue. Recently, we have prepared a new series of amorphous phosphate materials based on *pyrophosphate* anions, $M_2(P_2O_7).xH_2O$ (M = Ca, Sr; $3.8 < x < 4.2$),[2] which, unlike some calcium orthophosphate phases that readily crystallize, appear to be more stable over time, making them more interesting as potential biomaterials. A series of characterizations have thus been carried out on these phases, including the analysis of pair distribution functions (PDF) derived from synchrotron X-ray data, and ^{1}H and ^{31}P solid state NMR. In order to learn more about the structure of these systems, it thus appears as essential to characterize in detail the local environment of the metal cations (Ca or Sr). However, both calcium-43 and strontium-87 are challenging nuclei for NMR, because they are low-gamma quadrupolar isotopes of low natural abundance. In this project, a series of Ca and Sr pyrophosphate phases, both crystalline and amorphous, were characterized at ultra-high magnetic field (850 MHz), using ^{43}Ca RAPT MAS and ^{87}Sr WURST-QCPMG-VOCS experiments.[3,4]

^{43}Ca NMR spectroscopy of Ca-pyrophosphates.

Four different Ca-pyrophosphate phases were characterized by ^{43}Ca solid state NMR at 20 T: crystalline $Ca_2P_2O_7.4H_2O$, and three amorphous phases (amorphous Ca-pyrophosphate "ACaPPi", and 2 amorphous products resulting from its heat treatment at 140 and 220 °C). As expected from the XRD crystal structure, 2 peaks were observed for crystalline $Ca_2P_2O_7.4H_2O$, which correspond to the 2 crystallographic Ca sites. In contrast, the ^{43}Ca NMR spectra of the amorphous phases are much broader, due to the presence of a larger distribution in Ca local environments. In addition, the ^{43}Ca signal slightly broadens upon heat treatment, which suggests that by heating the amorphous sample to moderate temperatures (like 140 and 220°C) a further increase in local disorder around the calcium occurs. This could be one of the reasons for the high thermal stability of these phases.

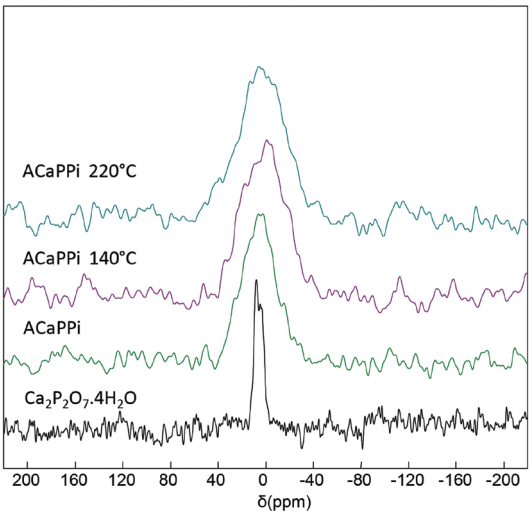

Figure 1. Natural abundance ^{43}Ca MAS NMR spectra of crystalline and amorphous Ca pyrophosphates.

^{87}Sr NMR spectroscopy of Sr-pyrophosphates

Static ^{87}Sr NMR spectra of crystalline $Sr_2P_2O_7$ and of amorphous $Sr_2P_2O_7$ □ x H_2O "ASrPPi" (before and after heat-treatment at 220°C) were recorded at 20 T, using the DFS WURST QCPMG pulse sequence (Figure 2). For the crystalline sample, two Sr sites with different quadrupolar parameters C_q can be identified in the static spectrum, in agreement with the XRD crystal structure, and with GIPAW calculations of the ^{87}Sr NMR parameters of this phase. In contrast, no signal was observed for the amorphous phase ASrPPi, and only a weak signal was obtained for the related amorphous phase "ASrPPi 220°C", which was prepared by heat treatment of ASrPPi at 220°C. The difficulties in recording the ^{87}Sr NMR spectra of the amorphous phases can be related to the broader distribution in Sr local environments in the amorphous phases, as well as the presence of water molecules in the vicinity of the strontium. Indeed, it is only after the heat treatment of ASrPPi at 220°C, which helps diminish the number of water molecules and OH-groups around the Sr, that it becomes possible to obtain an ^{87}Sr NMR spectrum at natural abundance.

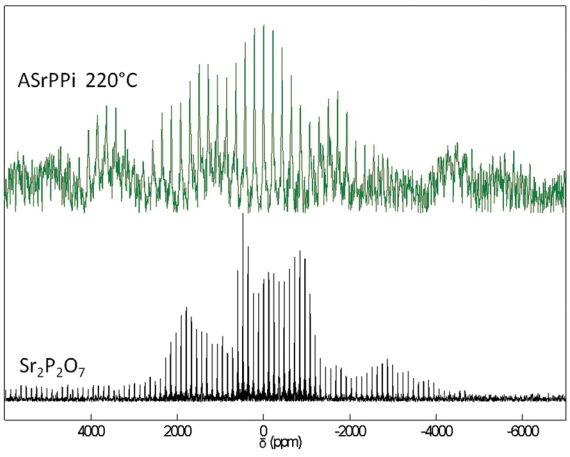

Figure 2. Natural abundance ^{87}Sr static NMR spectra of crystalline and amorphous Sr Pyrophosphates, recorded using the DFS WURST QCPMG pulse sequence. The total experimental time required for crystalline $Sr_2P_2O_7$ and ASrPPi 220°C were 4 hours (1 offset) and 25 hours (1 offset) respectively.

References

1. Li, Y.; Weng W. *J. Mater. Sci.* **2007** *18*, 2303.
2. Slater, C.; Laurencin, D.; Burnell, V.; Smith, M. E.; Grover, L. M.; Hriljac, J. A.; Wright, A. J. *J. Mater. Chem.* **2011**, *21*, 18783.
3. Bonhomme, C.; Gervais, C.; Folliet, N.; Pourpoint, F.; Coelho Diogo, C.; Lao, J.; Jallot, E.; Lacroix, J.; Nedelec, J.-M.; Iuga, D.; Du, J.; Hanna, J. V.; Smith M. E.; Laurencin, D. *submitted*.
4. Li, A.; Wang, D.; Xiang, J.; Newport, R. J.; Reinholdt, M. X.; Mutin, P. H.; Vantelon, D.; Bonhomme, C.; Smith, M. E.; Laurencin, D.; Qiu D. *J. Non Cryst. Solids* **2011**, *357*, 3548.

Global Supplier of NMR consumables and Stable Isotope Enriched products

www.cortecnet.com

Contact & Address:
Philippe Corcos, CEO
15/17, rue des Tilleuls
78960 Voisins-Le-Bretonneux, France
Tel: +33 (0)1 30 12 11 31
pcorcos@cortecnet.com

CortecNet
Innovation Accelerator in Life Science

Company

Since more than 15 years, CortecNet is known as one of the most reliable supplier of NMR consumables and Stable Isotope Enriched products.

CortecNet is composed of a team of analytical engineers capable to understand and fulfill all your needs.

Over the years, CortecNet has developed a strong professional network including thousands of academic labs and industrial companies all around the world.

Products

CortecNet has developed strong partnerships with key analytical suppliers like Bruker, New Era, Wilmad, SGE… .

CortecNet is specialized in NMR & EPR consumables (rotors, inserts, NMR tubes) and Stable Isotope enriched compounds including metals (^{29}Si, ^{43}Ca, ^{87}Sr), ^{17}O-labeled water, gases, deuterated solvents and custom ^{13}C, ^{15}N, ^{2}H labeled compounds.

We also recently expanded our line of services by providing high quality labeled protein standards for liquid and solid state NMR spectroscopy (Giotto Biotech).

We kindly invite you to visit our website (**www.cortecnet.com**) to discover all our products, download our catalogs and take advantage of our incredible weekly discounts on selected products.

JEOL-NMR Probes

advanced technology and performance

Royal Probe:

High 1H sensitivity

Improved inverse detection

Broad (LF) tuning range

Auto-tuning

Wide VT capability

1mm CPMAS Probe:

MAS Speeds 1KHz to 80KHz

Spinning stability <10Hz

Sample Volume 0.8µL

Excellent 1H sensitivity and resolution

Strong RF field

+44 (0)1707 377117

JEOL
www.jeol.com

euro.sales@jeol.com

BRUKER

Life science

Proteomics

Metabolomics

Materials science

Powering Discovery

Analytical chemistry

Pharmaceuticals

Microanalysis & imaging

Complete molecular confidence

Cutting-Edge Instrumentation
For Pioneering Research

- The world's highest magnetic field NMR system (1 GHz) - AVANCE™ 1000
- Breaking the optical diffraction limit, unprecedented lateral resolution in optical surface profiling - AcuityXR™
- The world's highest resolution FT-IR spectrometer - IFS 125
- Record-setting ultra-high field 17 Tesla preclinical MRI - BioSpec® 170/25
- Unrivalled scan speed from the first ion trap MS system with dual ion funnel transfer - amaZon

Contact us for more details: +44 (0)24 7685 5200
info@bruker.co.uk www.bruker.com

Innovation with Integrity

Design by Mustard: www.mustardhot.com

Advantage West Midlands
www.advantagewm.co.uk

BBSRC
bioscience for the future

EPSRC
Engineering and Physical Sciences Research Council

investing in your future
European Regional Development Fund
European Union

Dr Dinu Iuga (Facility Manager)
Department of Physics
University of Warwick
Coventry CV4 7AL

T +44 (0) 24 761 50814
F +44 (0) 24 761 50897
E D.Iuga@warwick.ac.uk
W http://go.warwick.ac.uk/850mhz/

UNIVERSITY OF CAMBRIDGE
Durham University
University of Glasgow
The University of Nottingham
UNITED KINGDOM · CHINA · MALAYSIA
University of St Andrews
THE UNIVERSITY OF WARWICK